Microwave Aperture Synthesis Radiometers for Earth Observation: Application to the SMOS Mission

A.Camps, Associate Professor
Dept. of Signal Theory and Communications
Universitat Politècnica de Catalunya

http://www.tsc.upc.edu/prs

Disclaimer:

• The materials of this tutorial have been obtained from a wide range of sources: from peer-reviewed journal papers and books, to publicly distributed technical notes and presentations from ESA and companies involved in the SMOS project.

• No specific mention has been made to each figure, table … and in any case the its authorship is not claimed by the lecturer of this course.

Acknowledgements:

• This course has been mainly extracted from the materials prepared by A. Camps, I. Corbella and N. Duffo for a 2-day course at INDRA premises in support to the development of the SMOS ground segment.
• The lecturer acknowledges the contributions of his co-authors and the rest of the UPC radiometry team.

Outline of the course:

1. Introduction

How can sea surface salinity be measured remotely?

• Using **microwave radiometry at L band**, as first proposed by C. Swift and R. McIntosh in 1983 (!!!):

C.T. Swift and R.E. McIntosh, "Considerations for Microwave Remote Sensing of Ocean-Surface Salinity," IEEE Trans. Geoscience Electronics, Vol. G.E.-21, no. 4, pp. 480-491, October 1983.

• In 1995, at the "Soil Moisture and Ocean Salinity" Worshop organized at ESTEC, microwave radiometry at L-band is still considered as the most promising technique to remotely measure Soil Moisture and Ocean Salinity, BUT using Aperture Synthesis Techniques

• Taking advantge of the MIRAS developments in the 90's, **in 1998 SMOS is proposed to ESA and in May 1999 is selected as the 2nd opportunity mission of the Earth Explorer series** with a (at least) two fold objective: to measure frequenctly and globally the SOIL MOISTURE and the OCEAN SALINITY.

1.1 Basic Radiometry Concepts

• **Introduction: The brightness.**

Gases radiate at discrete frequencies determined by the difference of energetic levels $f = \frac{E_2 - E_1}{h}$

The black-body (*bb: ideal*) radiates according to Plank's law

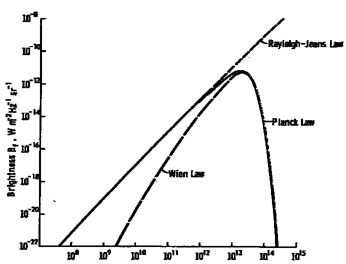

mW IR VIS

In thermodynamic equilibrium:
- Absorbs all incident energy
- Re-emits all absorbed energy

$$B_{bb}(f) = \frac{2hf^3}{c^2}\frac{1}{e^{\frac{hf}{k_B T}} - 1}\left[W \cdot m^{-2} \cdot Sr^{-1} \cdot Hz^{-1}\right]$$

$$\xrightarrow[f \to 0]{} \frac{2k_B}{\lambda^2} T$$ *Rayleigh-Jeans Law*

• Power collected by an antenna surrounded by a "black body":

$$P_{cn} = \frac{1}{2} A_{ef_R} \int_{f_0 - B/2}^{f_0 + B/2} \iint_{4\pi} \frac{2 k_B T}{\lambda^2} \cdot t(\theta,\varphi) \cdot \mathrm{d}\Omega \;\; \mathrm{d}f \approx k_B T \;\; B \;\; (B << f_0)$$

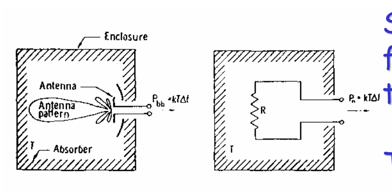

Same power as the one available from a resistor at the same physical temperature (Nyquist, 1928):

THERMAL NOISE

• The **brightness emitted by real bodies**: "gray bodies"

- *Do not absorb all incident energy:*
- *Part is reflected,*
- *Part is absorbed, which is then re-emitted directionally*

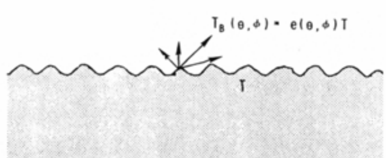

Brightness temperature and emissivity:

$$B(\theta,\varphi) = \frac{2 \;\; k_B}{\lambda^2} T_B(\theta,\varphi) \triangleq \frac{2 \;\; k_B}{\lambda^2} \;\; e(\theta,\varphi) \; T$$

$$0 \leq e \;\; (\theta,\varphi) \leq 1$$

- **Contributions to the noise power incident at the antenna:**

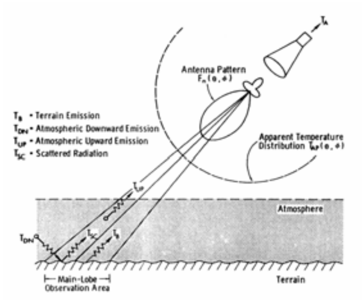

- From the **object** to which it is pointing (T_B), attenuated by the atmosphere ($L_a(\theta)$)
- The **atmosphere** (T_{UP})
- Reflections from other sources (T_{DN}): Sun, Moon, galactic noise, atmosphere...
- Direct brightness temperature from other sources.

⇒Apparent brightness temperature

$$T_{AP}^{p}(\theta,\varphi)=\frac{1}{L_a(h,\theta,\varphi)}\left(T_B^{p}(\theta,\varphi)+T_{SC}^{p}(\theta,\varphi)\right)+T_{UP}(\theta,\varphi)$$

- Total noise power delivered by an antenna:

$$N = k_B \; T_A^{'} \; B$$

$$T_A^{'} = \eta_\Omega \; T_A \; + \; (1-\eta_\Omega)T_{ph\,ant.}$$

$$T_A = \frac{1}{\Omega_a}\iint_{4\pi} T_{AP}(\theta,\varphi)\; t(\theta,\varphi)\; d\Omega = MBE\;\bar{T}_{ML} \; + \; (1-MBE)\;\bar{T}_{SL}$$

$\bar{T}$ main beam $\bar{T}$ secondary lobes

Goals:
- High Main Beam Efficiency: MBE → **1**
- Low ohmic losses: η_Ω → **1**

• Earth remote sensing applications (not comprehensive)
Scientific requirements

Aplication	Spatial resolution* [km]	Radiometric sensitivity [K]	Frequencies [GHz]
Temperature profile	50	0.3	21, 37, ***55***, 90
Water vapor profile	15	0.5	21, 37, 90, ***180***
Wind speed (over sea)	2-50	1	***10***, 18
Sea surface temperatura	1-50	0.3	***6.6***, 10, 18, 21, 37
Sea surface salinity	1-10	0.3	***1.4***, 6.6
Oil slicks	0.5	0.3	6.6, ***37***
Soil moisture	3-25	1	***1.4***, 6.6
Snow cover	3-25	1	6.6, 10, ***18***, ***37***, 90
Sea ice concentration	1-5	2	***18***, ***37***, 90
Continental ice mapping	1-5	1	10, 18, ***37***
Rain rate over the ocean	10-25	0.5	10, ***18***, 21, 37
Rain rate over land	10-25	0.5	18, ***37***, ***90***, 180
Cloud liquid water content	1-5	1	21, ***37***, 90

*: Spatial resolution may vary depending on the application

History of space-borne radiometers (not comprehensive)

Year	Platform/Instrument	1.4 GHz	6 GHz	10 GHz	18 GHz	21 GHz	37 GHz	50-60 GHz	90 GHz	160 GHz	183 GHz	Res. Espacial (Km)
1962	Mariner				X	X						1.300
1968	**Cosmos 243**	**X**		X								**37**
1970	Cosmos 384					X	X					13
1972	Nimbus-5 ESMR				X							25
	NEMS					X	X	X(3)				180
1973	**Skylab** S-193			X								16
	S-194	**X**										**115**
1974	Meteor						X					
1975	Nimbus-6 ESMR						X					20 x 43
	SCAMS					X	X	X(3)				150
1978	DMSP SSM/T							X(7)				175
1978	Tiros-N MSU							X(4)				110
1978	Nimbus-7 SMMR		X	X	X	X	X					18 x 27
	Seasat SMMR		X	X	X	X	X					22 x 35
1982	DMSP SSM/I				X	X	X		X			16 x 14
1986	NOAA AMSU-A					X	X	X(12)	X			50
	AMSU-B								X	X	X(3)	15
1992	SSM/T-2								X	X	X	50
2002-04	Aqua AMSR/E		X	X	X	X	X		X			75x43-6x4
	AMSU				15	channels	from	15 to 90				40
2002	Envisat MWR					X	X	GHz				25
2007	**SMOS MIRAS**	**X**										30->60
2008	SAC/D Aquarius	X										76x94-96x156
2010	Hydros (cancelled Dec 05)	X										40

• **SMOS mission: launch date September 2007**

- **SMOS** is the second mission selected in the EARTH OBSERVATION OPPORTUNITY MISSION PROGRAMME of ESA

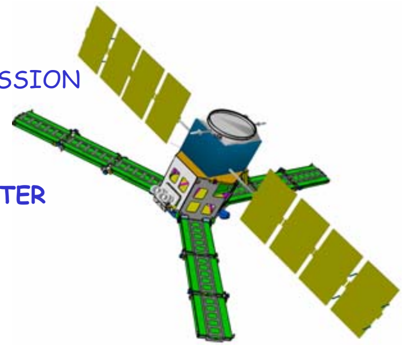

- **SMOS PayLoad Module (PLM)** is **MIRAS:** first **2D SYNTHETIC APERTURE RADIOMETER** for Earth observation.

- **Objectives:** soil moisture and ocean salinity measurements.
  ⇒ **L-band (!!)**

SMOS mission Objectives

Ocean: global SSS maps	0.1 psu every 10-30 days 200 km spatial resolution
Land: global SM maps and vegetation water content	0.035 m^3/m^3 every 3 days 0.2 Kg/m^2 60 km spatial resolution
Cryosphere:	Improved show mantle and multi-layered ice structure monitoring.

Technical Solution =

Microwave Radiometry by Aperture Synthesis

- **Innovative Method**
- Makes 2D brightness temperature images without mechanical antenna scanning
- Ideal case:

$$V(u,v)\,\alpha < b_1(t)\, b_2^*(t) >= F\left[\frac{T_B(\xi,\eta)-T_{ph}}{\sqrt{1-\xi^2-\eta^2}}\left|F(\xi,\eta)\right|^2\right]$$

- Achieves good spatial resolution (~50 km) with an array of small antennas (~20 cm)
- Smaller cost and more easily scalable

SMOS is a challenge:

Particularities of 2D aperture synthesis radiometers:

1) New type of instrument:

- Review of the fundamental equation
- Detail error model & error correction (calibration) algorithms
- Image reconstruction algorithms

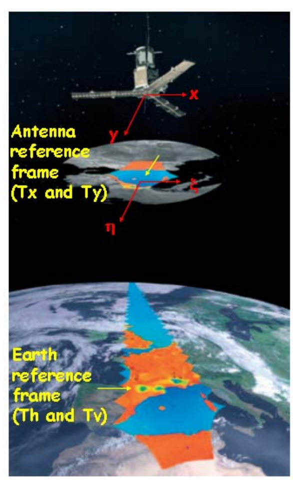

2) New type of observations:

- Multi-look and multi-angle observations:
  . different pixel size and orientation
  . different noise and precision for each pixel
- Polarization mixing:
  . Earth reference frane ↔ antenna reference frame

3) New L-band and multiangular ocean and soil emission models :

- Wide range of incidence angles (0°-60°)

4) New geophysical parameter retrieval algorithms taking into account issues 1, 2 and 3 above

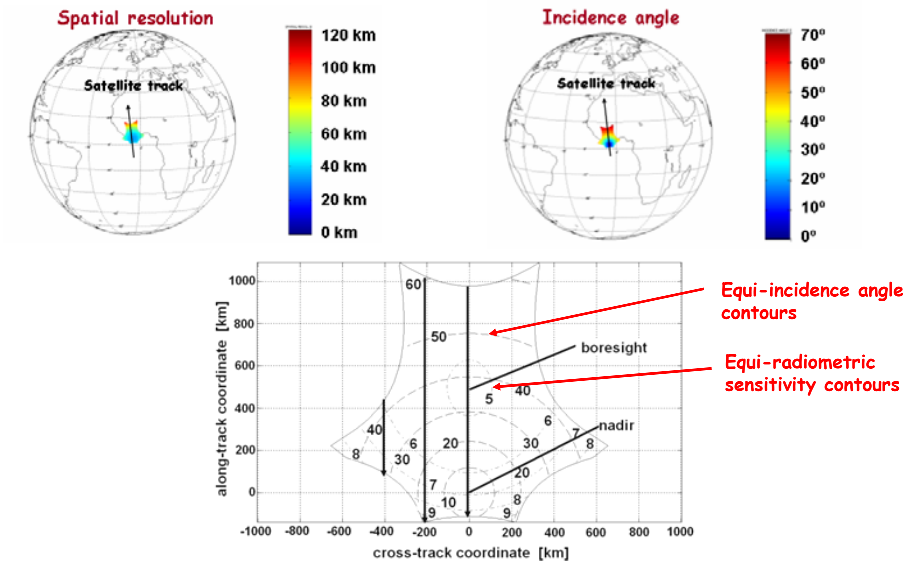

Orbital Considerations for SMOS:

Scientific measurements require a
- Sun-synchronous,
- dawn/dusk, and
- quasi circular orbit.

Orbital parameters:

• Mean altitude =	755.5 km
• Eccentricity =	0.001165
• Mean inclination =	98.416°
• Local Time Asc. Node =	6 AM
• Argument of Perigee =	90°
• Mean Anomaly =	306.3°

Note: The SUN is nearly always visible (97 % of the time) !!!

Mission Data:

Steering angle = 30°

Altitude = 755 km

β = 32 - 33° $\Rightarrow$ enlarge range of θ_i's

Antenna spacing = 0.875 λ

$\Rightarrow$ AF-FOV & 3-day revisit time !!

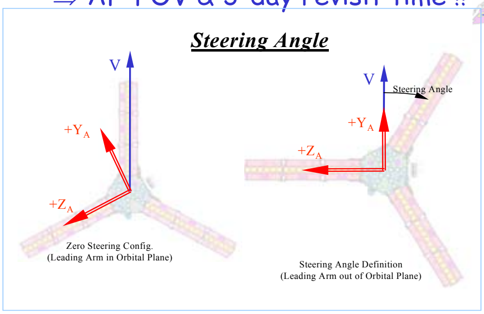

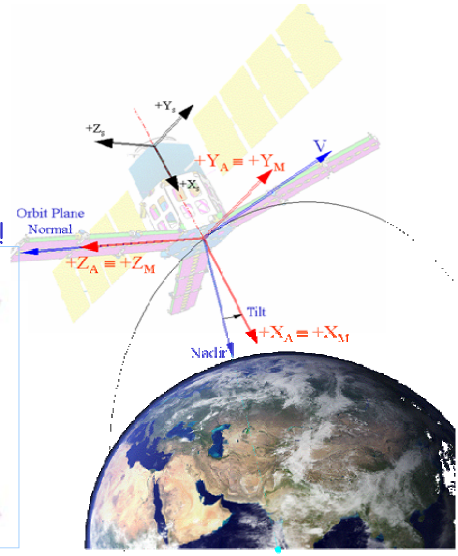

1.3. Stokes Emission Vector and Spectral Signatures

- **Stokes Vector**
  - Polarization Properties of Emitted/Scattered Radiation
  - Contains Directional Information

    E.g. wind Direction signal ~ two orders of magnitude smaller than wind Speed signal
  - Two ways of performing the measurements
    - Correlation of Primary Polarizations
    - Direct measure of ±45°, LHC, RHC

$$I_s = \begin{bmatrix} I \\ Q \\ U \\ V \end{bmatrix} = \begin{bmatrix} T_v + T_h \\ T_v - T_h \\ T_{45} - T_{-45} \\ T_{lhc} - T_{rhc} \end{bmatrix} \alpha \underbrace{\begin{bmatrix} \langle E_h E_h^* \rangle + \langle E_v E_v^* \rangle \\ \langle E_h E_h^* \rangle - \langle E_v E_v^* \rangle \\ 2\mathrm{Re}\langle E_v E_h^* \rangle \\ 2\mathrm{Im}\langle E_v E_h^* \rangle \end{bmatrix}}_{\text{As in full-polarimetric mode in SMOS}}$$

• Emissivity angular dependence of different flat surfaces:

$e_p(\theta) = 1 - \Gamma_p(\varepsilon_r, \theta)$

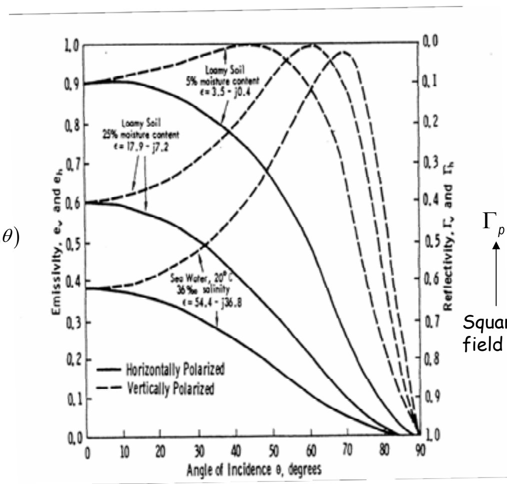

$\Gamma_p(\varepsilon_r, \theta)$

Squared Fresnel electric field reflection coefficient

• T_B sensitivity to different geophysical variables:

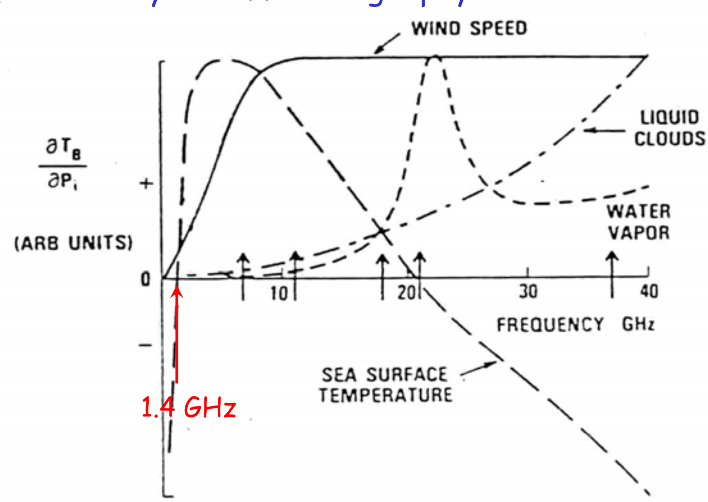

Soil Brightness Temperature: flat surface

ε_r(soil moisture, soil type, texture, porosity…) $\rightarrow T_B$(soil moisture, soil type, texture, porosity…)

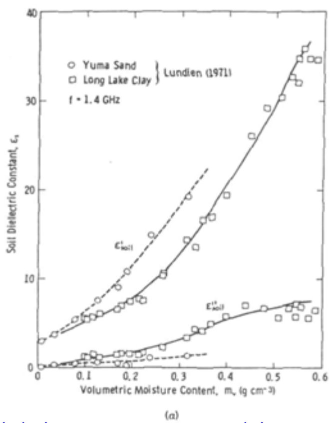

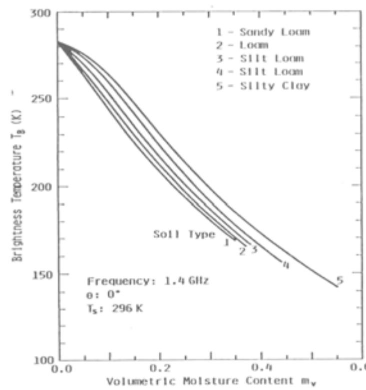

Several dielectric constant models exist: Wang, Dobson … (some depend also on soil type, density …)

Soil Brightness Temperature: roughness effects

$$T_{B,bare}^{p}(\theta) = \left[1-\Gamma_{bare}^{p}(\theta)\right]\ T_{soil}$$

$$\Gamma_{bare}^{p}(\theta) = \left[(1-Q)\ \ \Gamma_{spec}^{p}(\theta)+Q\ \ \Gamma_{spec}^{q}(\theta)\right]\ e^{-4\,k^2\,\sigma^2\,\cos^2\theta}$$

Polarization mixing parameter:

$$Q = 0.35\ \left(1-e^{-0.6\ \sigma_{cm}^2\ f_{GHz}}\right)$$

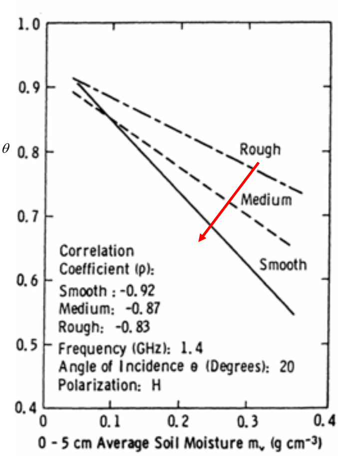

• Vegetation-covered brightness temperature:

At L-band the simple τ-ω model is used (T_{soil} = T_{veg}):

$$T_p = \left[\left(1+\frac{\Gamma_p^{bare}}{L_p^{veg}}\right)\cdot\left(1-\frac{1}{L_p^{veg}}\right)\cdot\left(1-\omega_p\right)+\left(\frac{1-\Gamma_p^{bare}}{L_p^{veg}}\right)\right]\cdot T_{soil}$$

$$\Gamma_{bare}^{p}(\theta)=\left[(1-Q)\ \ \Gamma_{spec}^{p}(\theta)+Q\ \ \Gamma_{spec}^{q}(\theta)\right]\ e^{-h_s}$$

$$L_p^{veg}=\exp\left(\frac{\tau_p}{\cos\theta}\right)$$

ω = single scattering albedo can be a function of polarization and incidence angle
τ = vegetation "opacity" depends mainly on the vegetation water content and can be a function polarization
Usually assumed to be rather constant, but may exhibit significant variations after intense rain events (if previously very dry, for example).
L_{veg} = attenuation through vegetation does not have to follow a $1/\cos(\theta)$ dependence
Scattering effects may become significant at large incidence angles

Remote Sensing of Soil Moisture with ESTAR (Electronically Steered Thinned Array Radiometer)

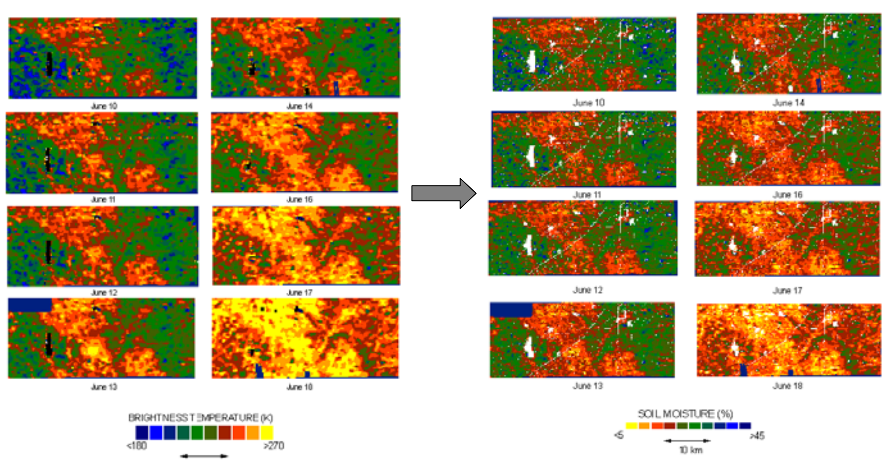

(http://hydrolab.arsusda.gov/RSatBARC/smresults.html)

The brightness temperature of the sea depends on

- the sea surface salinity, → Maximum sensitivity at P and L-bands:
  - 1400-1427 MHz reserved for passive observations
  - Atmospheric effects: minimum
- the temperature, and
- the sea state (wind, waves...) → **To be corrected**

SSS and SST dependence (θ = 0°)

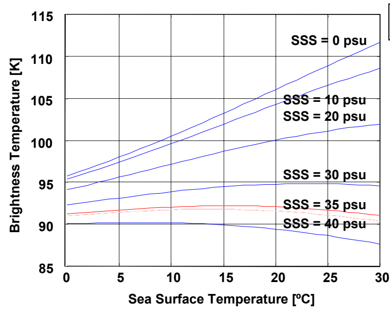

$$\underbrace{\underbrace{\big(1-\underbrace{\Gamma_{h,v}(\theta,SST,SSS)}_{\text{Fresnel reflection coefficient}}\big)}_{\text{Flat sea surface emissivity}}\cdot SST}_{T_B\text{ calm sea}}$$

$$T_{h,v}(\theta,SST,SSS)\approx\big(1-\Gamma_{h,v}(\theta,SST,SSS)\big)\cdot SST+\underbrace{\Delta T_{h,v}(\theta,param)}_{T_B\text{ variation due to sea state}}$$

Geophysical Parameters Retrieval in SMOS
Semi-empirical sea emission models: WISE & FROG field experiments

UPC
L-band
AUtomatic
RAdiometer

7 x 3 m pool
Array of 104 air difussers

Rain generator:
h = 10-13 m; R = 4000 mm/h

Geophysical model function derived from WISE/FROG:

- Sea roughness induced emissivity (WISE)

$$\boxed{T_B^{sea}(\theta, pol) = \left[1 - \Gamma^{Fresnel}(\theta, \varepsilon_r, pol)\right] \cdot T_s + \Delta T_B(\theta, pol, parameter)}$$

* Parameter = U_{10} * Parameter = SWH * Parameter = U_{10} & SWH

$$\begin{cases} \Delta T_h \approx 0.25 \cdot (1+\theta/94^\circ) \cdot U_{10} \\ \Delta T_v \approx 0.24 \cdot (1-\theta/81^\circ) \cdot U_{10} \end{cases} \quad \begin{cases} \Delta T_h \approx 1.09 \cdot (1+\theta/142^\circ) \cdot SWH \\ \Delta T_v \approx 0.92 \cdot (1-\theta/51^\circ) \cdot SWH \end{cases} \quad \begin{cases} \Delta T_h \approx 0.12 \cdot (1+\theta/24^\circ) \cdot U_{10} + 0.59 \cdot (1-\theta/50^\circ) \cdot SWH \\ \Delta T_v \approx 0.12 \cdot (1-\theta/40^\circ) \cdot U_{10} + 0.59 \cdot (1-\theta/50^\circ) \cdot SWH \end{cases}$$

- Foam-induced emissivity (FROG)

$$\boxed{\begin{aligned} T_{B_{h,v}}^{Total} &= F(U_{10}) \cdot T_{B_{h,v}}^{Foam} + \left[1 - F(U_{10})\right] \cdot T_{B_{h,v}}^{Sea} = \\ &= T_{B_{h,v}}^{Sea} + F(U_{10})\left[T_{B_{h,v}}^{Foam} - T_{B_{h,v}}^{Sea}\right] \end{aligned}}$$

  * H-pol: ~ 0.008 / mm at θ_i = 25°, ~ 0.005 /mm at θ_i = 50°
  * V-pol: ~ 0.005 / mm at θ_i = 25°, ~ 0.010 /mm at θ_i = 50°
  * Good agreement Reul-Chapron model with measurements if κ(SSS), and with WISE measurements if d ~ 8 mm

- Rain-perturbed sea surface emission:
  * estimated impact ~ 0.08 K at 160 mm/h at θ_i = 25°, and at H- and V-polarizations
  * Accurately predicted by SSA model +
  + Craeye-Sobieski-Bliven rain-perturbed sea surface spectrum

Incidence angle θ	25°	30°	35°	40°	45°	50°
$\Delta T_h = T_{h(with\ rain)} - T_{h(without\ rain)}$ [K]	0.0786	0.0921	0.0849	0.0555	0.0958	0.0339
$\Delta T_v = T_{v(with\ rain)} - T_{v(without\ rain)}$ [K]	0.0738	0.0829	0.0899	0.0914	0.1536	0.0884

- Oil-slicks: negligible effect for 48 μm thickness in fresh and salt water, but it does affect the sea surface roughness

Remote Sensing of Sea Salinity: First Results

- 1996: first SSS map with real aperture radiometer (SLFMR)
- 1999: first SSS map with synthetic aperture radiometer (ESTAR)

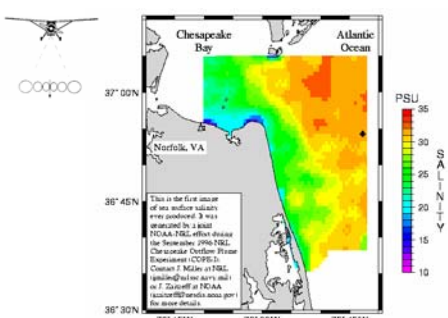

SSS map derived from the "Scanning Low Frequency Microwave Radiometer (SLFMR) airborne salinity mapper".
(J. Miller, NRL y J. Zaitzeff, NOAA/NESDIS).

Error = 1 psu

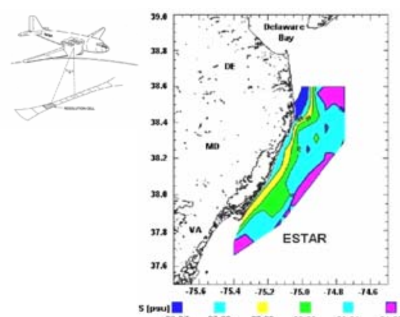

SSS map derived from the "Electronically Steered Thinned Array Radiometer (ESTAR)",
(D. M. LeVine et al., NASA Goddard).

Error = 0.3 psu

1.4. Atmospheric and Ionospheric Effects at L-band

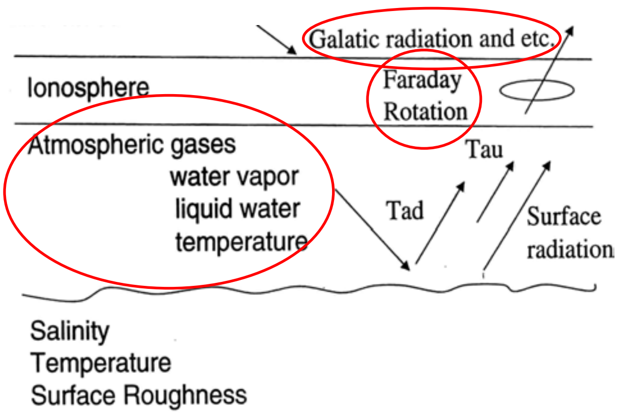

Atmospheric effects:

- As a first approximation the atmosphere can be approximated by a stratified set of attenuators at a given physical temperature.
- Hydrometeors, specially rain, increase the losses (both by absorption k_a and scattering k_s), and add contributions to the measured brightenss temperature.

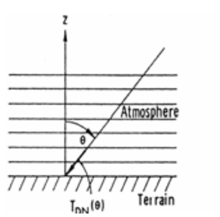

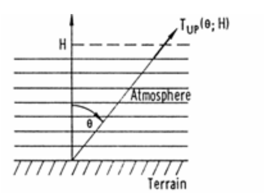

$$T_{UP}^{Atm}(\theta,H)=\sec\theta \int_0^H k_a(z')\ T(z')\ e^{-\tau(z',H)\sec\theta} dz',\ T_{DN}^{Atm}(\theta,H)=\sec\theta \int_0^\infty k_a(z')\ T(z')\ e^{-\tau(0,z')\sec\theta} dz'$$

$$\downarrow \qquad\qquad \downarrow$$

$$e(z')=k_a(z') \qquad\qquad e(z')=k_a(z')$$

$$\tau(z',H)=\int_{z'}^{H} k_a(z)\ dz \ \text{"opacity"}$$

- The atmosphere also **attenuates external noise sources**

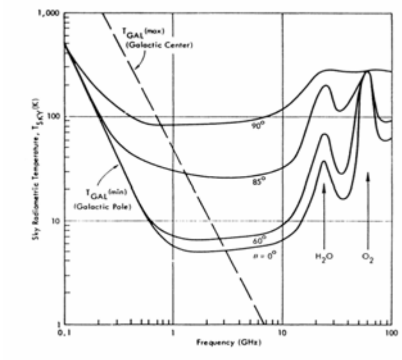

- **Galactic noise:** Passive observations below 1 GHz not feasible

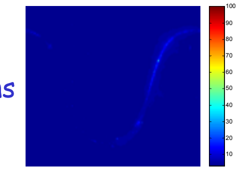

(1420 MHz sky map included in SEPS)

- **Cosmic noise:** $T_{cos} \approx 2.7$ K

- **Sun** and **Moon** reflections (if visible)

$$T_{DN} = T_{DN}^{Atm} + \left(T_{Gal} + T_{Cos} + T_{Sun} + T_{Moon}\right) e^{-\tau(0,\infty)\sec\theta}$$

Total Attenuation for One-way Vertical Transmission through the Atmosphere

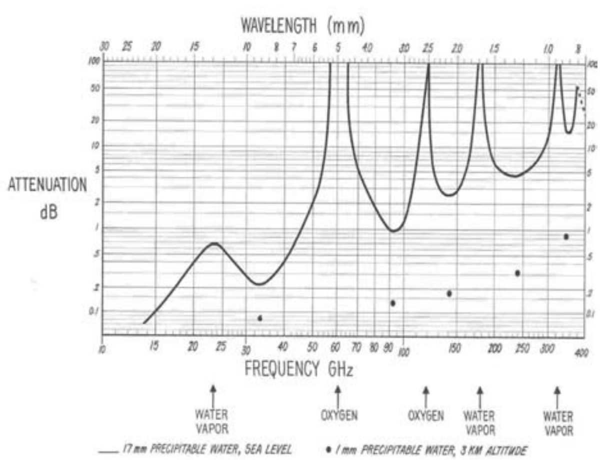

Correction of T_B images in the Earth's reference frame:

⇒ previous correction of Faraday and geometric corrections

- From T_B on top of the atmosphere to T_B over the Earth's surface:

$$T_p^{data} = T_p\, L(\theta) - \left[\Gamma_p(\theta) \frac{T_{SKY}}{L(\theta)} + T_{UP\ atm}(\theta)\, L(\theta) \right] - \Gamma_p(\theta) T_{DN\ atm}(\theta)$$

$L(\theta)$, T_{SKY}, $T_{UP\ atm}(\theta)$ and $T_{DN\ atm}(\theta)$ must account for:

- **Oxigen absorption** : error in surface temperature = 7 °C and in surface pressure = 14 mb
- **Water vapor**: negligible or based on climatological values
- **Clouds:** negligible
- **Rain:** usually negligible (only need to flag pixels with rain)
- **Sun** direct and reflected: Relies on Sun cancellation algorithms ? Estimates 5-10% error. Flag contaminated pixels.
- **Moon:** can be a problem... Direct: no problem, reflected ? Probably not.
- **Galactic noise reflected** (in the extended AF-FOV and in the AF-FOV: T_{SKY} term) MUST BE CORRECTED: BIG IMPACT ⇒ Galactic noise maps + surface scattering models

Over sea → validity TBC; Over land → lack of accurate models

Ionospheric effects:

- Small losses ⇒ contributions to T_{up}, T_{dn} and $L_{ionosphere}$
- VTEC + Geomagnetic field ⇒ Faraday rotation

Global distribution of Faraday rotation for local time of 6 am (left) and noon (right). The data are for high solar activity (June 1989), an altitude of 675 km, and looking perpendicular to the satellite heading to the right at incidence angles as indicated (20, 30, 40, and 50 degrees).

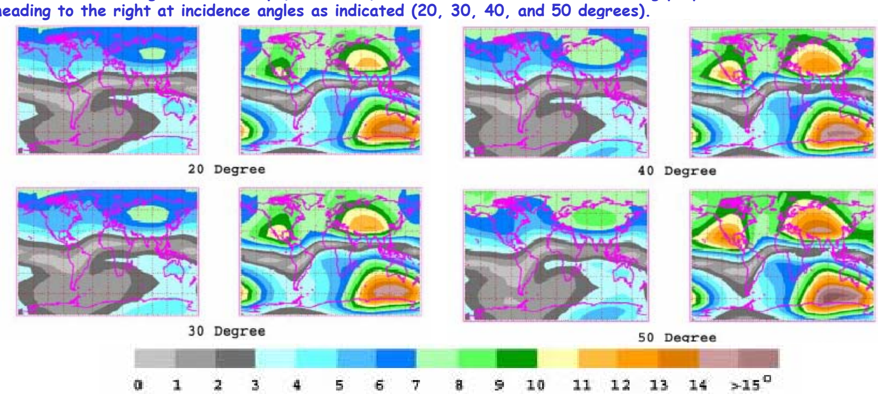

Global distribution of the error in brightness temperature as a function of incidence angle due to neglecting Faraday rotation at 6 am (left) and noon (right). The data are for high solar activity (June 1989; Rz = 158) and for a sensor at altitude of 675 km and looking perpendicular to the satellite heading to the right. The surface is ocean with S = 35 psu and T = 20 C.

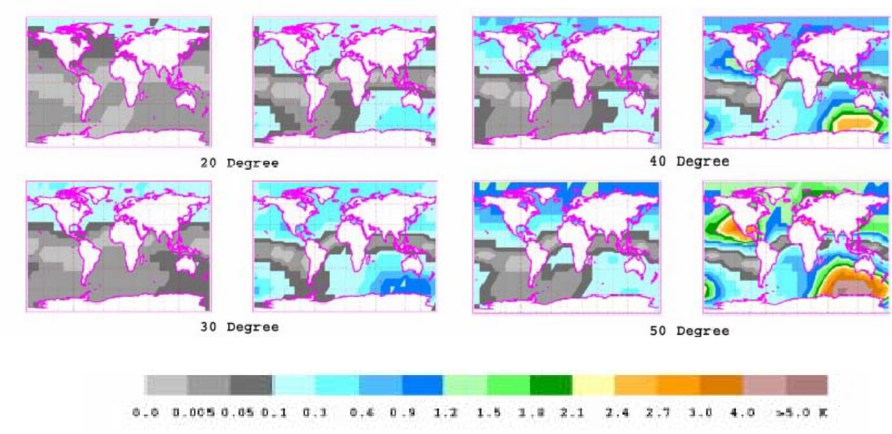

Ionospheric attenuation and emission: SSS = 35 psu, SST = 20°C

June 6 AM (top), 12 PM (bottom)
T↑ = Tup; T↓ = Tdn scattered over the ocean

IONOSPHERIC ATTENUATION AND EMISSION (6 AM)

Location		Rz	VTEC (TECU)	τ (10^{-4} Neper)	ΔT (mK)	T↑ (mK)	T↓ (mK)
Latitude	Longitude						
30 N	220 E	158.4	19.9	2.64	2.18	20.87	16.08
		8.5	6.4	1.45	1.20	4.75	3.51
0	220 E	158.4	20.6	2.47	2.04	23.01	18.22
		8.5	8.6	1.19	0.98	5.31	5.06
30 S	220 E	158.4	12.7	1.00	0.83	9.35	7.54
		8.5	3.6	[illegible]	[illegible]	[illegible]	[illegible]
30 N	330 E	158.4	24.9	3.51	2.89	31.42	23.98
		8.5	7.1	[illegible]	[illegible]	[illegible]	[illegible]
0	330 E	158.4	20.3	2.49	2.05	22.81	17.91
		8.5	8.0	1.11	0.91	4.79	4.39
30 S	330 E	158.4	9.5	0.65	0.53	5.38	4.60
		8.5	3.2	0.27	0.22	1.01	0.83
30 S	60 E	158.4	5.3	0.31	0.25	1.83	1.68
		8.5	2.2	0.21	0.17	0.65	0.48
75 N	160 E	158.4	18.7	3.32	2.74	17.70	22.86
		8.5	6.3	2.19	1.80	6.08	4.40

IONOSPHERIC ATTENUATION AND EMISSION (NOON)

Location		Rz	VTEC (TECU)	τ (10^{-4} Neper)	ΔT (mK)	T↑ (mK)	T↓ (mK)
Latitude	Longitude						
30 N	220 E	158.4	39.8	11.43	9.42	77.34	57.46
		8.5	14.2	5.00	4.12	18.49	13.52
0	220 E	158.4	45.0	13.42	11.06	99.21	78.06
		8.5	17.3	5.81	4.78	22.22	19.41
30 S	220 E	158.4	37.9	10.22	8.42	80.89	59.12
		8.5	9.0	3.26	2.69	10.32	7.59
30 N	330 E	158.4	43.5	12.37	10.20	89.77	67.04
		8.5	13.8	[illegible]	[illegible]	[illegible]	[illegible]
0	330 E	158.4	48.3	14.47	11.92	113.48	87.74
		8.5	17.7	[illegible]	[illegible]	[illegible]	[illegible]
30 S	330 E	158.4	35.7	9.98	8.22	75.06	54.73
		8.5	11.3	3.64	3.00	13.08	9.76
30 S	60 E	158.4	39.8	10.68	8.80	85.87	63.13
		8.5	9.8	3.46	2.85	11.82	8.57
75 N	160 E	158.4	20.1	6.11	5.034	24.57	28.29
		8.5	6.7	2.60	2.134	7.29	5.27

Solar activity in terms of the sunspot number Rz: Rz = 12-month, running mean centered on the middle of the month of interest.

2. The MIRAS Concept

2.1 Antenna Size Considerations

Until present **all Earth observation microwave radiometers are real aperture radiometers**.

The simplest version is the **total power radiometer** (TPR):

(conceptually identical to the LICEFs' PMS, needed to denormalize the visibility samples!!)

$$V_{out}=GT_A+(GT_{rec}+offset)$$

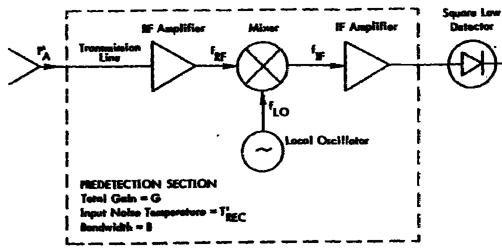

$$\Delta T=\frac{T'_A+T'_{REC}}{\sqrt{B\tau}}=\frac{T_{sys}}{\sqrt{B\tau}}$$

$$\Delta T = T_{SYS}\left[\frac{1}{B\tau}+\left(\frac{\Delta G_S}{G_S}\right)^2\right]^{\frac{1}{2}}$$

- **Total power Radiometer Calibration**

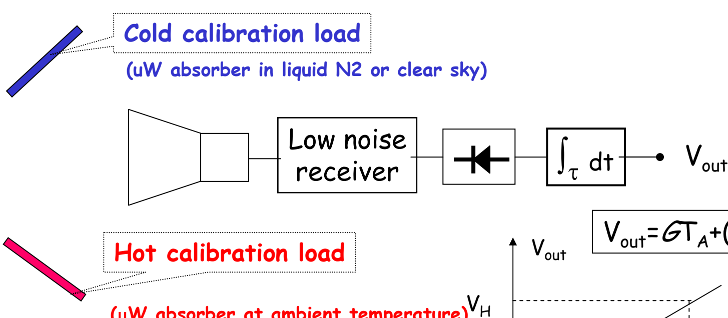

$$V_{out}=GT_A+(GT_{rec}+offset)$$

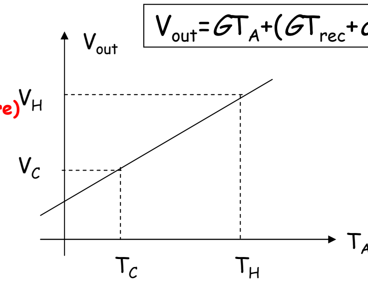

Image formation in aperture synthesis radiometers

- Image is formed by pointing the beam towards each pixel.
- Spatial resolution determined by the antenna size.

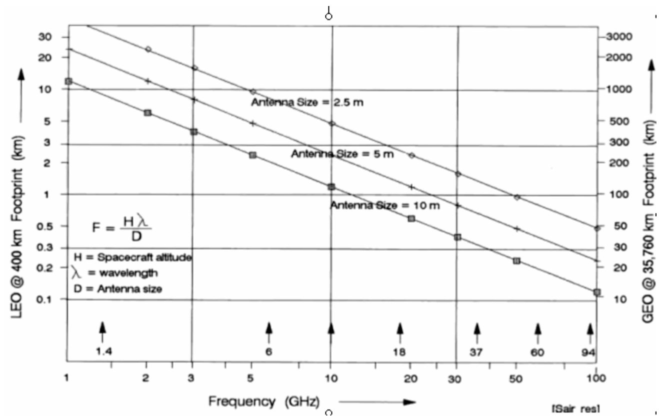

SCAN CONFIGURACIONS:

a) Cross-track scan

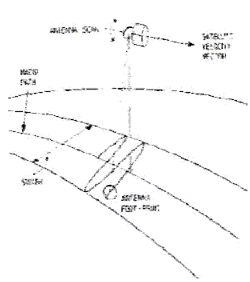

b) Conical scan

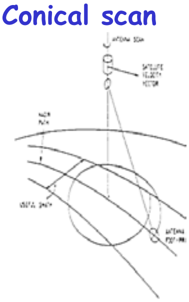

c) Push-broom

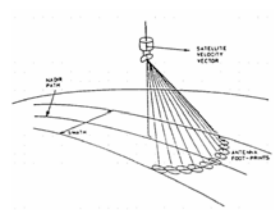

θ_{inc} constant over the surface

Aperture Synthesis Microwave Radiometry :

VLA, New Mexico, Socorro

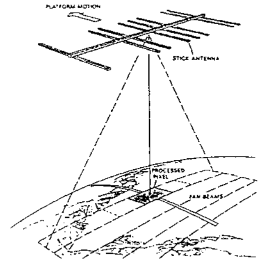

ESTAR

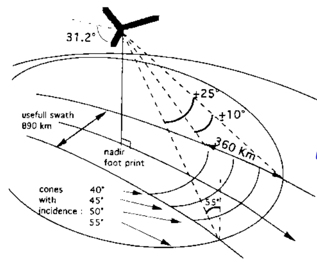

MIRAS

$$V(u,v)\alpha < b_1(t)b_2^*(t) >= F\left[\frac{T_B(\xi,\eta)-T_{ph}}{\sqrt{1-\xi^2-\eta^2}}|F(\xi,\eta)|^2\right]$$

Aperture Synthesis Microwave Radiometry: (cont')

- **Differences between radio-astronomy and Earth observation**
- **In radio-astronomy:**

- Large antenna spacing
- Very narrow field of view (FOV)
- Obliquity factor (1/cos θ) can be approximated by 1
- Antenna patterns are approximatedly constant (amplitude and phase) over the FOV
- Typically quasi-point sources imaged over cold background

→ super-resolution image reconstruction algortihms can be used

2.3. Aperture Synthesis Techniques: Overview

2.3.1. Fundamentals

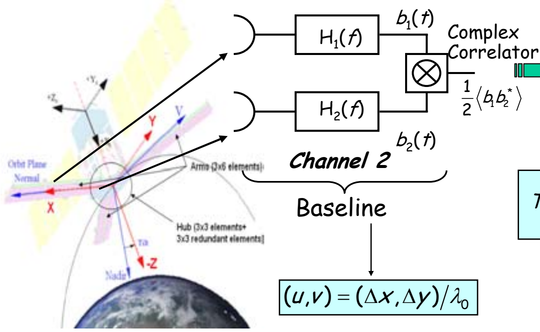

$$V(u,v) = \frac{1}{k_B\sqrt{B_1 B_2}\sqrt{G_1 G_2}}\,\frac{1}{2}\langle b_1(t)\, b_2^*(t)\rangle$$

$$T(\xi,\eta) = \frac{F_{n1}(\xi,\eta)\, F_{n2}^*(\xi,\eta)}{\sqrt{\Omega_1\Omega_2}}\,\frac{T_B(\xi,\eta) - T_{ph\,rec}}{\sqrt{1-\xi^2-\eta^2}}$$

$$(u,v) = (\Delta x, \Delta y)/\lambda_0$$

$$(\xi,\eta) = (\sin\theta\cos\varphi, \sin\theta\sin\varphi)$$

(u,v): antenna spacing normalized to the wavelength
set of (u,v) points depend on the antenna separation and the array geometry
= set of spatial frequencies where the visibility function V(u,v) is sampled

Ideal case: -Identical antenna patterns
-Negligible spatial decorrelation
-No antenna positioning errors

2D Fourier Transform

$$V(u,v) = F\,[T(\xi,\eta)]$$

2.3.2. Imaging

Antenna Positions

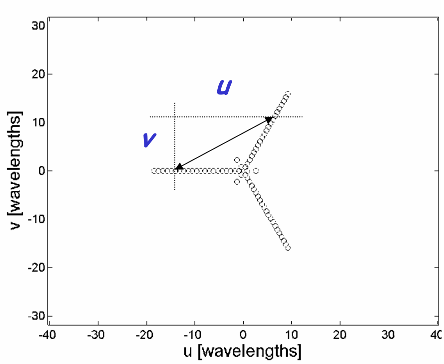

Spatial frequencies (u,v)

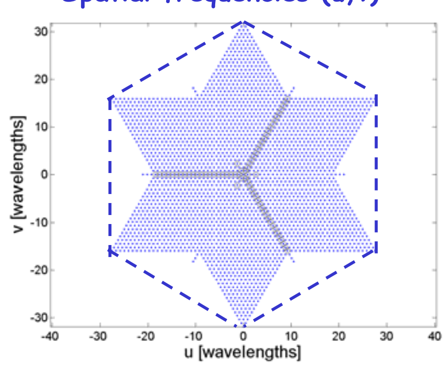

$$(u,v) = (\Delta x, \Delta y)/\lambda_0$$

21 elements + 2 redundant elements/arm
Antenna spacing d = 0.875λ

Hexagonal grid in (u,v) plane
Nyquist criterion: d< $\lambda/\sqrt{3}$

Periodic extension of the "visibility" samples in the (u, v) domain:

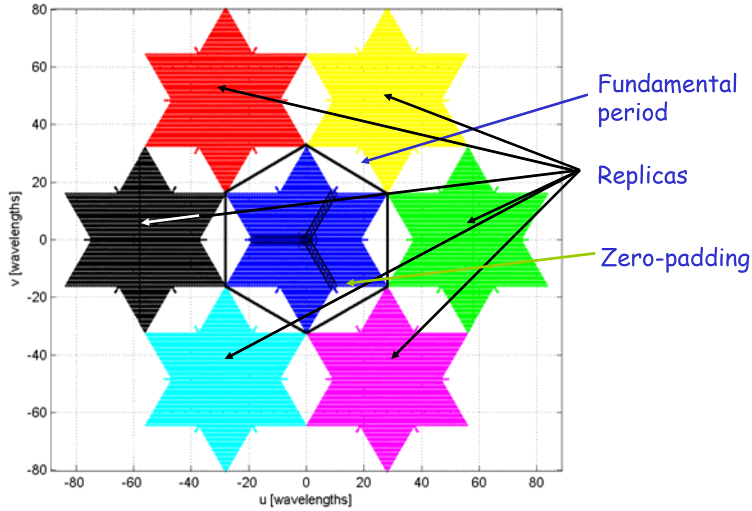

Ideal case: imaging using an Inverse Hexagonal Fourier Transform + antenna pattern & obliquity factor compensation

$$\boxed{V(u,v) = F\,[T(\xi,\eta)]}$$

$$T(\xi,\eta) = \frac{|F_n(\xi,\eta)|^2}{\Omega} \frac{T_B(\xi,\eta) - T_{ph\,rec}}{\sqrt{1-\xi^2-\eta^2}}$$

ÓPTIMO: (ξ,η) = malla recíproca de la malla (u,v)

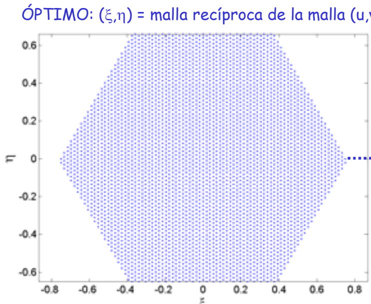

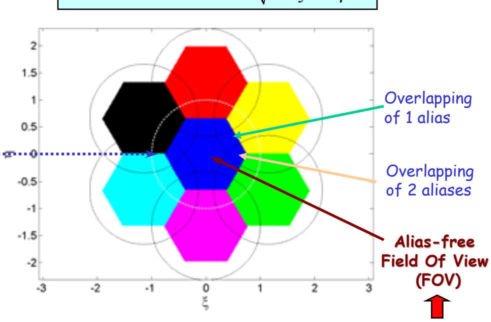

If d ≥ λ√3 ⇒ only one part of the fore hemisphere can be imaged = AF-FOV

In SMOS the "**alias-free FOV**" can be **enlarged** since part of the alias images are the "cold" sky (including the galaxy!) ⇒ T_B image limitaded by Earth replicas

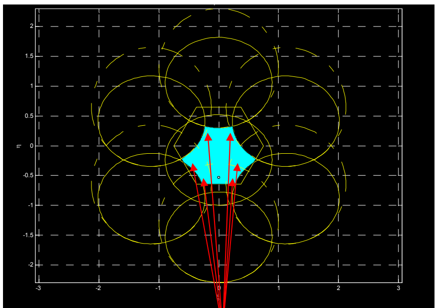

Extension of Alias-Free FOV

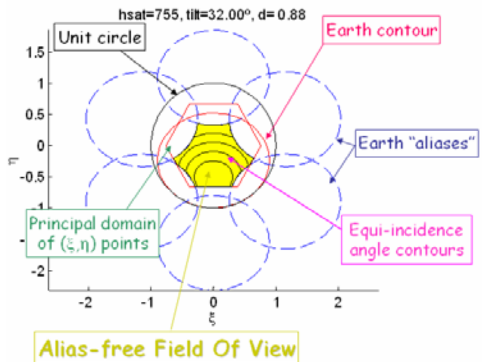

2.3.3. Dual-polarization and full-polarimetric aperture synthesis radiometers

Dual-polarization radiometer:

MIRAS has dual-pol antennas, but only one receiver
⇒ polarizations have to be measured sequentially, with an integration time of 1.2 s each

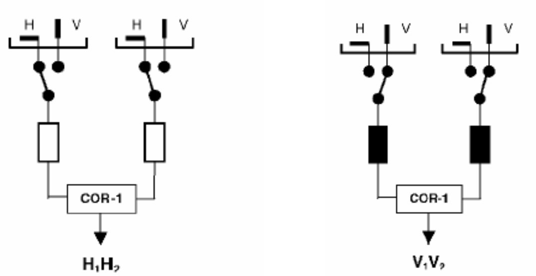

Full-polarimetric mode:

- If one receiver per polarization, the imaging process would be the same with the first antenna in one polarization, and the second one in the other polarization.
- An alternating sequence was devised to measure all cross-correlations.

Note: the zero-baseline is measured by a polarimetric radiometer (the 3 NIRs in the hub)

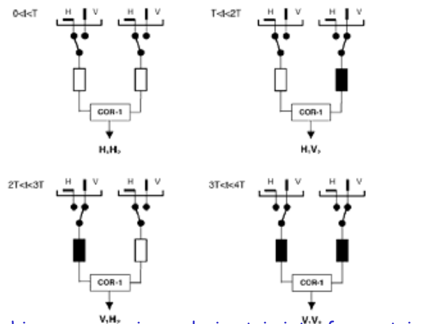

Switching sequence in a polarimetric interferometric radiometer of two elements, using T=1.2 s as the correlator integration time.

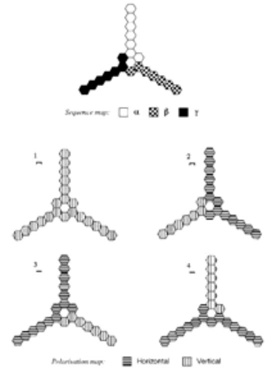

Polarization switching sequence theory applied to MIRAS.

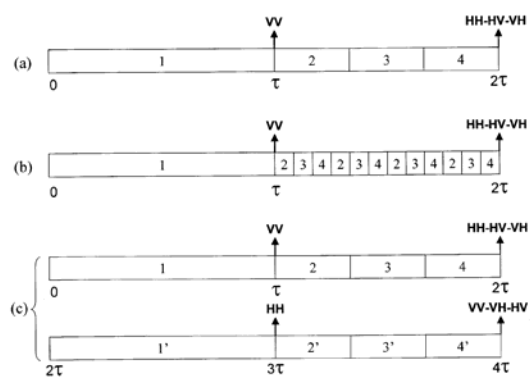

MIRAS full-polarimetric mode-switching sequences.
(a) Without interlacing of combined polarimetric measurements.
(b) With interlacing.
(c) Alternating polarization concept to achieve equisensitivity.
Interlacing minimizes blurring of the impulse response (or "array factor", AF)

2.3.4. Transformation from Antenna to Earth Reference Frames

At each snap-shot, inverting the transformation matrices requires knowledge of **Faraday and Geometric rotation angles** ($\varphi_{Faraday}$ and φ)

Dual-pol mode:

Matrix transformation:

Matrix is singular when A=B:
$\psi_{Faraday} - \psi_{geometry} = 45°$!!!

$$\begin{bmatrix} T_{xx} \\ T_{yy} \end{bmatrix} = \begin{bmatrix} A^2 & B^2 \\ B^2 & A^2 \end{bmatrix} \cdot \begin{bmatrix} T_{hh} \\ T_{vv} \end{bmatrix} \Rightarrow \overline{T}_{antenna} = \overline{\overline{M}}_{dual-pol} \cdot \overline{T}_{Earth}$$

$$A = \cos\left(\psi_{Faraday} - \psi_{geometry}\right)$$

$$B = \sin\left(\psi_{Faraday} - \psi_{geometry}\right)$$

Noise covariance matrix:

$$\overline{\overline{C}}^{antenna}_{dual-pol} = \begin{bmatrix} 1 & 0 \\ 0 & 1 \end{bmatrix} \sigma^2 \qquad \overline{\overline{C}}^{Earth}_{dual-pol} = \frac{1}{\left(A^4 - B^4\right)^2} \begin{bmatrix} A^4 + B^4 & -2A^2B^2 \\ -2A^2B^2 & A^4 + B^4 \end{bmatrix} \sigma^2 \quad [1]$$

Full-pol mode:

Matrix is never singular

$$\begin{bmatrix} T_{xx} \\ T_{xy} \\ T_{yx} \\ T_{yy} \end{bmatrix} = \begin{bmatrix} A^2 & AB & AB & B^2 \\ -AB & A^2 & -B^2 & AB \\ -AB & -B^2 & A^2 & AB \\ B^2 & -AB & -AB & A^2 \end{bmatrix} \begin{bmatrix} T_{hh} \\ T_{hv} \\ T_{vh} \\ T_{vv} \end{bmatrix} \Rightarrow \overline{T}_{antenna} = \overline{\overline{M}}_{full-pol} \cdot \overline{T}_{Earth}$$

Noise covariance matrices in odd and even snap-shots:

$$\overline{\overline{C}}^{antenna}_{full-pol} = \begin{bmatrix} 1 & 0 & 0 & 0 \\ 0 & 3 & 0 & 0 \\ 0 & 0 & 3 & 0 \\ 0 & 0 & 0 & 3 \end{bmatrix} \sigma^2; \; \overline{\overline{C}}^{Earth}_{full-pol} = \begin{bmatrix} A^4+6A^2B^2+3B^4 & -2A^3B & -2A^3B & -2A^2B^2 \\ -2A^3B & 3A^4+4A^2B^2+3B^4 & -2A^2B^2 & -2AB^3 \\ -2A^3B & -2A^2B^2 & 3A^4+4A^2B^2+3B^4 & -2AB^3 \\ -2A^2B^2 & -2AB^3 & -2AB^3 & 3A^4+6A^2B^2+B^4 \end{bmatrix} \sigma^2 \quad [2]$$

$$\overline{\overline{C}}^{antenna}_{full-pol} = \begin{bmatrix} 3 & 0 & 0 & 0 \\ 0 & 3 & 0 & 0 \\ 0 & 0 & 3 & 0 \\ 0 & 0 & 0 & 1 \end{bmatrix} \sigma^2; \; \overline{\overline{C}}^{Earth}_{full-pol} = \begin{bmatrix} 3A^4+6A^2B^2+B^4 & -2AB^3 & -2AB^3 & -2A^2B^2 \\ -2AB^3 & 3A^4+4A^2B^2+3B^4 & -2A^2B^2 & -2A^3B \\ -2AB^3 & -2A^2B^2 & 3A^4+4A^2B^2+3B^4 & -2A^3B \\ -2A^2B^2 & -2A^3B & -2A^3B & A^4+6A^2B^2+3B^4 \end{bmatrix} \sigma^2$$

Amplification of the noise standard deviation in the transformation from the antenna reference frame to the earth reference frame
($1/\sigma$ times the square root of the noise covariance matrix elements).

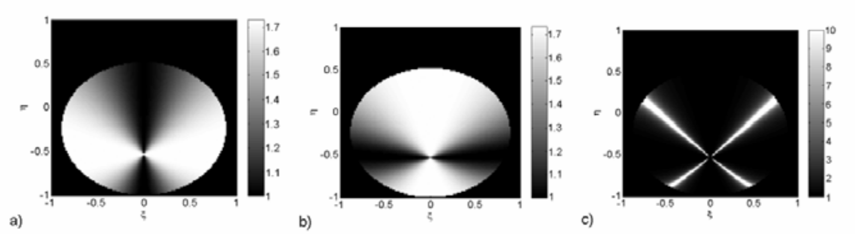

(a) Full-polarimetric mode at H-polarization odd period or V-polarization even period (element 4-4 in [2, top] or in 1-1 [2, bottom]),
(b) Full-polarimetric mode at V-polarization odd period or H-polarization even period (element 4-4 in [2, top] or 1-1 in [2, bottom), and
(c) Dual-polarization mode [element 1-1 or 2-2 in [1]: cross-like region is singular. Graybar truncated at 10 for better representation.

Example: The transformation from the Antenna Reference Frame (T_{xx}, T_{yy}) to the Earth Reference Frame (T_{hh}, T_{vh}) assumes a knowledge of Faraday and Geometric rotations.
In dual-pol mode singularities appear in the transformation.
In full-pol mode the noise is higher due to the shorter integration time

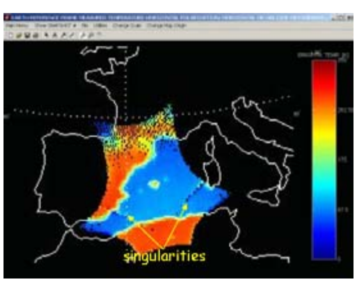

Dual-pol mode

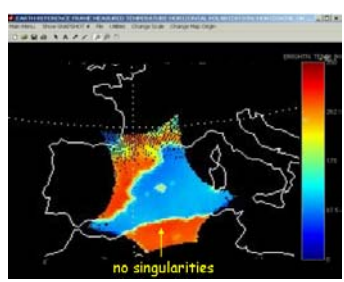

Full-pol mode

3. MIRAS Instrument Performance

3.1. Angular Resolution

$$V(u,v) = \frac{1}{\sqrt{\Omega_1\Omega_2}} \cdot \iint_{\xi^2+\eta^2\le 1} \frac{\left(T_B(\xi,\eta) - T_{ph}\right) F_{n1}(\xi,\eta) F_{n2}^*(\xi,\eta)}{\sqrt{1-\xi^2-\eta^2}} \tilde{r}_{n12}\left(-\frac{u\xi+v\eta}{f_0}\right) e^{-j2\pi(u\xi+v\eta)}\, d\xi\, d\eta$$

• The "ideal" brightness temperature image is formed by an inverse (discrete) Fourier transform of the measured visibility samples ($B = 0$):

$$\hat{T}(\xi,\eta) = \frac{1}{K}\Delta s \sum_m \sum_n W(u_{mn},v_{mn})\, V^0(u_{mn},v_{mn})\, e^{j2\pi(u_{mn}\xi+v_{mn}\eta)} = \iint_{\xi'^2+\eta'^2\le 1} T(\xi',\eta')\, AF^0(\xi-\xi',\eta-\eta')\, d\xi' d\eta'$$

Equivalent Array Factor:
same response as for an array of elements at (u,v) positions (except for the |(.)|²)

$$\Delta s = \frac{\sqrt{3}}{2} d^2$$

$$AF^0(\xi-\xi',\eta-\eta') = \Delta s \sum_m \sum_n W(u_{mn},v_{mn})\, e^{j2\pi(u_{mn}(\xi-\xi')+v_{mn}(\eta-\eta'))}$$

• The retrieved $\hat{T}(\xi,\eta)$ image is the 2D convolution of the original $T(\xi,\eta)$ image with the instrument's impulse response or ***equivalent array factor***:

$$\hat{T}(\xi,\eta) = F_H^{-1}\left[W(u,v) V^0(u,v) \right] = AF^0(\xi,\eta) * T(\xi',\eta')$$

Response with rectangular window Response with Blackmann window (rotational symmetry)

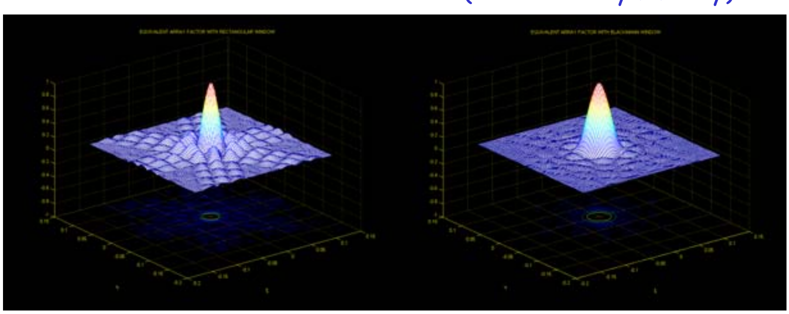

$$\Delta\xi_{-3dB}^{rect} \approx \frac{\pi/2}{\Delta u_{max}}; \quad e \le 10\% \text{ for } \Delta u_{max} \ge 15$$

$$\Delta u_{max} = 2\sqrt{3} N_{EL} d$$

$$MBE \approx 43\%$$

$$\Delta\xi_{-3dB}^{Blackmann} = 1.48\Delta\xi_{-3dB}^{rect}$$

$$MBE \approx 90\%$$

$$T_A' = MBE \cdot T_{main\ lobe} + (1-MBE) \cdot T_{secondary\ lobes}$$

$W(u_{mn},v_{mn})$: window to weight the visibility samples:
• reduces side lobes
• widens main lobe
• increases main beam efficiency (MBE)

• In the case of $B = 0$ the AF is space invariant.

• Fringe-washing effects ($W = B/f_0 \sim 0$) produce a radial smearing of the image of length L :

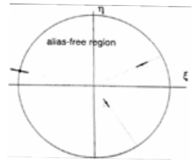

$$L = W\sqrt{\xi^2 + \eta^2}$$

- Peak amplitude decreases
- Response widens
- Total volume under AF remains constant

  $\Rightarrow T_B$ value ct. for homogeneous scenes

• The retrieved $\hat{T}(\xi,\eta)$ image is the 2D convolution of the original $T(\xi,\eta)$ image with the instrument's impulse response or ***equivalent array factor*** $AF(\xi,\xi',\eta,\eta')$ but it is space-variant

$$\hat{T}(\xi,\eta) = F_H^{-1}\left[W(u,v)\,V(u,v)\right] = AF(\xi,\xi',\eta,\eta') * T(\xi',\eta')$$

Position of the maximum

• Instrumental errors produce a negligible degradation of the AF.

If the window used is the same to image the pixels in all directions,
- in the ideal case the width of the AF is constant (right), but
-the projection over the Earth enlarges it due to increased distance and the projection $1/\cos(\theta_i)$. Orientation of ellipse is also changed

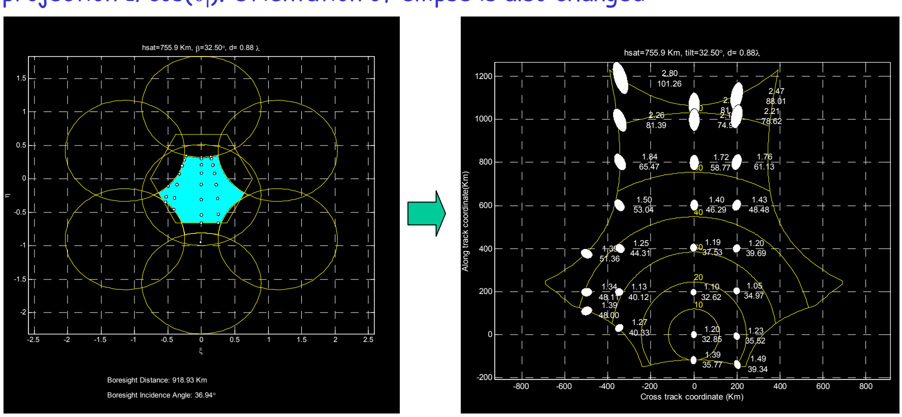

- Pixel axial ratio a/b
- Spatial resolution defined as geometric mean of axes

Windowing of the Visibility Samples

• In many cases the Blackman window is the preferably window function because, despite of a significant widening of the principal lobe, the Blackmann window function produces the best attenuation of the side lobes.

• However, applying the same window for all pixels in the FOV produces a significant distorsion of the pixels shape once projected over the Earth.

• This can be compensated by imaging each pixel with a properly designed window that compensates:

- the radial enlarging (window more "rectangular", and less tapered) and
- the cosine projection (window more "rectangular" in the radial direction and more "tapered" in the perperdicular" direction

• Windows can be designed for any specific "constant" spatial resolution on Earth

⇒ This is called "strip adaptive" processing:

Not worth to use IHFFTs, but to apply a IHDFT to each pixel.

Adaptive window to compensate pixels' distorsion pixels are more "circular":

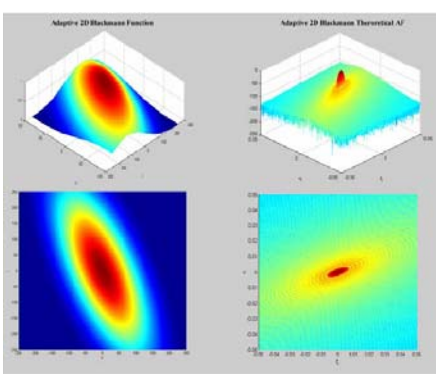

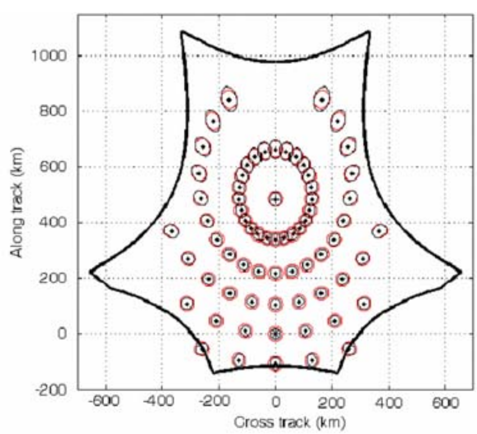

Resulting pixels:

The higher the spatial resolution the lower the resulting efficiency, up to a point where it is useless

Efficiency of an adaptive Blackmann function for circular pixels of 50 km.

ID	ξ	η	$\sqrt{a \cdot b}\,(km)$	a/b	$2E_1/\Delta\zeta_{-3dB}$	$2E_2/\Delta\zeta_{-3dB}$	δ(deg)	Eff	$Eff/Eff_{Blackmann}$
1	+0.00	-0.54	32.38	1.20	1.53490633	1.22050588	0.00	0.8786	1.0600
2	+0.31	-0.51	36.20	1.24	1.30608439	1.25623300	77.80	0.8682	1.0475
3	-0.12	-0.61	34.56	1.32	1.52109277	1.22081945	-25.55	0.8781	1.0594
4	-0.38	-0.28	38.67	1.10	1.16991005	1.25388626	-16.52	0.8598	1.0373
5	+0.00	-0.10	36.51	1.18	1.38470540	1.19006734	0.00	0.8681	1.0473
6	-0.40	-0.04	45.00	1.27	0.98094982	0.95561598	84.38	0.8226	0.9924
7	+0.29	+0.13	56.05	1.61	0.95317709	0.71324803	-47.36	0.7975	0.9621
8	-0.18	+0.21	61.06	1.78	0.96558678	0.60227971	26.68	0.7862	0.9485
9	+0.62	-0.22	58.46	1.62	0.65263750	0.98347758	20.52	0.7940	0.9579
10	+0.20	+0.29	77.62	2.20	0.81519902	0.43091755	-27.03	0.7372	0.8894
11	-0.24	+0.34	96.39	2.69	0.66368510	0.31253072	30.61	0.6768	0.8165

3.2. Radiometric Performance: definition of terms

Error maps: $\Delta T_B(\xi,\eta,t)$			
Random errors (noise due to finite integration time)	**Temporal average**	Zero	0
	Temporal standard deviation	**Radiometric sensitivity**	$\Delta T_{sensitivity} \approx \sqrt{\frac{\sum_{i=1}^{M}\left(\hat{T}_B(\xi,\eta,t_i)-\left\langle \hat{T}_B(\xi,\eta,t)\right\rangle_t\right)^2}{M-1}}$
Systematic errors (instrumental errors)	**Spatial average**	**Radiometric bias** (scene bias)	$\Delta T_{bias} = \frac{1}{N}\sum_{i=1}^{N}\left(\left\langle \hat{T}_B(\xi_i,\eta_i,t)\right\rangle_t - T_B(\xi_i,\eta_i)\right)$
	Spatial standard deviation	**Radiometric accuracy** (pixel bias)	$\Delta T_{accuracy} \approx \sqrt{\frac{\sum_{i=1}^{N}\left(\left\langle \hat{T}_B(\xi_i,\eta_i,t)\right\rangle_t - T_B(\xi_i,\eta_i)\right)^2}{N-1}}$

3.2.1. Radiometric Sensitivity:

Smallest variation in brightness temperature that can be measured by the instrument. It is related to the random noise introduced by instrument elements.

Analytic signals at elements output:

$$b_1(t) = [s_{i1}(t) + n_{i1}(t)]\cos(\omega_0 t) + [s_{q1}(t) + n_{q1}(t)]\sin(\omega_0 t)$$
$$b_2(t) = [s_{i2}(t) + n_{i2}(t)]\cos(\omega_0 t) + [s_{q2}(t) + n_{q2}(t)]\sin(\omega_0 t)$$

In-phase and quadrature signals at elements output:

$$i_1 = b_1(t)\cos(\omega_{LO} t) = \frac{1}{2}[s_{i1}(t) + n_{i1}(t)]\cos(\Delta\omega t) + \frac{1}{2}[s_{q1}(t) + n_{q1}(t)]\sin(\Delta\omega t)$$
$$q_1 = b_1(t)\sin(\omega_{LO} t) = -\frac{1}{2}[s_{i1}(t) + n_{i1}(t)]\sin(\Delta\omega t) + \frac{1}{2}[s_{q1}(t) + n_{q1}(t)]\cos(\Delta\omega t)$$
$$i_2 = b_2(t)\cos(\omega_{LO} t) = \frac{1}{2}[s_{i2}(t) + n_{i2}(t)]\cos(\Delta\omega t) + \frac{1}{2}[s_{q2}(t) + n_{q2}(t)]\sin(\Delta\omega t)$$
$$q_2 = b_2(t)\sin(\omega_{LO} t) = -\frac{1}{2}[s_{i2}(t) + n_{i2}(t)]\sin(\Delta\omega t) + \frac{1}{2}[s_{q2}(t) + n_{q2}(t)]\cos(\Delta\omega t)$$
$$\Delta\omega = \omega_0 - \omega_{LO}$$

Mean and standard deviation at correlator's output:

(assuming Gaussian receivers' frequency response)

$$\boxed{V_r(u,v) = E_\tau[p_r(t)] = E_\tau[i_1(t) i_2(t)]}$$
$$\boxed{\sigma_{p_r}^2 = \frac{1}{2\sqrt{2}B\tau}\left[(T_A + T_R)^2\left(1 + e^{-\pi\left(\frac{2\Delta f}{\sqrt{2}B}\right)^2}\right) + V_r^2(u,v)\left(1 + e^{-\pi\left(\frac{2\Delta f}{\sqrt{2}B}\right)^2}\right) - V_i^2(u,v)\left(1 - e^{-\pi\left(\frac{2\Delta f}{\sqrt{2}B}\right)^2}\right)\right]}$$

$$\boxed{V_i(u,v) = E_\tau[p_i(t)] = E_\tau[q_1(t) i_2(t)]}$$
$$\boxed{\sigma_{p_i}^2 = \frac{1}{2\sqrt{2}B\tau}\left[(T_A + T_R)^2\left(1 + e^{-\pi\left(\frac{2\Delta f}{\sqrt{2}B}\right)^2}\right) + V_i^2(u,v)\left(1 + e^{-\pi\left(\frac{2\Delta f}{\sqrt{2}B}\right)^2}\right) - V_r^2(u,v)\left(1 - e^{-\pi\left(\frac{2\Delta f}{\sqrt{2}B}\right)^2}\right)\right]}$$

Radiometric sensitivity in synthetic T_B images:

$$\Delta T(\xi,\eta) = \Omega_{ant}\left(\frac{\sqrt{3}}{2}d^2\right)\sum_m \sum_n W(u_{mn},v_{mn})\left[\Delta V_r(u_{mn},v_{mn}) + j\Delta V_i(u_{mn},v_{mn})\right] e^{j2\pi(u_{mn}\xi+v_{mn}\eta)}$$

Further considerations:

- Errors in the visibility samples are hermitian:

$$V^*(u,v) = \left\{\frac{1}{2}E\left[b_1(t)b_2^*(t)\right]\right\}^* = \frac{1}{2}E\left[b_2(t)b_1^*(t)\right] = V(-u,-v)$$

- Error correlation is negligible:

$$E\left[\Delta V_{12}(t+t_d)\Delta V_{34}^*(t)\right] = \frac{V_{13}V_{24}^*}{B\tau}\,\mathrm{sinc}\left(\frac{t_d}{\tau}\right)$$

Radiometric sensitivity:

$$\boxed{\Delta T(\xi,\eta) = \Omega_{ant}\left(\frac{\sqrt{3}}{2}d^2\right)\frac{T_A+T_R}{\sqrt{B\tau_{eff}}}\alpha_W\frac{\alpha_{LO}}{\alpha_F}\sqrt{N_V}}$$

N_V : number of (u,v) points

Impact of noise correlation in the radiometric sensitivity in synthetic T_B images:

- The radiometric sensitivity follows "somehow" the T_B image

$T_B(\xi,\eta)$ $\sigma_{TB}(\xi,\eta)\sqrt{(B\cdot\tau)}$

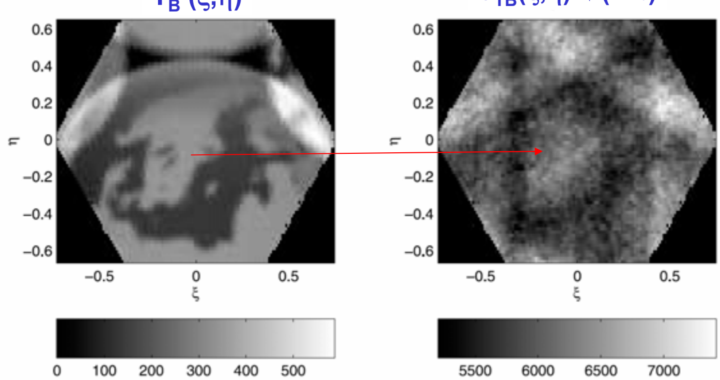

3.2.2. Radiometric bias and accuracy

Need to understand MIRAS' architecture first, error sources, their calibration and the measurements required

A baseline BASICS OF PLM

ELECTRICAL ARCHITECTURE

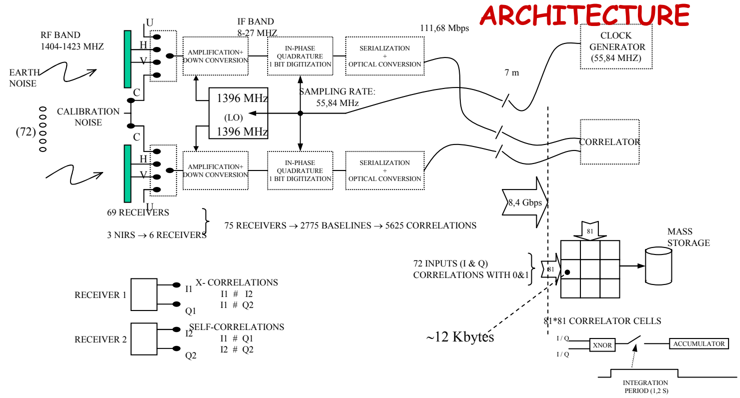

MIRAS : - computes visibility samples from correlations of I/Q signals at IF (close to zero)
- 1 bit/2 level digital correlators are used (easier integration)

Error model:

$$\begin{bmatrix}\mu_{12r}\\ \mu_{12j}\end{bmatrix} = \frac{1}{\sqrt{\langle |b_1|^2\rangle}\sqrt{\langle |b_2|^2\rangle}}\begin{bmatrix}\Re e\\ \Im m\end{bmatrix}\left\{\langle b_1 b_2^*\rangle\right\} = \frac{1}{\sqrt{\langle |b_1|^2\rangle}\sqrt{\langle |b_2|^2\rangle}}\begin{bmatrix}\langle i_1 i_2\rangle\\ \langle q_1 i_2\rangle\end{bmatrix} = g_1 g_2 \begin{bmatrix}\Re e\\ \Im m\end{bmatrix}\{V_{12}\}$$

$$= g_1 g_2 \begin{Bmatrix}\tilde r_{ni_1i_2}(0)\\ \tilde r_{nq_1i_2}(0)\end{Bmatrix}\frac{1}{\sqrt{\Omega_1\Omega_2}}\cdot\left[\begin{matrix}\Re e\\ \Im m\end{matrix}\left\{\iint_{\xi^2+\eta^2\le 1}\frac{\left(T_B(\xi,\eta)-T_{rec}\delta_{pq}\right)F_{n1}(\xi,\eta)F_{n2}^*(\xi,\eta)}{\sqrt{1-\xi^2-\eta^2}}\begin{Bmatrix}\tilde r_{ni_1i_2}(\tau)\\ \tilde r_{nq_1i_2}(\tau)\end{Bmatrix}e^{-j2\pi\left(u_{12}\xi+v_{12}\eta+w_{12}\sqrt{1-\xi^2-\eta^2}\right)}\,d\xi\,d\eta\right\}\right] + \begin{bmatrix}\mu_{12roff}\\ \mu_{12joff}\end{bmatrix}$$

Fringe-washing function at the origin

$$\boxed{\tilde r_{12}(0) = g_{12}e^{j(\theta_1-\theta_2+\theta_{12})}}$$

Separable amplitude errors:

$$\boxed{g_1 = \sqrt{\frac{1}{T_{sys,1}}}\qquad g_2 = \sqrt{\frac{1}{T_{sys,2}}}}$$

System Temperatures

Antenna radiation voltage patterns (errors function of (ξ,η)) and antenna solid angles (cross-polar patterns not included)

Normalized Fringe-washing Function (shape):

$$\boxed{\tilde r_{n12}(\tau) = \frac{\tilde r_{12}(\tau)}{\tilde r_{12}(0)}}$$

$$\boxed{\tau = -\frac{u_{12}\xi + v_{12}\eta + w_{12}\sqrt{1-\xi^2-\eta^2}}{f_0}}$$

Antenna position errors:
$(u_{12}, v_{12}, w_{12}) = (x_2-x_1, y_2-y_1, z_2-z_1)/\lambda$

Offset errors :
- LO leakage
- ADCs errors
- ...

Diferent frequency responses between I and Q channels responsable for fase, quadrature and amplitude errors (separables and not separables).

Error classification and correction techniques:

Error type	Procedure
1) **Offset errors** (μ_{12r} , μ_{12i}):	Uncorrelated noise (1) + 1/0 unbalance
2) **Quadrature errors** (θ_{q1}, θ_{q2}):	Distributed Noise Injection (1)
3) **Non-separable in phase and amplitude errors** (θ_{12}, g_{12})	Centralized Noise Injection (2) (only shortest baselines)
4) **Separable phase errors** (θ_1, θ_2)	Distributed Noise Injection (1)
5) **Separable amplitude errors** (g_1,g_2)	PMS: T_{HOT}/T_{COLD}
6) **Antenna temperature** (T_A)	3 NIRs
7) **Antenna radiation voltage patterns:** $F_{n1,2}(\xi,\eta)$	Anechoic chamber measurements + redundant space calibration(3) + image reconstruction algorithm
8) **Fringe-washing function:** $r_{n1,2}(\xi,\eta)$	Correlation at different time lags (4, 5) (correlated noise injection) + image reconstruction algorithm
9) **Antenna position errors:** ($\Delta u,\Delta v,\Delta w$)	Image reconstruction algorithm

(1) F. Torres, A. Camps, J. Bará, I Corbella, R. Ferrero, "On-board Phase and Modulus Calibration of Large Aperture Synthesis Radiometers: Study Applied to MIRAS," IEEEE Transactions on Geoscience and Remote Sensing, Vol 34, No 5, pp 1000-1009, July 1996
(2) I. Corbella, F. Torres, A. Camps, J. Bará, "A New Calibration Technique for Interferometric Radiometers, " Proceedings of the SPIE, Europto Series, Vol 3498, pp. 359-366, 1998
(3)A. Camps, F. Torres, P. Lopez-Dekker, S. J. Frasier, "Redundant Space Calibration Of Hexagonal And Y-Shaped Beamforming Radars and Interferometric Radiometers", International Journal of Remote Sensing, Vol. 24, pp. 5183-5196, 20 Diciembre 2003
(4) A. Camps, F. Torres, J. Bará, I. Corbella, and F. Monzón, "Automatic Calibration of Channels Frequency Response in Interferometric Radiometers," Electronics Letters, 21st January 1999, Vol 35, No 2, pp. 115-116
(5) R. Butora, M. Martín-Neira, A.L. Rivada-Antich, "Fringe-washing function calibration in aperture synthesis microwave radiometry," Radio Science, Volume 38, Issue 2, pp. 15-1, DOI 10.1029/2002RS002695

RADIOMETRIC ERROR BUDGET: How it is computed (1/2)

- Individual contributions are calculated based on analysis of system.
- Sensitivities calculated by analysis and with instrument simulator (SEPS), assuming IFFT (simplest, algorithm-independent, and worst-case image reconstruction)
- EM and FM measurement data included as available
- Instrument should perform better than EB, depending on ground processing (Flat Target Response and image reconstruction algorithms can improve image quality significantly)

SNAP-SHOT	Param. value (1 s)	Units	Param. sens. to Tph	Units	Sens. to error (K/unit)	Rad. Sens. (random error)	Rad. bias. Scene bias	Rad. Accur. Pixel Bias	Data Source	
T-T0 (T0=25ºC) 2ºC peak orbit temperature drift	0	ºC								
TA	150	K								
TR (NF=2.45 dB)	226	K								
Polarization (X = 1, Y = 0, XY=2)	0									
FUNDAMENTAL LIMITATIONS						2,40	0,00	0,05		
Discretization								0,05	E	
Thermal noise (Dual-Pol. τ=1.2 s; Full-Pol τ=0.8 s)	1,2	s				2,40			M	Measured
ANTENNA ERRORS						0,00	0,00	1,45		
Antenna voltage pattern phase ripple	0,33	deg	0		1,11			0,36	R	
Antenna voltage pattern amplitude ripple	0,57	%	0		0,8			0,45	R	Requirem.
Antenna XP	1,58E-03		0		90			0,14	M	
Switch isolation	1,80E-03		0		90			0,16	M	
Antenna mismatch	0	lin	0		0			0,00	M	
Geometric position uncertainty (x-y)	0,62	mm	0		1,99			1,22	M	
Geometric position uncertainty (z)	0,62	mm	0		0,4			0,24	M	Study
Array arm thermo-elastic deformation:In-plane	0,15	deg	0,015	deg/ºC	0,2			0,03	E	
Array arm thermo-elastic deformations:Off-plane	0,15	deg	0,015	deg/ºC	2			0,30	E	
Hub arm thermo-elastic deformation:In-plane	0,06	deg	0,005	deg/ºC	3,37			0,20	E	
Hub arm thermo-elastic deformation:Off-plane	0,06	deg	0,005	deg/ºC	3,45			0,20	E	
Antenna rotation(3)	5,60E-05		0		90			0,00	E	
Pointing accuracy	0,00E+00		0		0			0,00	E	
Antenna voltage pattern dependency on frequency	0,00E+00		0		0			0,00	E	
Antenna-LICEF XP measured via TRFOP	0		0		0			0,00	E	

RADIOMETRIC ERROR BUDGET: How it is computed (2/2)

AMPLITUDE ERRORS									
NOISE INJECTION RADIOMETER: V(0,0)						**0,19**	**0,49**	**0,00**	
NIR: Sensitivity $2T_{sys}/\sqrt{B\tau}$	0,196	K	0		1	0,19			M
NIR: Bias error	0,00891	K	0,013	K/ºC	1		0,01		M
NIR: Gain error	-0,0033	-	0	/ºC	150		-0,50		M
RECEIVER & BASELINE AMPLITUDE ERRORS	**1,77**	**%**				**0,00**	**0,00**	**0,88**	
Amplitude calibration residual error	0,1	%	0		0,15			0,02	E
NDN Sij relative amplitude	0,037	dB	0		8,1			0,30	M
PMS sensitivity due to thermal noise	0,059	%	0		1,1			0,06	E
Low-frequency PMS random gain fluctuation	0,075	%	0		1,1			0,08	E
PMS linearity error:	0,25	%	0		1,1			0,28	M
Reciever input path Sij relative amplitude	0,01	dB	0		8,1			0,08	R
Antenna losses relative amplitude	0,02	dB	0		8,1			0,16	M
Error in the relative noise injected by CAS	0,67	%	0		0,5			0,34	M
Amplitude error due to mismatch at calibration planes	1,2	%	0		0,5			0,60	M
FWF(0) modulus error on distributed calibration	1,5	%	0		0,21			0,32	E
PHASE ERRORS	**1,47**	**deg**				**0,00**	**0,00**	**0,40**	
In-phase calibration residual error	0,018	deg	0		0,27			0,00	E
NDN Sij relative phase uncertainty	1,27	deg	0		0,27			0,34	M
Receiver input path Sij relative phase uncertainty	0,5	deg	0		0,27			0,14	R
Path antenna plane to antenna geometric center	0,5	deg	0		0,27			0,14	E
Residual quadrature error	0,014	deg	0		0,36			0,01	E
Phase error due to mismatch at calibration planes	0,13	deg	0		0,27			0,04	E
In-band freq dependent quadrature error	0	deg	0		0,025			0,00	E
FWF(0) phase error on distributed calibration	0,15	deg	0		0,38			0,06	E
OTHER SOURCES OF ERROR						**0,00**	**0,00**	**1,02**	
Sampling skew error	0,52	ns	0		0,76			0,40	M
Sampling jitter error	0,03	ns	0		5			0,15	M
Comparators threshold and U-noise injection correction	0,50	cu	0		0,83			0,42	R
SELF-RFI&FLAT TARGET RESPONSE correction	1,00	cu	0		0,83			0,83	R
TOTAL RMS Sum (K)						**2,40**	**0,49**	**2,02**	
TOTAL radiometric sensitivity						2,40			
TOTAL radiometric accuracy [RMS sum of pixel bias&scene bias]								2,08	

(Sample working SMOS error budget: not the final one)

RADIOMETRIC ERROR BUDGET: Current Performances

- Current PLM performances vs Requirements

Radiometric Sensitivity (K)	Req't	X-Pol	Y-Pol
Ocean Salinity (150K) - Boresight	2,5	2,32	2,33
Ocean Salinity (150K) - 32°	4,1	3,80	3,82
Soil Moisture (220K) - Boresight	3,5	2,77	2,77
Soil Moisture (220K) - 32°	5,8	4,54	4,54

- Radiometric Accuracy

Radiometric Accuracy (K)	Req't	X-Pol	Y-Pol
Radiometric Systematic Error (TA=273 K)	3,7	**4,22**	2,46
Measurement Accuracy (TA=298 K)	4,1	**4,59**	2,65

Large disparity between X and Y due to NIR behavior

- Important Flight Model HW measurements still missing: Antenna, Receiver and NIR (NIR EM performance data available soon).

4. MIRAS Instrument Calibration

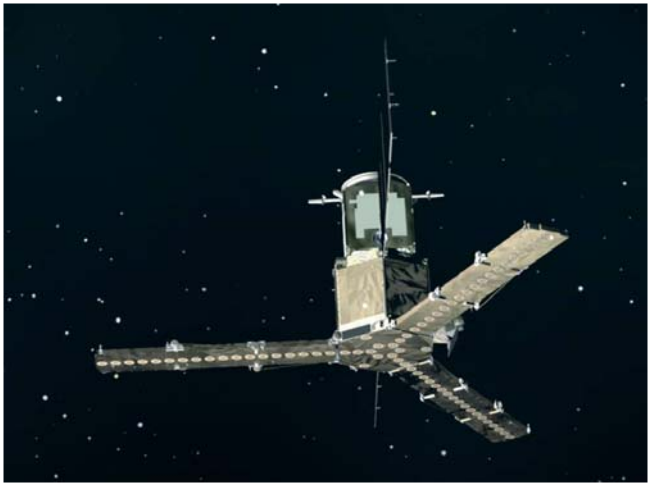

MIRAS consists of a central structure (hub) and 3 deployable arms, each of which has 3 segments.

4.1 MIRAS' Topology

4.1.1. Array topology

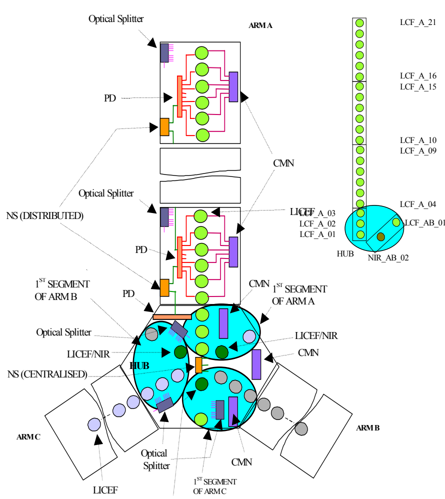

• 69 antenna elements (LICEF)

• Equally distributed over the 3 arms and hub

• The acquired signal is transmitted to a central correlator unit, which computes the complex cross-correlations of all signal pairs.

Unit	In the arms	In the Hub	Total
LICEF	3 x 3 x 6	3 x 4	66
LICEF/NIR	-	3 x 1	3
CMN	3 x 3 x 1	3 x 1	12
CCU	-	1	1
NS (distributed)	3 x 3 x 1	-	9
NS (centralised)	-	1	1
PD (2 to 8)	3 x 3 x 1	3 x 1	12
Optical Splitter (1 to 8)	3 x 3 x 1	3 x 1	12
Optical Splitter (2 to 12)	-	1	1
TRANSMITTERS	-	2	2
FILTERS	-	2	2
X-ANTENNA	-	1	1

4.1.2. Receivers' architecture:

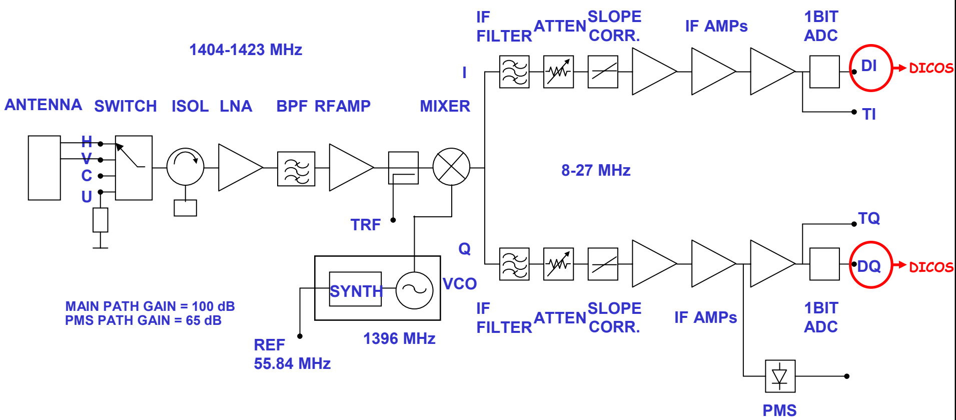

4.1.3. NIR architecture

The Noise Injection Radiometer (NIR) is fully polarimetric and operates at 1.4 GHz

3 NIRs in the hub for redundancy.

Functions:

- precise measurement of $V_{pq}(0,0) = T_{Apq}$ for mean value of $T_{Bpq}(\xi,\eta)$ image.
- measurement of noise temperature level of the reference noise source of Calibration Subsystem (CAS) → absolute amplitude reference

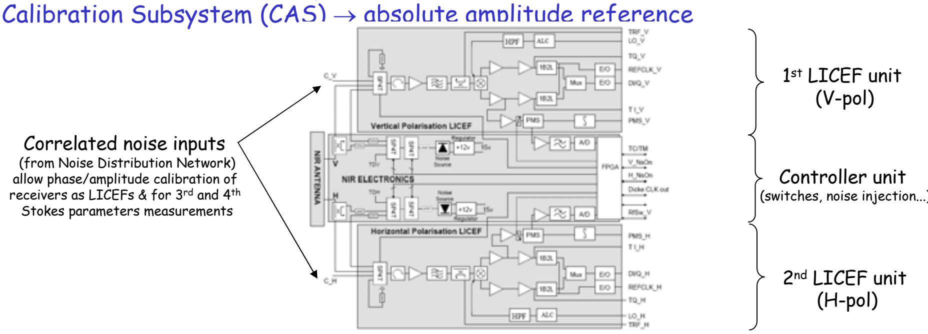

Modes of operation:

NIR-A mode: Measuring antenna temperature

$$T_U = \eta\,(T_A + T_{NA}) + (1-\eta)\,T_A \quad\Rightarrow\quad \boxed{T_A = T_U - \eta\, T_{NA}}$$

Calibration using sky look (T_{A0}): $T_{NA} = \dfrac{T_U - T_{A0}}{\eta_0}$

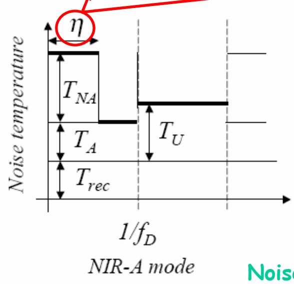

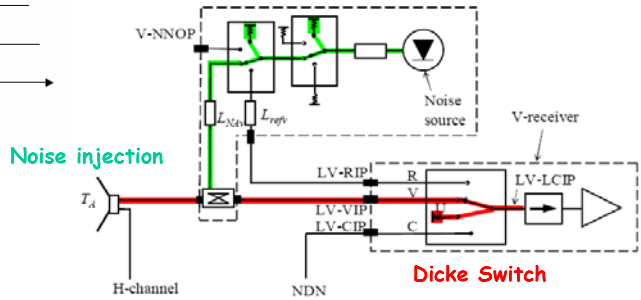

NIR-R mode: Measuring CAS temperature

$$T_{NDN} = \eta\,(T_{ref} + T_{NR}) + (1-\eta)\,T_{ref} \quad\Rightarrow\quad \boxed{T_{NDN} = T_{ref} + \eta\, T_{NR}}$$

Calibration using sky look (T_{A0}) in NIR-AR mode (next slide)

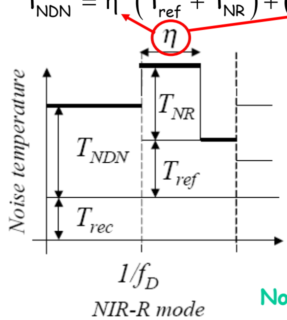

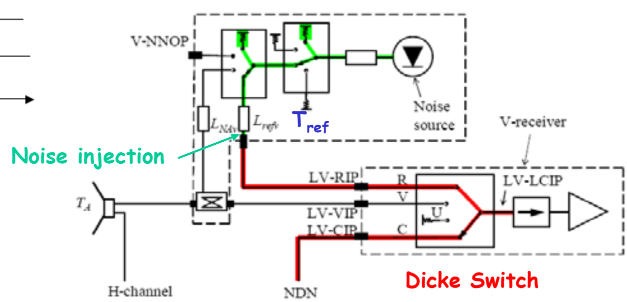

NIR-AR mode & cold sky: Calibrating NIR-R mode

$$T_{NA} + T_{A0} = \eta\ (T_{ref} + T_{NR}) + (1-\eta)\ T_{ref}$$

$$\boxed{T_{NR} = \frac{T_{NA} + T_{A0} - T_{ref}}{\eta}}$$

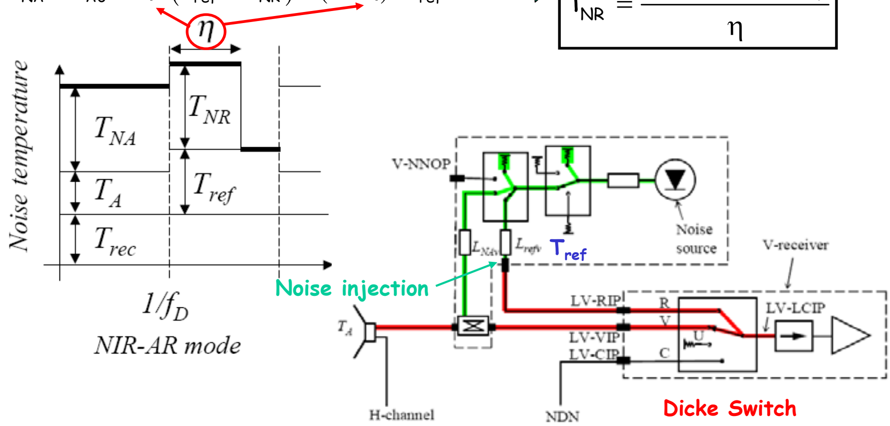

4.1.4. DIgital COrrelator System (DICOS)

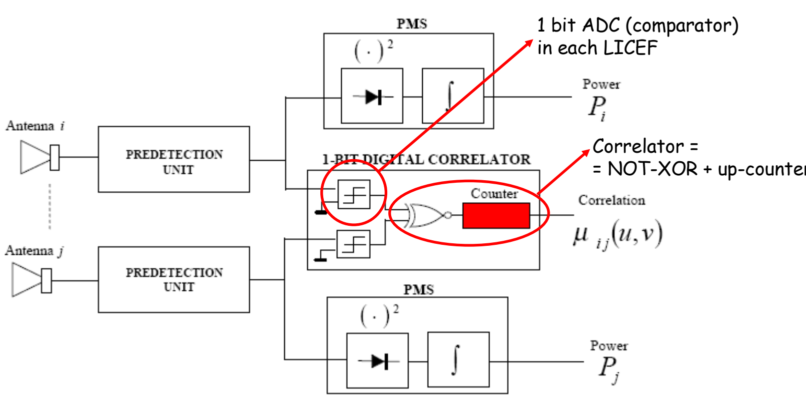

Digital signals from each LICEF are transmitted to DICOS to compute the complex cross-correlations of all signal pairs.

• Lower half: II-correlations: $N_r, N_c \rightarrow Z_r \rightarrow \mu_r \rightarrow V_r$

• Upper half: IQ-correlations: $N_i, N_c \rightarrow Z_i \rightarrow \mu_i \rightarrow V_i$

• Diagonal: IQ-correlations of same element (θ_q: quadrature errors)

• Correlations of I and Q signals with 0's and 1's to compensate comparators' threshold errors

• Correlations of 0's and 0's and 1's and 1's = N_{cmax}

• N_{Cmax} = 65437 for dual-pol mode (= $f_{CLK} \cdot \tau_{int}$)

N_{Cmax} = 43625 for full-pol mode

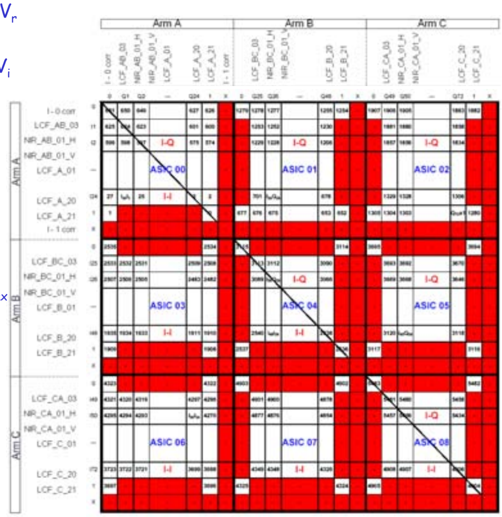

• Total number of products:
  - •2556 correlations Ik-Ij
  - •2556 correlations Ik-Qj
  - •72 correlations Ik-Qk
  - •72 correlations I-0
  - •72 correlations Q-0
  - •72 correlations I-1
  - •48 correlations Q-1
  - •36 control correlations between 1 and 0 channels (4 for each ASIC)

4.1.5. CAlibration System (CAS)

Noise sources needed to calibrate the instrument.

HUB ARMS

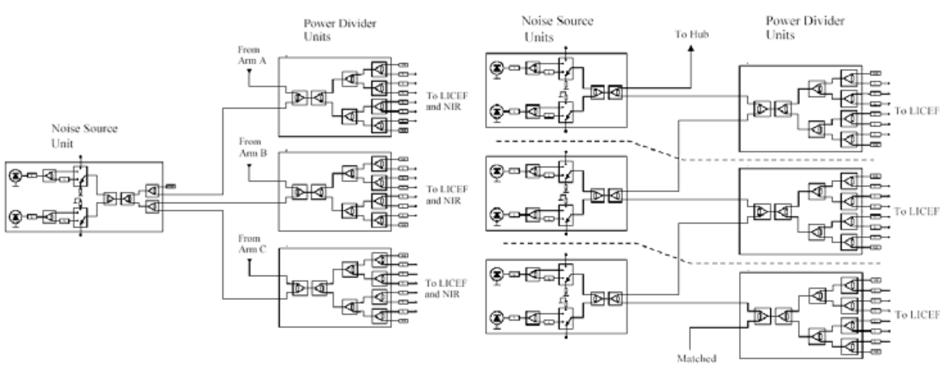

4.1.6. Power Measurement System (PMS)

- Acts as a total Power Radiometer in each LICEF
- Needed to denormalize the "normalized" correlations (1 bit/2 level)

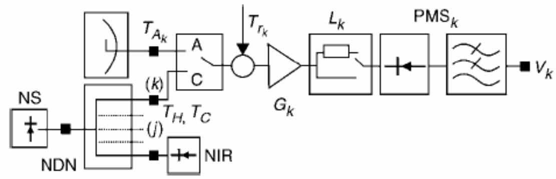

4.2. MIRAS calibration

Main differences between the calibration of an standard radiometer (real aperture) and an interferometric radiometric such as MIRAS

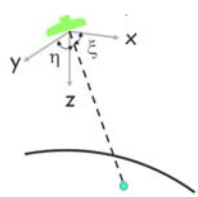

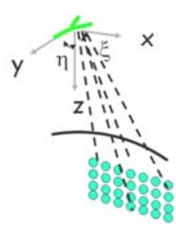

A **real aperture radiometer** requires only an external absolute calibration (gain and offset correction): T_{hot} & T_{cold}

A **synthetic aperture interferometric radiometer** requires:
- an internal relative error correction of each visibility sample (prevent image aberration) +
- an external absolute calibration (gain and offset correction: equivalent to "brightness" and "contrast" adjustment)

An **interferometric radiometer** is **calibrated** by a **two-step procedure:**

1. **Relative internal instrument error correction:**
   To prevent image aberration.
   Applied to each visibility sample, prior to image inversion.
   Based on instrument error model + correlated/uncorrelated + hot/warm measurements through CAS

2. **Absolute external calibration.**
   Same stage as for a real aperture radiometer.

MIRAS: steps 1 and 2 are mixed, and also involves image reconstruction.

Calibration is understood as the algorithm to retrieve $\widehat{V}_{kj}$ from the instrument measurement output

Calibration Concept: Brief sketch

- Items that need calibration:
  - NIR Gain and Offset
  - PMS gain and offset (receiver and baseline amplitude errors)
  - Fringe-washing function FWF (amplitude and phase errors)
  - Noise that is injected to receivers during calibration
  - Correlator Offsets
- Types of Calibration:
  - Internal: injection of correlated or uncorrelated noise to the receivers
  - External: observation of known target:
    - NIR absolute calibration
    - Flat-Target Transformation: to calibrate antenna pattern errors
  - CAS Calibration: performed by NIR during internal calibration
  - Correlator Calibration: injecting known signals

IN-ORBIT CALIBRATION HEADLINES

Cal Modes	Type	Description and objectives

Deep Sky view	External	• NIR absolute calibration:
		  ○ Antenna branch injected noise
		  ○ Reference branch injected noise
		• Deep sky imaging: FLAT TARGET RESPONSE (Corbella Offset correction)
		• Current baseline two calibrations per month.

Moon Pointing	External	• Antenna relative phase validation/correction • Commissioning phase and validation activitites
Long Calibration	Internal	• U-noise injection (internal correlated noise correction) • C-noise injection (FWF shape) • C-noise injection (part of the orbit) Monitoring parameter temperature drift

Short Calibration	Internal	• C-noise injection:
		  ○ PMS calibration
		  ○ FWF at the origin

Selfcalibration	Internal	• Calculation of normalized complex correlations:
		  ○ Sampler offset correction (1-0 correction)
		  ○ Quadrature correction

4.2.1. MIRAS internal calibration

Instrumental errors correction: set of measurements and mathematical relations to remove instrumental errors → INTERNAL INSTRUMENT CALIBRATION

Error model

• Characterizes the instrument behavior **independently** of the input signal.
• It can be characterized by suitable internal known signals injected at its input: correlated/uncorrelated and hot/cold noise injection.

Basic measurements = visibility samples = complex cross-correlation of the signals $b_k(t)$ and $b_j(t)$ collected by each pair of channels (antennas + receivers)

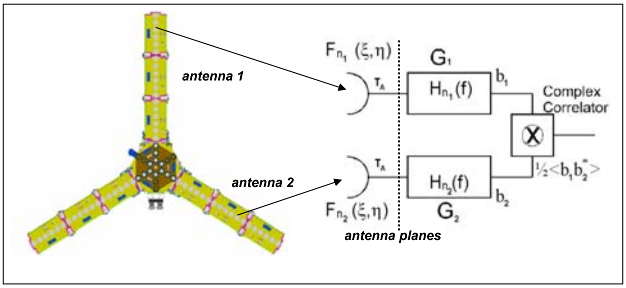

$$V_{kj}(u,v) = \frac{E\left[b_k(t)b_j^*(t)\right]}{2k\sqrt{B_k B_j}\sqrt{G_k G_j}}$$

- G_k and G_j: available power gains of the chains,
- B_k and B_j: equivalent noise bandwidths.

Visibility samples: dimensions of Kelvin

Instrument outputs

1. The **outputs of the instrument** to start the calibration procedure are:
   - Correlator (DICOS) counts N_c: I_k-I_j, Q_k-I_j, Q_k-I_k, I_k-1, Q_k-1, I_k-0, Q_k-0
   - PMS voltages (V_k)
   - NIR output (T_N)

2. The **required ancillary data** are:
   - S-parameters of the noise distribution network (NDN) relative to the NIR path
   - Antenna efficiency
   - S-parameters of the receiver's input switch relative to the CL path

Parameters characterized by ground measurements

LICEF switch S-parameters	
Symbol	S_{LCk}, S_{LHk}, S_{LVk}
Units	Module: dB Phase: deg
Procedure	Ground measurements between CIP_k, HIP_k and VIP_k to $TRFOP_k$ respectively. Measurements performed prior to antenna assembling.
Measurement accuracy	Applies to relative measurements $\frac{S_{LCk}}{S_{LVk}}, \frac{S_{LCk}}{S_{LHk}}$ Relative module: 0.15 dB (3 sigma) Relative phase: 1.5 deg (3 sigma)
Comments	Used to perform calibration plane translation from CIP_k to VIP_k and HIP_k.
Sensitivity of PMS gain to T_{ph}	
Symbol	$S_{G_{PMSk}}^{\Delta T_{ph}}$
Units	%/°C
Procedure	Ground characterization of PMS_k vs temperature. Actualized during commissioning phase and dedicated orbits.
Measurement accuracy	TBD after EM tests
Comments	Used to correct the effect of temperature drift in-between PMS calibrations

Sensitivity of PMS offset to T_{ph}	
Symbol	$S_{V_{offk}}^{\Delta T_{ph}}$
Units	mV/°C
Procedure	Ground characterization of PMS_k vs temperature. Actualized during commissioning phase and dedicated orbits.
Measurement accuracy	TBD after EM tests
Comments	Used to correct the effect of temperature drift in-between PMS calibrations
PMS linearity term	
Symbol	A
Units	mV/K²
Procedure	Deflection method
Measurement accuracy	±10% peak-to-peak deviation in the operational temperature range
Comments	Used to correct 2nd order PMSk response $v_k = v_{offk} + G_k T_{sys} + a_k T_{sys}^2$

CAS S-parameters	
Symbol	S_{k0}
Units	Module: dB Phase: deg
Procedure	Ground measurements between port "0" (nominal and redundant Noise Sources in NS4 positions) and CIP_k. ***Any cable used to connect the output of the NDN to the CIPk connector at LICEF is part of the NDN itself and must be included in the S-parameters measurements.***
Measurement accuracy	Applies to relative measurements: $\frac{S_{k0}}{S_{r0}}$, where port "*r*" is the reference branch. Relative module: 0.045 dB (3 sigma) Relative phase: 1.5 deg (3 sigma) Measurement accuracy must be achieved in all temperature operation range.
Comments	Used to perform: ♦ Amplitude calibration: plane translation from CIP_r (reference port) to CIP_k (LICEF "*k*" port) ♦ Phase calibration: CAS phase correction (C-Noise injection).

Antenna on-ground measurements

Normalized phase and amplitude antenna patterns CO and X	
Symbol	$F_n(\xi,\eta)$
Units	Module: dB Phase: deg
Procedure	Antenna patterns measurements relative to boresight at TUD.
Measurement accuracy	According to antenna errors specification in [2]
Comments	Used in the image reconstruction algorithms
Antenna ohmic efficiency at H and V polarizations	
Symbol	$\eta_H,\ \eta_V \qquad \eta < 1$
Units	Linear magnitude
Procedure	Relative amplitude by estimation of antenna ohmic efficiency dispersion relative to its mean value. Performed by CASA-EADS.
Measurement accuracy	0.15 dB (3 sigma) [[i]].
Comments	Accuracy corresponds to parameter dispersion due to mechanical tolerances. Used to translate the amplitude of calibrated visibilities from VIP_k/HIP_k planes to VAP_k/HAP_k planes. Assumed to be constant in temperature

[i]Antenna efficiency 08.06.04 Quiterio García. CASA

Antenna pattern absolute phase (during Image Validation Test at ESTEC facilities)	
Symbol	ϕ_H, ϕ_V
Units	Deg
Procedure	Measured during IVT test at ESTEC
Measurement accuracy	3/√2 deg (3 sigma)
Comments	Used to translate the phase of calibrated visibilities from VIP_k/HIP_k planes to VAP_k/HAP_k planes. Assumed to be constant in temperature

Instrumental Error Correction:

Correlator offset correction

• Correlation counts N_c provided by DICOS for each pair of receiver outputs converted to digital correlation, using:

$$Z = 2\frac{N_c}{N_{c_{MAX}}} - 1$$

N_c: correlation counts: is an integer ranging from 0 to $N_{c\,MAX}$

$N_{c\,MAX}$: the maximum number of counts (function of the sliding window and the integration time used

Z: digital correlation, a real number ranging from -1 to +1

$$N_{c_{MAX}} = 2^{N_b} - 1$$

N_b: the number of bits of the readout from the accumulator

Normalized correlation of the corresponding analog Gaussian signals related to the digital correlation of the clipped signals by the known relation [Hagen & Farley, 1973]:

$$\mu = \sin\left(\frac{\pi}{2}Z\right) \Longrightarrow$$ only valid for comparators having zero offset

The digital correlation Z, when samplers threshold is present is related to the analog normalized correlation μ by:

$$Z = \frac{2}{\pi}\arcsin\mu - \frac{2}{\sqrt{1-\mu^2}}\left(\mu X_{01}^2 + \mu Y_{01}^2 - 2X_{01}Y_{01}\right)$$

X_{01} and Y_{01} are parameters computed from the measured digital correlations of each signal with all ones (Z_1) and all zeroes (Z_0)

No linear equation

Iterative method with initial guess: $\mu = \sin\left(\frac{\pi}{2}Z\right)$

$$\left.\begin{matrix} X_{01} \\ Y_{01} \end{matrix}\right\} = \frac{1}{4}(Z_0 - Z_1)$$

μ is also a real number ranging from -1 to +1

Visibility denormalization and corrected visibility

Normalized cross-correlation between the receiver output signals is:

$$\mu_{kj} = \mu_{kj}^{ii} + j\,\mu_{kj}^{qi}$$ which can be written as

$$\mu_{kj} = \frac{1}{\sqrt{T_{sys_k}T_{sys_j}}}\left(\mathrm{Re}\left[\tilde{r}_{kj}^{ii}(0)\hat{V}_{kj}\right] + j\,\mathrm{Im}\left[\tilde{r}_{kj}^{qi}(0)\hat{V}_{kj}\right]\right)$$

$\tilde{r}_{kj}^{\alpha\beta}(0)$ is the fringe washing function at the origin for the corresponding pair of filters indicated by the sub-superscripts, the system temperatures of the denominator are given by:

$$T_{sys} = T_a + T_r$$

$\hat{V}_{kj}$ is the ***corrected* visibility** (receiver *k* at *p*-pol and receiver *j* at *q*-pol) which, assuming both receivers at the same physical temperature T_{ph}, is given by

$$\hat{V}_{kj}^{pq} = \iint_{\xi^2+\eta^2\leq 1} \frac{T_B(\xi,\eta)-\delta_{pq}T_{ph}}{\sqrt{1-\xi^2-\eta^2}} \cdot \frac{F_{n_k}(\xi,\eta)}{\sqrt{\Omega_{a_k}}} \cdot \frac{F_{n_j}(\xi,\eta)}{\sqrt{\Omega_{a_j}}} \cdot \bar{\tilde{r}}_{kj}\left(-\frac{u\xi+v\eta}{f_0}\right) \cdot e^{-j2\pi(u\xi+v\eta)} d\xi d\eta$$

where the bar over the fringe washing function means normalized to unity at the origin, that is:

$$\bar{\tilde{r}}_{kj}(t) = \frac{\tilde{r}_{kj}^{\alpha\beta}(t)}{\tilde{r}_{kj}^{\alpha\beta}(0)}$$

is assumed to be the same for all superscript combinations (switch positions)

Fringe-washing function:

$$\bar{\tilde{r}}_{kj}(t) = \frac{\tilde{r}_{kj}^{\alpha\beta}(t)}{\tilde{r}_{kj}^{\alpha\beta}(0)}$$

The fringe-washing function at the origin carries the information of the in-phase and quadrature errors, as well as the non-separable amplitude and phase errors.

For a given baseline (*kj*) the two fringe washing functions of the (*ii*) and (*qi*) signals can be written approximately as:

$$\left.\begin{aligned} \tilde{r}_{kj}^{ii}(0) &= g_{kj} e^{-j\left(\alpha_{kj}+Q_{kj}\right)} \\ \tilde{r}_{kj}^{qi}(0) &= g_{kj} e^{-j\left(\alpha_{kj}+Q'_{kj}\right)} \end{aligned}\right\}$$

g_{kj} amplitude of FWF at the origin,
α_{kj} includes the in-phase and non-separable phase error,

$$\alpha_{kj} = \theta_{0j} - \theta_{0k} - \theta_{kj}$$

Q_{kj} and Q'_{kj} depend on the quadrature error

$$Q_{kj} = \frac{\theta_{qj}}{2} - \frac{\theta_{qk}}{2} \qquad Q'_{kj} = \frac{\theta_{qj}}{2} + \frac{\theta_{qk}}{2}$$

$$\tilde{r}_{kj}^{ii}(0) = g_{kj} e^{-j(\alpha_{kj}+Q_{kj})} \qquad \tilde{r}_{kj}^{qi}(0) = g_{kj} e^{-j(\alpha_{kj}+Q'_{kj})}$$

$$\mu_{kj} = \frac{1}{\sqrt{T_{sys_k} T_{sys_j}}} \left(\mathrm{Re}\left[\tilde{r}_{kj}^{ii}(0) \hat{V}_{kj} \right] + j\,\mathrm{Im}\left[\tilde{r}_{kj}^{qi}(0) \hat{V}_{kj} \right] \right)$$

Defining:

$$\begin{cases} M_1 = \cos Q'_{kj} + j \sin Q_{kj} \\ M_2 = \cos Q_{kj} + j \sin Q'_{kj} \end{cases}$$

Then:

$$\boxed{\hat{V}_{kj} = \underbrace{\sqrt{T_{sys_k} T_{sys_j}} \frac{1}{g_{kj}}}_{\text{Amplitude calibration}} \underbrace{e^{j\alpha_{kj}}}_{\text{Phase calibration}} \underbrace{\frac{1}{\cos \theta_{qk}} \left(\mathrm{Re}\left[M_1 \mu_{kj} \right] + j \,\mathrm{Im}\left[M_2 \mu_{kj} \right] \right)}_{\text{Quadrature corrected normalized correlation}}}$$

Quadrature error:

The quadrature error of a receiver θ_{qk} is directly estimated from the measured normalized cross-correlation between its in-phase and quadrature outputs:

$$\theta_{qk} = -\arcsin\left(\mu_{kk}^{qi} \right)$$

Real-time correction while the instrument is measuring a scene or the injected signal used for amplitude and phase calibration.

$$\boxed{M_{kj} = \frac{1}{\cos \theta_{qk}} \left(\mathrm{Re}\left[M_1 \mu_{kj} \right] + j\,\mathrm{Im}\left[M_2 \mu_{kj} \right] \right)}$$

System Temperatures

For H,V and U positions the needed system temperature at H and V planes are computed from the ones at C plane by a simple plane translation

WARM (TS1) and the HOT (TS2) temperatures synthesized by common external noise source and injected at port "0" of the NDN to be distributed to each LICEF.

Equivalent external temperatures at the calibration plane of the LICEF units (ports "*k*" and "*j*" of the NDN) are TCS2k, TCS2j, TCS1k and TCS1j

Temperatures measured by the NIR: *TNS1* and *TNS2* (port "1" of the NDN) at NIR plane

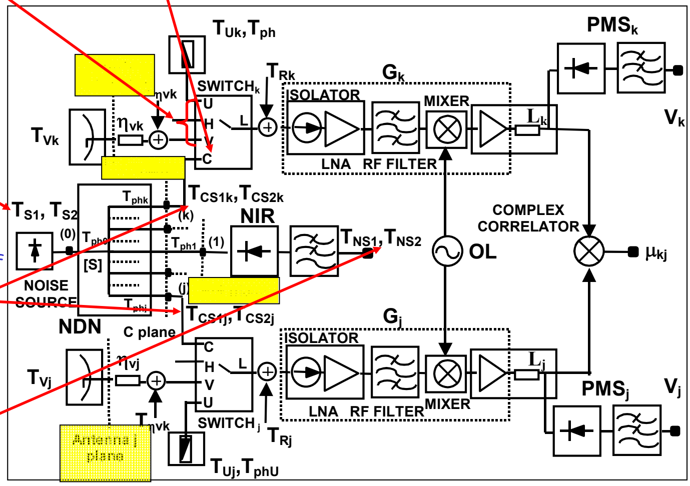

The four-point measurement technique:

- Two known external temperatures *TC1* (warm) and *TC2* (hot).
- Overall system gain switched between G and G/L by means of an attenuator

With or without attenuator

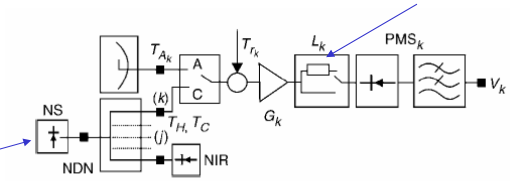

Two noise sources

$V_k = V_{offk} + G_k T_{sys}$ where $T_{sys} = T_{ext} + T_r$

$$T_{sys} = \frac{V - V_{off}}{G}$$

$$\begin{cases} V_{1k} = V_{offk} + G_k^C\, T_{sysC_k}^{WARM}, & V_{3k} = V_{offk} + \dfrac{G_k^C}{L_k} T_{sysC_k}^{WARM} \\ V_{2k} = V_{offk} + G_k^C\, T_{sysC_k}^{HOT}, & V_{4k} = V_{offk} + \dfrac{G_k^C}{L_k} T_{sysC_k}^{HOT} \end{cases}$$

$$\left.\begin{aligned} T_{sysC_k}^{WARM} &= T_{C1} + T_{r_k} \\ T_{sysC_k}^{HOT} &= T_{C2} + T_{r_k} \end{aligned}\right\} \; T_{sysC_k}^{HOT} - T_{sysC_k}^{WARM} = T_{C2} - T_{C1} = \frac{|S_{k0}|^2}{|S_{10}|^2}(T_{N2} - T_{N1})$$

Independent of T_r

The desired parameters can be readily obtained as:

$$G_k = \frac{v_{2k} - v_{1k}}{T_{C2} - T_{C1}} = \frac{v_{2k} - v_{1k}}{T_{N2} - T_{N1}} \cdot \frac{|S_{10}|^2}{|S_{k0}|^2} \quad \Longrightarrow \text{Two known external temperatures}$$

$$v_{offk} = \frac{v_{2k}v_{3k} - v_{1k}v_{4k}}{(v_{2k} - v_{4k}) - (v_{1k} - v_{3k})} \quad \Longrightarrow \text{Direct from PMS measurements}$$

System temperature at C-plane:

$$T_{sys_k}^{C} = \frac{v_K - v_{off}}{G_K} = \frac{v_K - v_{off}}{v_{2k} - v_{1k}} \cdot \frac{|S_{k0}|^2}{|S_{10}|^2}(T_{N2} - T_{N1})$$

System temperature at antenna-plane (used to denormalize μ's):

$$\boxed{T_{sys_k}^{p} = \left(\frac{v_K - v_{off}}{v_{2k} - v_{1k}} \frac{|S_{k0}|^2}{|S_{10}|^2}(T_{N2} - T_{N1})\right)\frac{|S_{LCk}|^2}{|S_{Lpk}|^2 \eta_{pk}}; \qquad p = V- \quad or \quad H-pol}$$

If second order model for the PMS has to be considered:

$$v_k = v_{offk} + G_k T + a_k T^2$$

$\hat{a}_k$ ancillary data is needed to subtract the 2nd order contribution using an estimate of Tsys computed from the linear model:

$$v_{ik}^{(2)} = v_{ik}^{(1)} - \hat{a}_k \left[T_{sysk}^{C(1)}\right]^2$$

Centralized and distributed calibration

Correlated noise is injected to the receivers in two steps: first the "even" sources and then using the "odd" ones

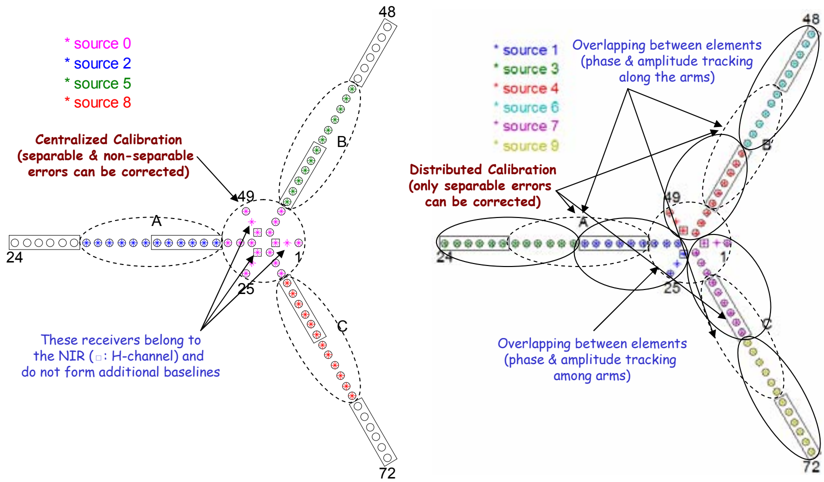

PMS CALIBRATION

Distributed calibration

Considerations: All receivers in the hub and the first and second sections of the arms are driven twice (for even and odd noise sources), while some receivers in the third section are only driven once.

h	ℓ	m	n	ℓ	m	n	ℓ	m	n
HUB	ARM A			ARM B			ARM C		
0	1	2	3	4	5	6	7	8	9
1	1	7	13	25	31	37	49	55	61
2*	2*	8	14	26*	32	38	50*	56	62
3**	3**	9	15	27**	33	39	51**	57	63
4	4	10	16	28	34	40	52	58	64
5	5	11	17	29	35	41	53	59	65
6	6	12	18	30	36	42	54	60	66
25	7	13	19	31	37	43	55	61	67
26*	8	14	20	32	38	44	56	62	68
27**	9	15	21	33	39	45	57	63	69
28	10	16	22	34	40	46	58	64	70
29	11	17	23	35	41	47	59	65	71
30	12	18	24	36	42	48	60	66	72
49									
50*									
51**									
52									
53									
54									

* NIR-LICEF H input ** NIR-LICEF V input

De-normalized visibilities and correlation temperatures

De-normalized quadrature-corrected visibilities computed from quadrature-corrected normalized correlations and system temperatures:

$$V_{kj}^{HH} = \sqrt{T_{sys_k}^{HH} T_{sys_j}^{HH}}\, M_{kj}^{H} \qquad V_{kj}^{UH} = \sqrt{T_{sys_k}^{UH} T_{sys_j}^{UH}}\, M_{kj}^{U}$$

$$V_{kj}^{VV} = \sqrt{T_{sys_k}^{VV} T_{sys_j}^{VV}}\, M_{kj}^{V} \qquad V_{kj}^{UV} = \sqrt{T_{sys_k}^{UV} T_{sys_j}^{UV}}\, M_{kj}^{U}$$

For all baselines sharing a common noise source the *de-normalized correlation temperatures* for both warm and hot states are computed:

$$T_{kj}^{C_1} = \sqrt{T_{sys_k}^{C_1C} T_{sys_j}^{C_1C}}\, M_{kj}^{C_1} \qquad T_{kj}^{C_2} = \sqrt{T_{sys_k}^{C_2C} T_{sys_j}^{C_2C}}\, M_{kj}^{C_2}$$

$\Rightarrow$ phase and amplitude correction factors or fringe washing constants for all receivers connected to a given distribution network

Phase and amplitude (G_{kj}) correction factor

The theoretical correlation when a WARM and HOT temperatures are injected via the NDN is given, respectively by:

$$S_{k0}S_{j0}^{*}(T_{S2}-T_{ph}) = \sqrt{T_{sys_k}^{C_2C} T_{sys_j}^{C_2C}}\, \underbrace{\frac{1}{g_{kj}}}_{G_{kj}^{-1}} \underbrace{e^{j\alpha_{kj}} \frac{1}{\cos\ \theta_{qk}} \left(\mathrm{Re}\left[M_1\, \mu_{kj}^{C_2}\right] + j\ \ \mathrm{Im}\left[M_2\, \mu_{kj}^{C_2}\right]\right)}_{M_{kj}^{C_2}}$$

$$S_{k0}S_{j0}^{*}(T_{S1}-T_{ph}) = \sqrt{T_{sys_k}^{C_1C} T_{sys_j}^{C_1C}}\, \underbrace{\frac{1}{g_{kj}}}_{G_{kj}^{-1}} \underbrace{e^{j\alpha_{kj}} \frac{1}{\cos\ \theta_{qk}} \left(\mathrm{Re}\left[M_1\, \mu_{kj}^{C_1}\right] + j\ \ \mathrm{Im}\left[M_2\, \mu_{kj}^{C_1}\right]\right)}_{M_{kj}^{C_1}}$$

NDN contribution removed by subtracting these two quantities

$$S_{k0}S_{j0}^{*}(T_{S2}-T_{S1}) = G_{kj}^{-1}\left(\sqrt{T_{sys_k}^{C_2C} T_{sys_j}^{C_2C}}\, M_{kj}^{C_2} - \sqrt{T_{sys_k}^{C_1C} T_{sys_j}^{C_1C}}\, M_{kj}^{C_1}\right)$$

G_{kj} Correction factor:

$$G_{kj}^{C} = \frac{\sqrt{T_{sys_k}^{C_2C} T_{sys_j}^{C_2C}}\, M_{kj}^{C_2} - \sqrt{T_{sys_k}^{C_1C} T_{sys_j}^{C_1C}}\, M_{kj}^{C_1}}{S_{k0} S_{j0}^{*} \left(T_{S2} - T_{S1}\right)}$$

System temperatures measured by PMS

$$T_{sys_{k,j}}^{C_1C} = \frac{v_{1k,j} - v_{off}}{v_{2k,j} - v_{1k,j}} \frac{\left|S_{k,j0}\right|^2}{\left|S_{10}\right|^2} \left(T_{N2} - T_{N1}\right)$$

$$T_{sys_{k,j}}^{C_2C} = \frac{v_{2k,j} - v_{off}}{v_{2k,j} - v_{1k,j}} \frac{\left|S_{k,j0}\right|^2}{\left|S_{10}\right|^2} \left(T_{N2} - T_{N1}\right)$$

External sources measured by NIR

$$T_{N_2} - T_{N_1} = \left(T_{S_2} - T_{S_1}\right) \left|S_{10}\right|^2$$

$$G_{kj}^{C} = \frac{M_{kj}^{C2} \sqrt{\left(v_{2k} - v_{offk}\right)\left(v_{2j} - v_{offj}\right)} - M_{kj}^{C1} \sqrt{\left(v_{1k} - v_{offk}\right)\left(v_{1j} - v_{offj}\right)}}{\sqrt{\left(v_{2k} - v_{1k}\right)\left(v_{2j} - v_{1j}\right)}} \frac{\left|S_{k0}\right|\left|S_{j0}\right|}{S_{k0} S_{j0}^{*}}$$

Depends on normalized correlations, PMS linearity and NDN phase unbalance

Translation from CIP to HIP and from HIP to HAP (CIP to VIP and from VIP to VAP)

$$G_{kj}^{p} = G_{kj}^{C} \underbrace{\frac{\bar{S}_{Lpk} \bar{S}_{Lpj}^{*}}{\bar{S}_{LCk} \bar{S}_{LCj}^{*}}}_{\text{CIP to } p\text{IP}} \underbrace{e^{j(\phi_{pk} - \phi_{pj})}}_{p\text{IP to } p\text{AP}}$$

p = V- or H-pol

$\bar{S} = S/|S|$

G_{kj} Correction factor in distributed calibration and residual offset correction

• Baselines formed by receivers not sharing a common noise source: constants computed using a separate approach for the amplitude and for the phase:

- The amplitude assumed to be equal to the average of the previous ones
- The phase is obtained from the following set of equations using a pseudo-inverse:

$$Arg(G_{kj}^{p}) = \theta_k - \theta_j \longrightarrow$$

Applied to all known G_{kj} separately for H and V

$$G_{lm}^{p} = \left|G_{kj}^{p}\right| e^{j(\theta_l^p - \theta_m^p)}$$

• Subtraction of the **visibility offset** measured while injecting uncorrelated noise and dividing by the phase and amplitude correction factor:

$$\hat{V}_{kj}^{p} = \frac{V_{kj}^{pp} - V_{kj}^{Up}}{G_{kj}^{p}}$$

The corrected visibility $\hat{V}_{kj}^{p}$ is the final output of the calibration procedure

Fringe-washing function estimation

• The fringe-washing indicates the decorrelation of the signals from a given direction for a given baseline.

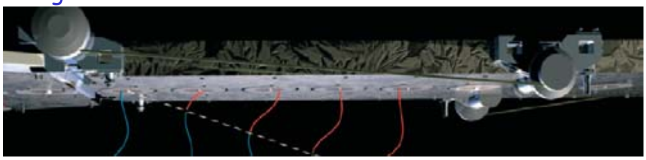

• Relevant for image reconstruction algorithm, since it appears inside the integral to be inverted.

• Not part of the calibration, measured during the centralized noise injection mode by switching DICOS to measure additional correlations at $-T_s$, and $+T_s$ time delays, being T_s the sampling period

• For every hub baseline approximated by a sinc function (amplitude) and a 2nd order polinomial (phase).

• For other baselines a closure relationship proposed by M. Martín-Neira can be used provided the frequency responses are not too different

Shape of FWF: Centralized calibration

Module of FWF is modeled by means of a sinc function:

$$\left|G_{kj}(\tau)\right| \approx A \cdot \mathrm{sinc}(B \cdot (\tau - C))$$

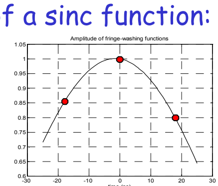

Phase of FWF is modeled by means of a 2nd order function:

$$\Phi_{kj}^{S}(\tau) \approx D^S \cdot \tau^2 + E^S \cdot \tau + F^S$$

$$\bar{G}_{kj}^{C}(-T_s) = \frac{M_{kj}^{C}(-T_s)}{M_{kj}^{C}(0)} e^{-j2\pi f_{IF} T_s}$$

$$\bar{G}_{kj}^{C}(+T_s) = \frac{M_{kj}^{C}(+T_s)}{M_{kj}^{C}(0)} e^{j2\pi f_{IF} T_s}$$

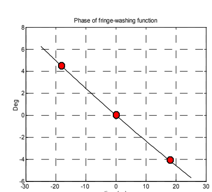

Temperature change from calibration

$$\Delta T_{ph} = T_{phL1k} - T_{phL0k}$$

LICEF Temperature sensor. It is different in H, V modes from U mode.

LICEF temperature during PMS calibration

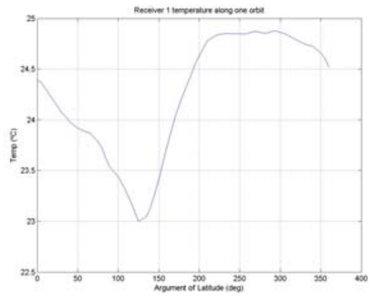

Computation of PMS$_k$ gain and offset at measurement temperature

$$G^{C}_{PMS1_k} = G^{C}_{PMS0_k}\left(1 + S^{G_0}_{T_{ph}}\frac{1}{100}\Delta T_{ph}\right)$$

$$V_{off1_k} = V_{off0_k} + S^{V_{off0}}_{T_{ph}}\Delta T_{ph}$$

4.2.2. MIRAS External Calibration:

- External Calibration used for:
  - NIR absolute Calibration: known cold scene
  - Flat-Target Response: known homogeneous scene
- Perturbations (Sun, Earth through backlobes, attitude mispointing,...) to be minimized during observation (pointing close to zenith, Sun in backlobes)
- One full orbit assigned (TBC)

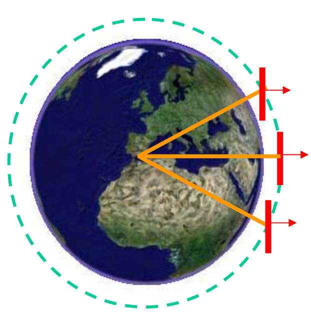

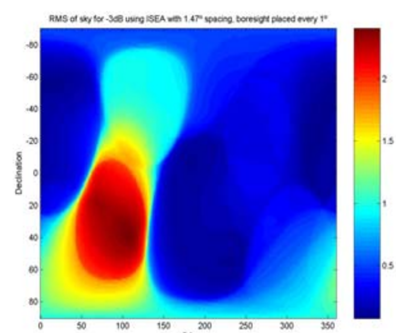

NIR – Amplitude Calibration

- Antenna Brightness Temperature – V(0,0)
- Amplitude of on-board noise diodes – PMS

The PMS readings used to de-normalize the baselines.

2 REFERENCES ARE NEEDED

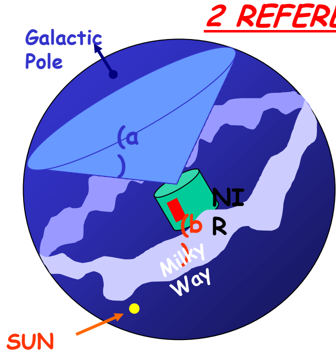

a) The Cold Sky

Inertial pointing of MIRAS to or near the galactic poles.

b) One Matched Load
It is placed in NIR.
Its physical temperature is ambient and is well monitored.

FTT and NIR

The Flat Target Transformation (FTT)

- Transformation of the "Corbella equation" by applying the FTT

- FTT requires imaging of a "Flat Target" to get the instrument "Flat Target Response"

-A "Flat Target":

1.- is completely unpolarised
2.- has the same brightness temperature in any direction
3.- its brightness temperature does not change in time

- The cold sky regions near the galactic poles are good approximations of Flat Targets:

$$T_p^v = T_p^h = 3.5\ K$$

$$T_p^{vh} = T_p^{hv} = 0\ K$$

The Flat Target Response:

-The Flat Target Response is defined by:

$$V_{ij}^{\alpha\alpha,pq}(u,v;1) \equiv \frac{1}{\sqrt{\Omega_i \Omega_j}} \iint_{\xi^2+\eta^2 \le 1} F_{n,i}^{\alpha,p}(\xi,\eta) F_{n,j}^{\alpha,q*}(\xi,\eta) \frac{1}{\sqrt{1-\xi^2-\eta^2}} \tilde{r}_{ij}\left(-\frac{u\xi+v\eta}{f_o}\right) e^{-j\,2\pi(u\xi+v\eta)} d\xi d\eta$$

$$V_{ij}^{pq}(u,v;T_o-T_r) = (T_o-T_r)\ V_{ij}^{\alpha\alpha,pq}(u,v;\ 1)$$

defining:

$$\Delta V_{ij}^{pp}(u,v) \approx \frac{\bar{T}_B^{pp}-T_r}{T_p-T_r}\ V_{ij}^{pp}(u,v\ ;\ T_p-T_r)$$

Then the differential visibilities to be processed are:

$$\breve{V}_{ij}^{pp}(u,v) = V_{ij}^{pp}(u,v) - \Delta V_{ij}^{pp}(u,v)$$

Antenna characterization:

On-ground Characterization: Antenna Test Campaign (DTU) + Image Validation Test (Maxwell)

- Antenna Patterns needed in image reconstruction algorithms.
- Measurement requirements: ±0.05dB and ±0.5°

•Assumed to remain constant during the mission lifetime:

-Some image reconstruction algorithms claim that they can be inferred in orbit from "known" measurements

-On-ground antenna patterns to be validated using bound of Corbella eqn.

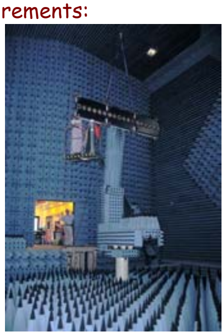

Image Validation Test (Maxwell)

- *Stability tests*
- *Sensitivity circles measurement*
- *Polarization switch control*
- *Phase and Amplitude recovery*
- *ABSOLUTE PHASE BETWEEN ELEMENTS*

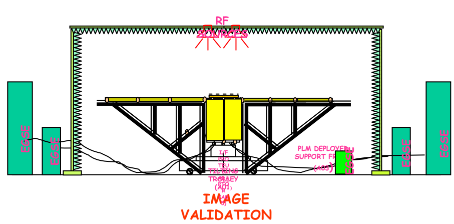

In orbit antenna pattern validation

- Comparison of cold Sky visibilities with model

$$\left|dV_{ij}^{pq}(u,v;1)\right| \le R_F \cdot \frac{1}{2\pi}\left|\iint_{\xi^2+\eta^2\le 1} \frac{\hat{D}(\xi,\eta)}{\sqrt{1-\xi^2-\eta^2}} e^{-j2\pi(u\xi+v\eta)} d\xi d\eta\right|; \quad R_F = 0.5\%$$

$$\hat{D}(\xi,\eta) = \frac{4\pi}{\Omega}\left|\hat{F}_n(\xi,\eta)\right|^2$$

Instrument stability verification

- on-ground stable external targets (Dome-C / antarctica, rainforest…)
- synthetic beam (Sun response? without Sun cancellation algorithm)
- end-to-end verification

4.3. Calibration Timeline

- Two external calibrations per month (Moon observation optional)
- 4 Short Internal Calibrations per 5 orbits:
  PMS gain and FWF(0) calibration.
  Noise at two levels is injected, and also measured by NIR.
  Lasts 16 epochs.
- One Long Internal Calibration per month:
  PMS gain and offset (C-noise: 60 epochs), FWF(0) and FWF shape (30 epochs), and visibility offset (U-noise: 75 epochs).
  Full orbit devoted to it.
- Frequency of calibration depends on drift and thermal behavior, and therefore will be updated during commissioning

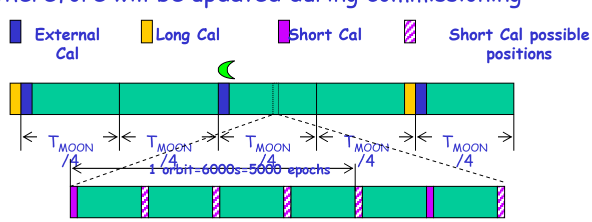

Summary of calibration measurements and requirements:

- Cold Sky as Flat Target

- NIR is used for amplitude calibration

- CAS is used for in-phase and FWF correction

- The U-load and the 0-1 correlations offsets removal

- IQ correlations remove the quadrature error.

- The timeline is in sync with the Moon for verification

- Full calibration orbits provide temperature drifts

- Cold sky views provide NIR calibration and FTR for FTT

- Short calibrations allow to track drifts outside calibrated range

5. Image Reconstruction Algorithms

Real Aperture Radiometer:
1 step calibration

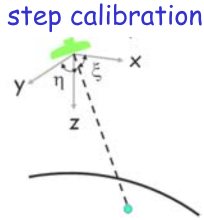

T_B imaging pixel by pixel through antenna scan:

1) Absolute calibration
External references:
T_{hot}, T_{cold}

Aperture Synthesis Radiometer:
2 step calibration

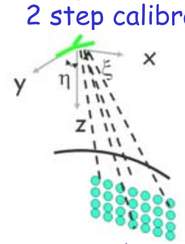

T_B imaging in a single snap-shot
(1 integration time = 1.2 s / polarization in dual-pol):

1) Receivers relative calibration (image "contrast")
- Error model (distorsions, artifacts, blurring…)
- Internal references (Tcorr, Tuncorr,…)

*** Image Reconstruction Algorithm ***

2) Absolute Calibration (image accuracy)
- External references
- T_{hot}/T_{cold}, ground truth, external calibration…

5.1. Image Reconstruction Algorithms: Ideal Situation

Antenna Positions | **Spatial frequencies (u, v)** | **Periodic extension**

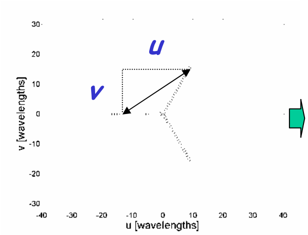

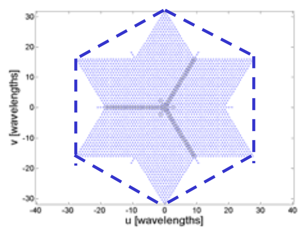

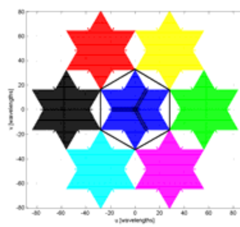

$$\boxed{V(u,v) = \mathcal{F}\left[T(\xi,\eta)\right]}$$

$$\boxed{T(\xi,\eta) = \frac{\left|F_n(\xi,\eta)\right|^2}{\Omega}\frac{T_B(\xi,\eta) - T_{ph\,rec}}{\sqrt{1-\xi^2-\eta^2}}}$$

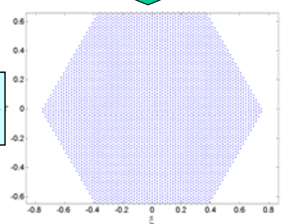

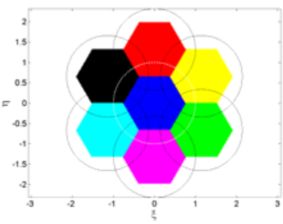

5.2. Image Formation Through a Fourier Synthesis Process

Even in the ideal case:
- Antenna spacing > $\lambda/\sqrt{3}$ ⇒ aliasing
- Gibbs phenomenon near the sharp transitions (mainly alias borders)

In the real case:
- Antenna patterns are different
- Receivers' frequency responses are different (⇒FWF different)
- Antenna positioning errors ⇒ $(u,v,w)_{real}$ different from $(u,v,0)_{ideal}$

⇒ IHFFT cannot be used as image reconstruction method
More sophisticated algorithms must be devised
But it will be good that the second ones tend to IHFFT in ideal conditions

… and obviously instrumental errors must be calibrated first!

5.3. Formulation of the Problem: Instrument Equation After Internal Calibration

$$V_{12}^{pq} = \frac{1}{\sqrt{\Omega_1 \Omega_2}} \iint_{\substack{\xi^2+\eta^2\le 1 \\ fore}} \frac{T_{pq}(\xi,\eta) - T_{rec}\delta_{pq}}{\sqrt{1-\xi^2-\eta^2}} F_{np1}(\xi,\eta) F^*_{np2}(\xi,\eta)\, \tilde{r}_{12}\left(-\frac{u_{12}\xi + v_{12}\eta + w_{12}\sqrt{1-\xi^2-\eta^2}}{f_0}\right)$$
$$\exp\left(-j2\pi\left(u_{12}\xi + v_{12}\eta + w_{12}\sqrt{1-\xi^2-\eta^2}\right)\right) d\xi\, d\eta$$

Includes:

1. "-T_{rec}" (Corbella eqn. term)

2. Fringe-washing function meas
from correlations at different
with correlated noise injected

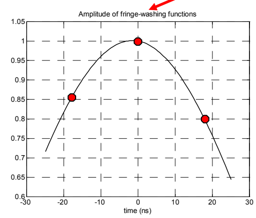

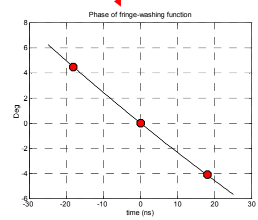

3. Antenna positioning errors (u_{12}, v_{12}, w_{12})

$$V_{12}^{pq} = \frac{1}{\sqrt{\Omega_1 \Omega_2}} \iint_{\xi^2+\eta^2\le 1} \frac{T_{pq}(\xi,\eta) - T_{rec}\delta_{pq}}{\sqrt{1-\xi^2-\eta^2}} F_{np1}(\xi,\eta) F^*_{np2}(\xi,\eta)\, \tilde{r}_{12}\left(-\frac{u_{12}\xi + v_{12}\eta + w_{12}\sqrt{1-\xi^2-\eta^2}}{f_0}\right)$$
$$\exp\left(-j2\pi\left(u_{12}\xi + v_{12}\eta + w_{12}\sqrt{1-\xi^2-\eta^2}\right)\right) d\xi\, d\eta$$

4. Antenna voltage pattern frequency-dependence can be minimized with the following weighted average

$$\frac{1}{4}F_{n1}(\xi,\eta,f_0 - B/2)F^*_{n2}(\xi,\eta,f_0 - B/2) + \frac{1}{2}F_{n1}(\xi,\eta,f_0)F^*_{n2}(\xi,\eta,f_0) + \frac{1}{4}F_{n1}(\xi,\eta,f_0 + B/2)F^*_{n2}(\xi,\eta,f_0 + B/2)$$

5. Extension to the polarimetric case including the co- and cross-polar patterns:

$$\begin{aligned}
\left(T_{xx}(\xi,\eta) - T_{rec}\right)F_{n\,x1}(\xi,\eta)F^*_{n\,x2}(\xi,\eta) &\to R_{x1}R^*_{x2}\left(T_{xx} - T_{rec}\right) + \left(R_{x1}C^*_{x2} + C_{x1}R^*_{x2}\right)T_{yx} + C_{x1}C^*_{x2}\left(T_{yy} - T_{rec}\right),\\
\left(T_{yy}(\xi,\eta) - T_{rec}\right)F_{n\,y1}(\xi,\eta)F^*_{n\,y2}(\xi,\eta) &\to C_{y1}C^*_{y2}\left(T_{xx} - T_{rec}\right) + \left(R_{y1}C^*_{y2} + C_{y1}R^*_{y2}\right)T_{yx} + R_{y1}R^*_{y2}\left(T_{yy} - T_{rec}\right),\\
T_{yx}(\xi,\eta)\,F_{n\,y1}(\xi,\eta)F^*_{n\,x2}(\xi,\eta) &\to C_{y1}R^*_{x2}\left(T_{xx} - T_{rec}\right) + \left(R_{y1}R^*_{x2} + C_{y1}C^*_{x2}\right)T_{yx} + R_{y1}C^*_{x2}\left(T_{yy} - T_{rec}\right),
\end{aligned}$$

5.4. Pre-processing of Visibility Samples:

1.Computation of auxiliary visibilities to extend the AF-FOV to the periodic Earth aliases :

a) Term corresponding to the physical temperature of the receivers (T_{rec}): $V_R^{pq}(u,v)$
Appears as an offset in the visibilities, except in V(0,0), which is measured by the 3 NIRs.

$$V_R^{pq} \triangleq \frac{1}{\sqrt{\Omega_1\Omega_2}} \iint_{\xi^2+\eta^2\le 1} \frac{-T_{rec}}{\sqrt{1-\xi^2-\eta^2}} \hat{F}_{n1}^{p}(\xi,\eta)\hat{F}_{n2}^{q*}(\xi,\eta)\hat{\tilde{r}}_{12}\left(-\frac{u_{12}\xi+v_{12}\eta+w_{12}\sqrt{1-\xi^2-\eta^2}}{f_0}\right)\exp\left(-j2\pi(u_{12}\xi+v_{12}\eta+w_{12}\sqrt{1-\xi^2-\eta^2})\right)d\xi d\eta\,,$$

b) $\bar{T}_A^{pq} = V^{pq}(0,0) = \sum_{\forall m} T_{A\,m,m}^{pq}/3$: weighted average of the 3 NIR measurements

c) Term corresponding to the sky: $V_{sky}(u,v)$,

$$V_{sky}^{pq} \triangleq \frac{1}{\sqrt{\Omega_1\Omega_2}} \iint_{\xi^2+\eta^2\subset sky} \frac{T_{B\,sky}^{pq}(\xi,\eta)}{\sqrt{1-\xi^2-\eta^2}} \hat{F}_{n1}^{p}(\xi,\eta)\hat{F}_{n2}^{q*}(\xi,\eta)\hat{\tilde{r}}_{12}\left(-\frac{u_{12}\xi+v_{12}\eta+w_{12}\sqrt{1-\xi^2-\eta^2}}{f_0}\right)\exp\left(-j2\pi(u_{12}\xi+v_{12}\eta+w_{12}\sqrt{1-\xi^2-\eta^2})\right)d\xi d\eta\,,$$

L-band noise map of the sky
(cosmic + galactic contributions)

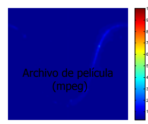

1. Computation of auxiliary visibilities to extend the AF-FOV to the periodic Earth aliases: (cont')

d) Term corresponding to the antenna back lobes, since there are two directions (θ,ϕ) and ($\pi-\theta,\phi$) that are imaged in the same (ξ,η) point:

$$V_{12}^{pq}\Big|_{back} = \frac{1}{\sqrt{\Omega_1\Omega_2}} \iint_{\xi^2+\eta^2\le 1} \frac{T_{pq,back}(\xi,\eta)-T_{rec}}{\sqrt{1-\xi^2-\eta^2}} \hat{F}_{np1}(\xi,\eta)\hat{F}_{np2}^{*}(\xi,\eta)\hat{\tilde{r}}_{12}\left(-\frac{u_{12}\xi+v_{12}\eta-w_{12}\sqrt{1-\xi^2-\eta^2}}{f_0}\right)\exp\left(-j2\pi\left(u_{12}\xi+v_{12}\eta-w_{12}\sqrt{1-\xi^2-\eta^2}\right)\right)d\xi d\eta$$

Note, however, that the uncertainty in the measured antenna patterns from the back side is large, and comparable to the value itself.

e) Term coming from a "constant" T_B within the land-covered region and a ocean-covered region so that differential visibilities are zero-mean:

$V_{Land}^{pq}(u,v) = T_{Land}^{pq}\bar{V}_{Earth}^{pq}(u,v)$ $\quad V_{Ocean}^{pq}(u,v)$: from ocean emission model

$$\boxed{\Delta V^{pq}(u,v) = V^{pq}(u,v) - V_R^{pq}(u,v) - V_{sky}^{pq}(u,v) - V_{back}^{pq}(u,v) - T_{Land}^{pq}\,\bar{V}_{Earth}(u,v) - V_{Ocean}(u,v)}$$

$$\bar{V}_{Land}^{pq} \triangleq \frac{1}{\sqrt{\Omega_1\Omega_2}} \iint_{\xi^2+\eta^2\subset Land\ on\ Earth} \frac{1}{\sqrt{1-\xi^2-\eta^2}} \hat{F}_{n1}^{p}(\xi,\eta)\hat{F}_{n2}^{q*}(\xi,\eta)\hat{\tilde{r}}_{12}\left(-\frac{u_{12}\xi+v_{12}\eta+w_{12}\sqrt{1-\xi^2-\eta^2}}{f_0}\right)\exp\left(-j2\pi(u_{12}\xi+v_{12}\eta+w_{12}\sqrt{1-\xi^2-\eta^2})\right)d\xi d\eta\,,$$

Note: this term will be recomputed once the Sun and Moon contributions are estimated

2. Cancellation of Sun and Moon effects:

- Make a "raw" T_B image using an IHFFT: $\hat{T}_B^{pq} = F^{-1}\left[V^{pq}(u,v) - V_R^{pq}(u,v)\right]$

The Sun is such a bright source that it completely masks the rest of the image.

- Estimate the image of a normalized (T_B=1 K) Sun and Moon if visible:

$$\hat{\bar{T}}^{pq}_{Sun/Moon,dir/ref} = F^{-1}\left[\bar{V}^{pq}_{Sun/Moon,dir/ref}(u,v)\right]$$

- Estimate T_B from the Sun as: $T^{pq}_{Sun,dir} = \hat{T}_B^{pq}\left(\xi_{Sun,dir}, \eta_{Sun,dir}\right) / \hat{\bar{T}}^{pq}_{Sun,dir}\left(\xi_{Sun,dir}, \eta_{Sun,dir}\right)$

- T_B Moon is much smaller and cannot be easily "seen" in the "raw" T_B image.

Then, assume it is ~ 250 K, or from radiotelescope measurements .

$$V^{pq}_{Sun/Moon,dir/ref}(u,v) = T^{pq}_{Sun/Moon,dir/ref} \cdot \bar{V}^{pq}_{Sun/Moon,dir/ref}(u,v)$$

2. Cancellation of Sun and Moon effects: (cont')

- Compute the contributions to the measured visibilities from the Sun and the Moon:

$$V^{pq}_{Sun/Moon,dir/ref}(u,v) = T^{pq}_{Sun/Moon,dir/ref} \cdot \bar{V}^{pq}_{Sun/Moon,dir/ref}(u,v)$$

- Compute the **differential visibilities** including the Sun and Moon contributions:

$$T^{pq}_{Land} \triangleq \frac{\bar{T}_A^{pq} - V^{pq}_{sky}(0,0) - V^{pq}_{back}(0,0) - V^{pq}_{Ocean}(0,0) - T'_{Sun,dir}\bar{V}^{pq}_{Sun,dir}(u,v) - T_{Sun,ref}\bar{V}^{pq}_{Sun,ref}(0,0) - T_{Moon,dir}\bar{V}^{pq}_{Moon,dir}(0,0) - T_{Moon,ref}\bar{V}^{pq}_{Moon,ref}(0,0)}{\bar{V}^{pq}_{Land}(0,0)}$$

$$\begin{aligned}\Delta V^{pq}(u,v) = {} & V^{pq}(u,v) - V_R^{pq}(u,v) - V^{pq}_{sky}(u,v) - T^{pq}_{Land}\,\bar{V}_{land}(u,v) - V_{ocean}(u,v) \\ & - T'_{Sun,dir}\bar{V}^{pq}_{Sun,dir}(u,v) - T_{Sun,ref}\bar{V}^{pq}_{Sun,ref}(u,v) - T_{Moon,dir}\bar{V}^{pq}_{Moon,dir}(u,v) - T_{Moon,ref}\bar{V}^{pq}_{Moon,ref}(u,v) \\ & - V^{pq}_{back}(u,v),\end{aligned}$$

Note: $V_R(0,0) = 0$ and $V^{pq}(0,0) = T_A^{pq}$ (without the $-T_{rec}$ term)

Instrument equation in terms of differential visibilities:

$$\Delta V^{pq} \triangleq \frac{1}{\sqrt{\Omega_1 \Omega_2}} \iint_{\xi^2+\eta^2 \subset Earth} \frac{\Delta T_B^{pq}(\xi,\eta)}{\sqrt{1-\xi^2-\eta^2}} \hat{F}_{n1}^{p}(\xi,\eta) \hat{F}_{n2}^{q*}(\xi,\eta) \hat{\tilde{r}}_{12}\left(-\frac{u_{12}\xi + v_{12}\eta}{f_0}\right) \exp(-j2\pi(u_{12}\xi + v_{12}\eta))\, d\xi\, d\eta ,$$

Where: $\Delta T_B^{pq}(\xi,\eta) \triangleq T_B^{pq}(\xi,\eta) - T_{Earth}^{pq}$

The equation is discretized

$$\boxed{W(u,v)\ \ \Delta V(u,v) = G\left[\Delta T^{dec}(\xi,\eta)\right]}$$

• The elements of the **G-matrix** correspond to the discretization of the integral equation (above), sampled at the (ξ,η) points of the (u,v) reciprocal grid (slide 66)
⇒ in the ideal case the image reconstruction process reduces to an IHFFT with all its well behaved properties (e.g. no error amplification).

• **Redundant visibilities** (same (u,v) point) are averaged to reduce noise ⇒ the corresponding equations are averaged as well.

5.5. Types of Image Reconstruction Algortihms
Solution of Instrument Equation in Terms of Differential Visibilities:

•**Direct**: G-matrix pseudo-inverse (used in ESTAR)

$$\boxed{\Delta T^{dec}(\xi,\eta) = \overbrace{\left(G^H G\right)^{-1} G^H}\left[W(u,v)\ \ \Delta V(u,v)\right]}$$ → OK for small arrays

•**Iterative methods (coded in SEPS)**:
Extended-CLEAN (UPC)
Stabilization + conjugate gradient (UPC):

$$\boxed{G^H W(u,v)\ \ \Delta V(u,v) = G^H G\left[\Delta T^{dec}(\xi,\eta)\right]}$$ → **Calibration**
+ Sun/Moon cancellation
+ Differential visibilities
+ G-matrix formulation
+ Image reconstruction
⇒ SMOS L1 Processor

Types of Image Reconstruction Algortihms (cont')

- **The Resolving Matrix Approach (CERFACS)**

Preliminary definitions:

DFT operator: $U: E \rightarrow \hat{E}$

$T \rightarrow UT = \hat{T}$

Zero-padding operator: $Z: \hat{\varepsilon} \rightarrow \hat{E}$

$\hat{T} \rightarrow Z\hat{T} = \hat{T}$

Modeling operator: $G: E \rightarrow F$

$T \rightarrow GT = V$

Solution of the problem:

$$\min_{T \in E} \left\| V - GT \right\|_F^2 \qquad (I - P_H)T = 0 \qquad P_H = U^*ZZ^*U$$

$$\min_{\hat{T} \in \hat{E}} \left\| V - A\hat{T} \right\|_F^2 \qquad A = GU^*Z$$

$$\boxed{A^*A\hat{T} = A^*V} \qquad \boxed{T_r = \left(A^*A\right)^{-1} A^*V}$$

Solution equivalent to G-matrix + conjugate-gradient, since in the computation ($G\Delta T$) no visibilities are added beyond the (u,v) points measured by MIRAS.

Example 1: Image reconstruction in the antenna reference frame (T_x, T_y)

Smooth transition from aliases ⇒ larger error
Need to leave guard pixels
Minimized by constant T_B Earth subtraction

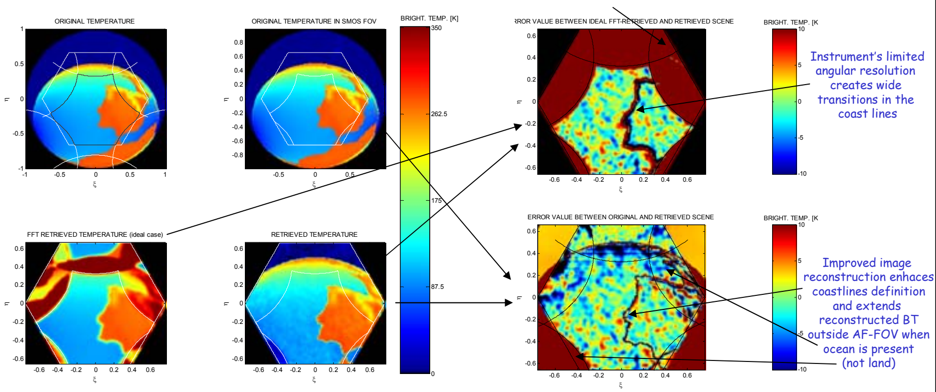

Example 2: Sun effects and their cancellation

The Sun appears in the E-AF-FOV …

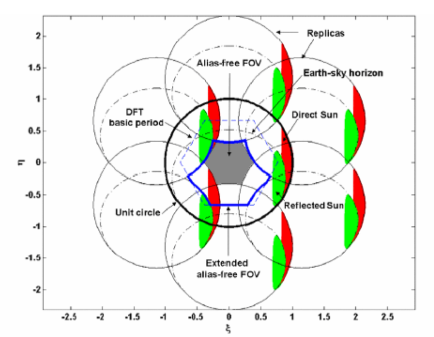

and nearly 97 % of the time!!

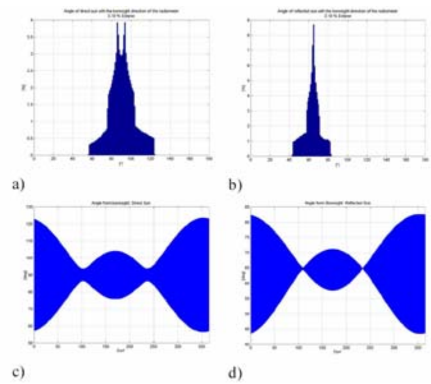

Direct sun direction

Specular reflection direction of the sun

Over land the effect is not so visible

No Sun

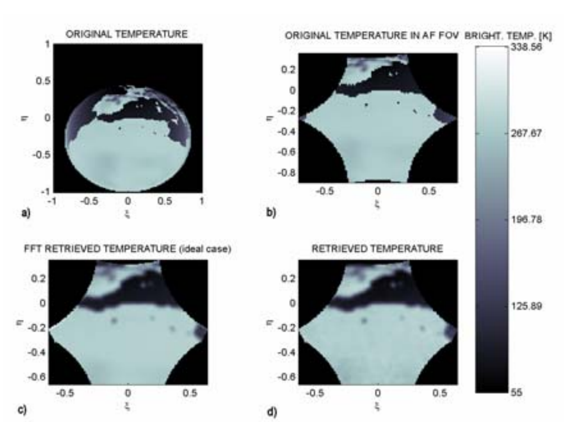

Sun present, but not cancelled

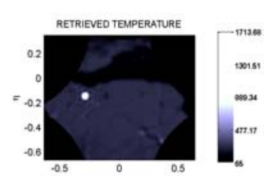

Sun present, and cancelled

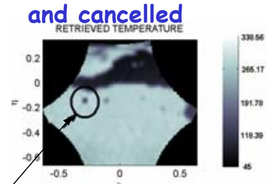

Residual error

Over sea the effect is more dramatic!
Sun glint not critical, imperfect direct Sun cancellation important

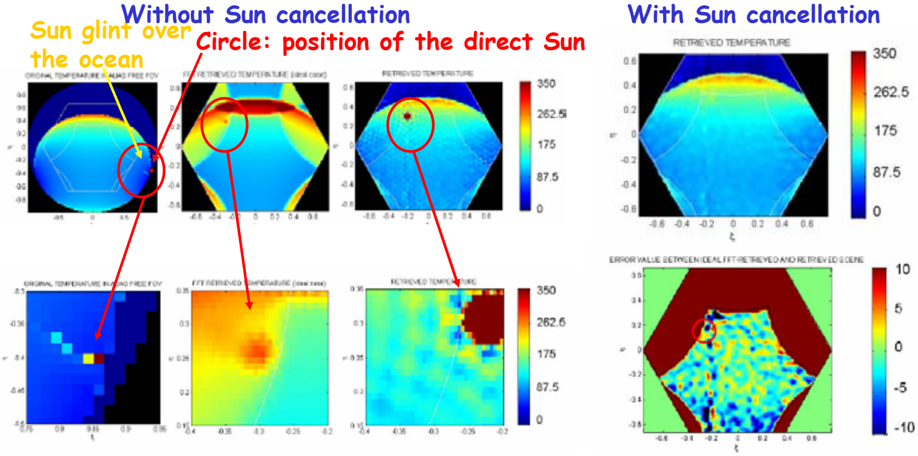

In AF-FOV, without Sun cancellation, rms radiometric errors can be ~22 K, while if it is cancelled they are ~3.4 K in front of 1.7 K if there is no Sun

Geolocalization: from director cosines grid to Earth reference frame grid

• ISEA family of grids seem to be the best option for the SMOS Products, but EASE-Grid has come to be popular amongst many of the Earth Observation missions of the USA, namely AQUA (NASA/NASDA) and AQUARIUS (NASA), which are particularly interesting for comparison with the SMOS products.

• Spatial partitioning of EASE-Grid is square-based and ISEA can be triangular, hexagonal or diamond-based:

- In its **hexagonal form, ISEA** has a **higher degree of compactness**, quantize the plane with the **smallest average error** and provides the **greatest angular resolution**.

-ISEA hexagonal possesses **uniform adjacency with its neighbours**, unlike the square EASE-Grid.

• Both grids have **uniform alignment** and are **based on a spherical Earth assumption**.

• **ISEA hexagonal at aperture 4 and resolution 9 (15km) is made up of 2,621,442 points and the EASE-Grid at 12km has 3,244,518 points.**

• EASE-Grid is congruent, whereas **ISEA is not congruent**, being impossible to decompose a hexagon into smaller hexagons or aggregate hexagons into larger ones. This would be a negative feature for real-time re-gridding, but in SMOS the grids will be pre-generated.

6. Retrieval of Geophysical Parameters

- Use of **multiangular information**:
  1. Horizontal (T_h) and vertical (T_v) polarizations or T_x and T_y
     + Faraday and geometric rotations corrections:
     Earth $\rightarrow$ Antenna: retrieval in antenna ref frame,
     Antenna $\rightarrow$ Earth: retrieval in Earth ref frame,
  2. First Stokes parameter: $I = T_x+T_y=T_h+T_v$
     (invariant to rotations)
- For each track:
  - SSS retrieval using SST and U_{10} (or sea state descriptor) as aux. data
  - SM retrieval using T, τ, ω, σ as aux. data

  Aux data must be of high accuarcy or if not it can be left as free param.
- Spatio-temporal averaging of results

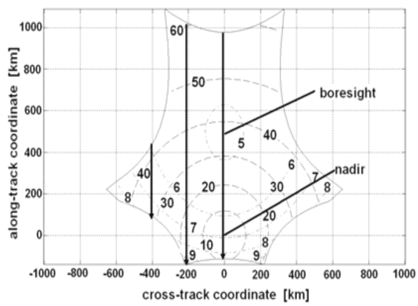

Simulated T_v and T_h for different ground-tracks:
a) no wind
b) wind = 10 m/s
SSS = 35 psu, SST = 15°C

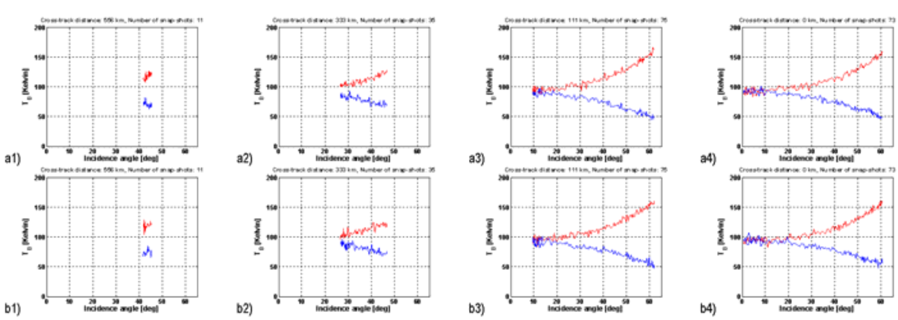

SSS Retrieval in one overpass:

• Multi-parameter retrieval ($U_{10\ eff}$, SST_{eff}, SSS) with appropriate aux data (with or without restrictions)

• External calibration first to compensate instrumental and modeling biases…

Covariance error matrix. Depends on:
• instrument observation mode (dual- or full-pol), and
• reference frame (Earth or antenna)

$$\varepsilon = \frac{1}{N_{obs}} \sum_n \left\{ \left[\bar{F}_{model}\left(\theta_n, \hat{\vec{P}}\right) - \bar{F}_{data}\left(\theta_n, \vec{P}\right) \right]^T \left(\bar{\bar{C}}^{Earth,\ Antenna\,/\,odd(n),\,even(n)}_{Full-pol\,/\,Dual-pol} \right)^{-1} \left[\bar{F}_{model}\left(\theta_n, \hat{\vec{P}}\right) - \bar{F}_{data}\left(\theta_n, \vec{P}\right) \right] \right\} + \cancel{\frac{\left(SSS - SSS_{ref}\right)^2}{\sigma^2_{SSS}}} + \frac{\left(SST - SST_{ref}\right)^2}{\sigma^2_{SST}} + \frac{\left(WS - WS_{ref}\right)^2}{\sigma^2_{WS}}$$

Restrictions.
- Can be added to help finding the solution
-Restriction on SSS found to be "too much" helpful: $SSS_{retrieved} = SSS_{ref}$ always

• F = I, $[T_h, T_v]$ or $[T_x, T_y]$
• x = vector of parameters on which T_B depends
• The retrieved U_{10} is not the actual wind speed, it is an effective wind speed that best describes the sea state at L-band (accounts for wind speed & sea state)

SSS retrieval: standard deviation in 1 over-pass:

SST = 5°C, 15°C, 25°C

SSS = 30 psu SSS = 35 psu SSS = 40 psu

U_{10} = 0 m/s

U_{10} = 10 m/s

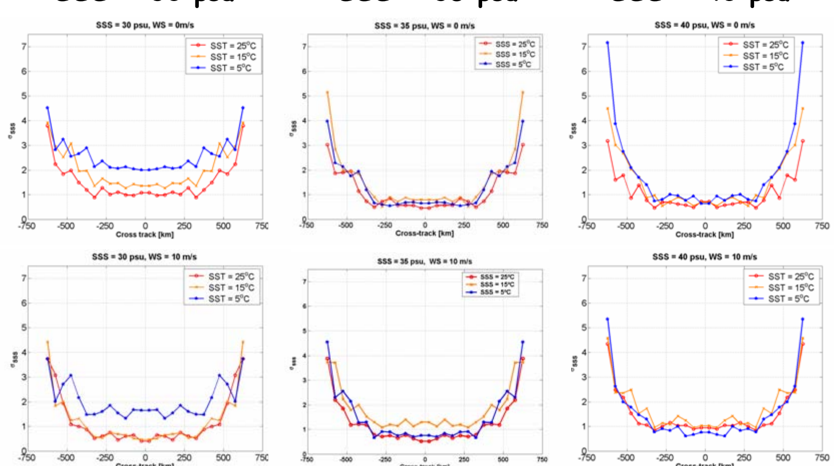

SSS retrieval: Spatio-temporal averaging:

Use of first Stokes parameter provides only a slight degradation of the retrieval, as compared to Tx,Ty or Th,Tv with "perfect" Faraday rotation correction

SSS = 35 psu, U_{10} = 10 m/s,
SST = 5°C (solid), 15°C (dashed), 25°C (dotted).
(I) (Tv & Th)

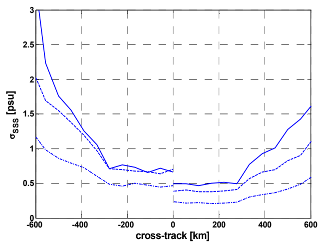

Retrieval in 1 overpass with different auxiliary parameters

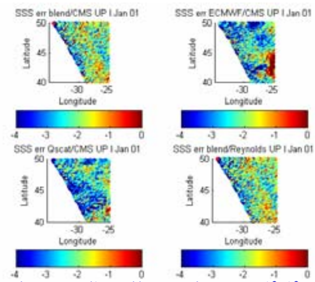

Temporal averaging (1 month)

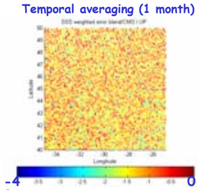

Temporal averaging (1 month) + spatial averaging 1°x1°

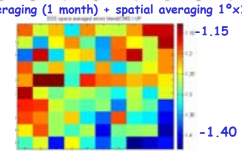

Simulated Tv and Th for different ground-tracks:

Over land T_B depends on: soil moisture (and soil type, density…),
surface roughness, veget. opacity, albedo and temp.

No veget.
flat soil
SM=0

No veget.
flat soil
SM=0.4

Dense veget.
Rough soil
SM=0

Dense veget.
Rough soil
SM=0.4

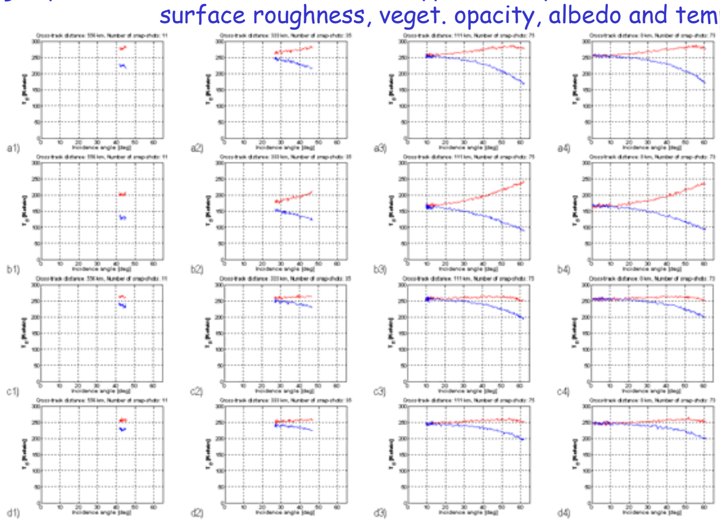

Not only the SM can be retrieved, but also vegetation parameters (τ: related to the vegetation water content):

Use of first Stokes parameter leads to very few eqns. and poor retrievals

Soil: flat (σ = 0), temperature = 290 K,
No vegetation: τ = 0 Nep, ω = 0
SM = 0% (solid), 20% (dashed), 40% (dotted).
(I) (Tv & Th)

Soil: very rough (σ = 1), temperature = 290 K,
Thick vegetation: τ = 1 Nep, ω = 0.1
SM = 0% (solid), 20% (dashed), 40% (dotted).
(I) (Tv & Th)

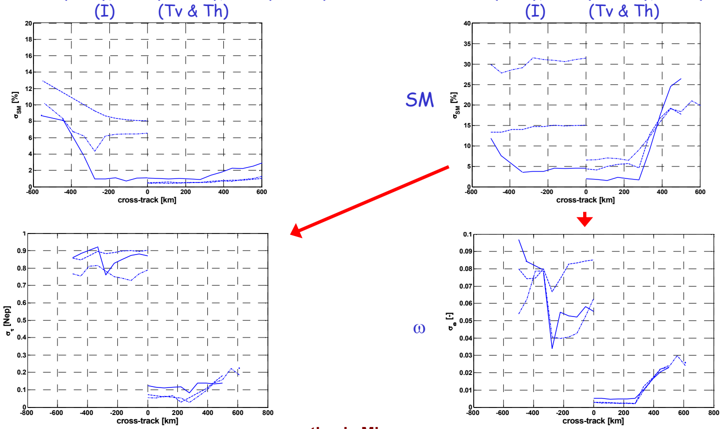

7. SEPS: The SMOS End-to-end Performance Simulator

Objectives:

- Analyze instrument's performance
- Develop geophysical parameters retrieval alg.
- Generate data packets for L1 processor developpers

Simulation tool:

- Propagates SMOS orbit
- Generates realistic T_B maps from geophysical params.
- Computes instrument's observables including detailed error model with in-orbit temperature depend.
- Applies error correction algorithms (int. calibration)
- Applies image reconstruction algorithm(s)
- Projects reconstructed T_B on the Earth

Antecedents:

- MIRAS Simulator (A. Camps, Ph D, 1996), SEPS v1.0 (2001) ...

Simulator Block Diagram & Basic Features

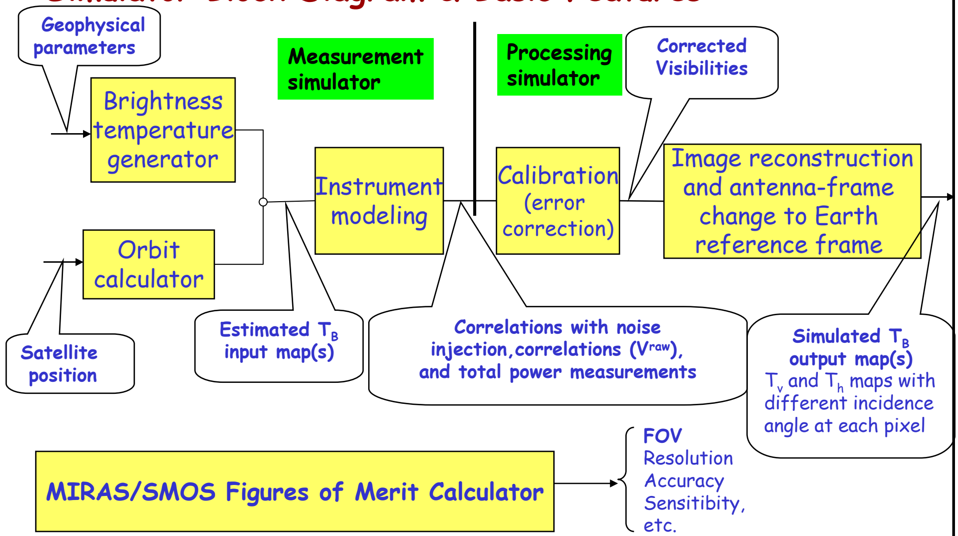

Level 0: SMOS observables = correlation products among all signal pairs collected by the array elements ("visibilities")

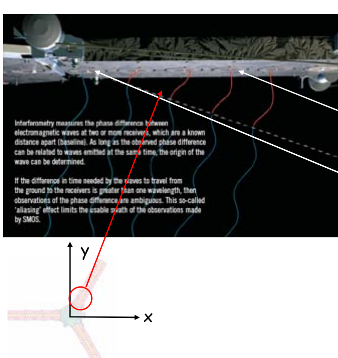

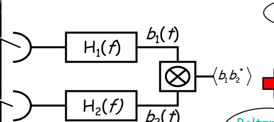

Spatial coordinates
Complex Correlation Products

$$V(u,v) = \frac{1}{k_B\sqrt{B_1 B_2}\sqrt{G_1 G_2}}\,\frac{1}{2}\left\langle b_1(t)\, b_2^*(t)\right\rangle$$

Boltzmann constant
Receivers Noise Bandwidth
Available Power Gain

Antenna Radiation Volatage Pattern
Brigthness Temperature
Physical Temperature of the receivers
Director Cosines

$$T(\xi,\eta) = \frac{F_{n1}(\xi,\eta)\, F_{n2}^*(\xi,\eta)}{\sqrt{\Omega_1\Omega_2}}\,\frac{T_B(\xi,\eta) - T_{ph}}{\sqrt{1-\xi^2-\eta^2}}$$

Antenna Solid Angle
Obliquity factor (cos(θ))

$$\boxed{(u,v) = (\Delta x, \Delta y)/\lambda_0} \quad \boxed{(\xi,\eta) = (\sin\theta\cos\varphi, \sin\theta\sin\varphi)}$$

(u,v) = spatial frequencies where $V(u,v)$ is sampled
depend on array geometry and inter-element spacing ("d")

Ideal case: 2D Fourier transform

$$\boxed{V(u,v) = F\left[T(\xi,\eta)\right]}$$

Non-ideal case: includes antenna positioning errors, receiver frequency response differences

Brightness Temperature Generator:

- T_H and T_v computed by the **radiative transfer equation** (models in bright.m)

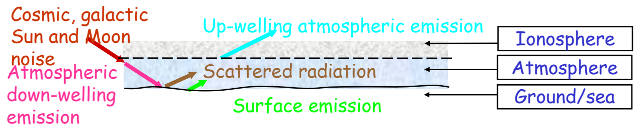

- Geophysical parameters from the CD set:
  - "Global Data Sets for Land-Atmosphere Models ISLSCP Initiative 1: 1987-1988 Vols 1-5"
  - 1° resolution: 180 x 360 matrices (text file or.mat binary file) land-sea mask at 1°/12 (ETOPO 5) + bilinear inter } Higher resolution maps can be used as input (developed in the frame of Synergy study)
  - Monthly variation
  - Parameters: . Atmosphere: liquid water, rain rate
    . Land: land, snow & vegetation albedos, soil surface temperature, moisture & roughness, vegetation height, snow depth,
    . Sea: surface salinity, temperature and wind speed, ice cover fract.
    . Galactic noise map from Reich and Reich [1986].
    . Ionosphere: Intenational Reference Ionosphere '95 model & International Geomagnetic Reference Field model

Improving Spatial Resolution At Coast Lines:

- Geophysical data on a 1° x 1° grid (~ 110 Km at the equator)
  ⇒ Data **resampled and bilinearly interpolated** in each region (land – sea)
  ⇒ **Masked with ETOPO5** (1° /12, ~ 10 Km at the equator)

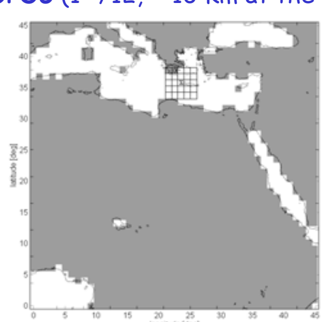

- Iced sea – sea lines do not have this improved resolution (1°x1°)

Sky Noise:

- Cosmic noise ≈ 2.7 K
- Galactic noise map from Reich and Reich [1986].

SEPS 4.0 includes the complete map, but bright sources still need to be added

Problem: Southern sky not mapped ⇒ ~ $f^{2.8}$ extrapolation of the 408 MHz map

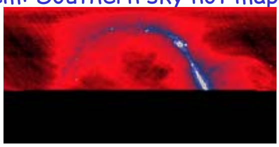

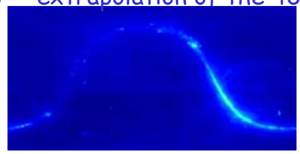

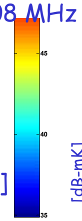

- Sun: T_B = 218.000 K [Fleury, '01]
  Ω_{sun} = 0.586°
- Moon: T_B = 250 K [Kopal, '69]
  Ω_{moon}= 0.586°

Direct + reflected = total

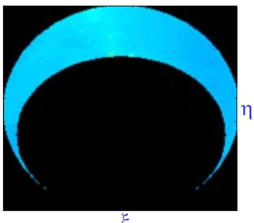

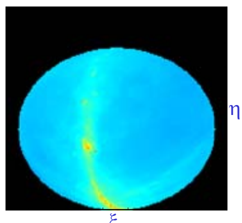

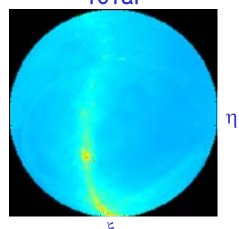

Atmosphere:

- Assumptions:
  - Air pressure at sea level P_0= 1013 mbar;
  - Air temperature at 2 m = 10°C;
  - Atmosphere height h_{atm}= 32 km (important θ > 80° : Earth's curvature)

Can be made pixel-dependent using appropriate input files.

- To speed up the T_B generator Liebe's model linear regressions at L-band used:

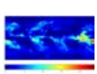

Global rain rate

LW : liquid water; AP : atmospheric pressure; ST : surface temperature

$$\theta_{eq} = \arccos\left(\frac{h_{atm}}{\sqrt{R_T^2\cos^2(\theta_{inc})+(2R_T+h_{atm})h_{atm}}-R_T\cos(\theta_{inc})}\right)$$

$$T_{UP} = \left[1.86 + 0.0029\,RR + 0.10\,LW + 0.0034\,(AP - P_0) - 0.011\,(ST - 283.15)\right]/\cos(\theta_{eq})$$

$$T_{DN} = \left[2.10 + 0.0029\,RR + 0.10\,LW + 0.0034\,(AP - P_0) - 0.011\,(ST - 283.15)\right]/\cos(\theta_{eq})$$

$$L_{atm} = \left[0.04024 + 0.000046\,RR + 0.0030\,WL + 0.000059\,(AP - P_0) - 0.00030\,(ST - 283.15)\right]/\cos(\theta_{eq})$$

Sea And Water Bodies:

- Assumptions:
  - Klein-Swift '77 dielectric permittivity model:
  - epsilon.m and epsiloni.m files can be replaced by the Ellison or Blanch-Aguasca models…
  - Linear fit of Hollinger's '71 wind dependence:

$$T_p(\theta_{inc}, SSS, SST, WS) = \left[1 - \Gamma_p^{sp}(\theta_{inc}, SSS, SST)\right] SST + \Delta T_p$$

$$\Delta T_{\substack{h \\ v}} = 0.2\left(1 \pm \frac{\theta_{inc}}{55^\circ}\right) WS$$

  - Iced sea: $\varepsilon_{r\ ice} = 3.0 - j\,0.25$

$$T_p(\theta_{inc}) = \left[1 - \Gamma_p^{sp}(\theta_{inc}, \varepsilon_{r\ ice})\right] SST$$

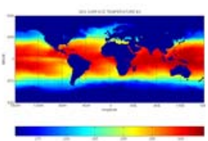

SST

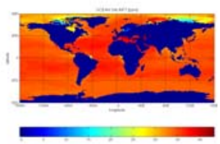

SSS

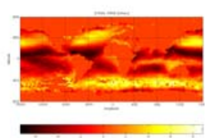

Zonal wind

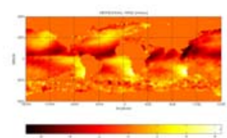

Meridional wind

Land:

- **Bare soil (Wang-Choudhury model)**: $T_{bareB,\,p}(\theta) = e_{bare\ p}(\theta, \sigma, f, W)\, T_{ph}$
- **Vegetation-covered soil**: 3-layer model

$$T_B^{canopy}(\theta) = \frac{1 - \Gamma_{air\text{-}veg}}{1 - \frac{\Gamma_{air\text{-}veg}\,\Gamma_{veg\text{-}soil}}{L_{veg}^2}} \left[\left(1 + \frac{\Gamma_{veg\text{-}soil}}{L_{veg}}\right)\left(1 - \frac{1}{L_{veg}}\right)(1 - a)\, T_{veg} + \frac{1 - \Gamma_{veg\text{-}soil}}{L_{veg}} T_{soil}\right]$$

- Dielectric permitivity computed with Matzler's and Kerr's formulas (e_veget.m)
- Mixing formula not implemented: lack of vegetation fraction cover data.

- **Dry snow-covered soil**: 3-layer model
  - Dielectric permittivity computed with the following formulas:
    - Iced soil: $\varepsilon_r = 3.15$
    - Snow: eps_ds.m, formulas from *Microwave Scattering and Emission Models, A.K. Fung, '94*
  - Snow extinction and albedo: kekas.m, formulas from *Microwave Remote Sensing, Ulaby et al., '86, pp 1606-1609*
  - Effective surface temperature and density: stros.m, formulas assuming exponential profiles vs. depth from *Tsang et al., '94.*

Ionosphere:

- Ionosphere parameters computed based on the Intenational Reference Ionosphere '95 model. It has been implemented in a set of Fortran functions by **Dieter Bilitza**, obtained from the National Space Science Data Center ftp server: ftp://nssdc.gsfc.nasa.gov/pub/models/ionospheric/iri/iri95/fortran_code/

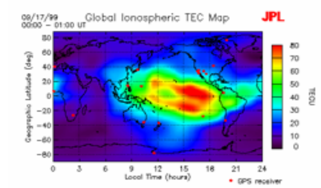

- Geomagnetic field computed based on the International Geomagnetic Reference Field model. It has been implemented in a set of Fortran functions, obtained from the National Space Science Data Center ftp server: ftp://nssdc.gsfc.nasa.gov/pub/models/geomagnetic/igrf/fortran_code/
- TEC used to compute ionospheric losses
- TEC and Earth's geomagnetic field data used to compute Faraday's rotation

Level 1a: Calibrated Visibility Samples ⇔ Error model

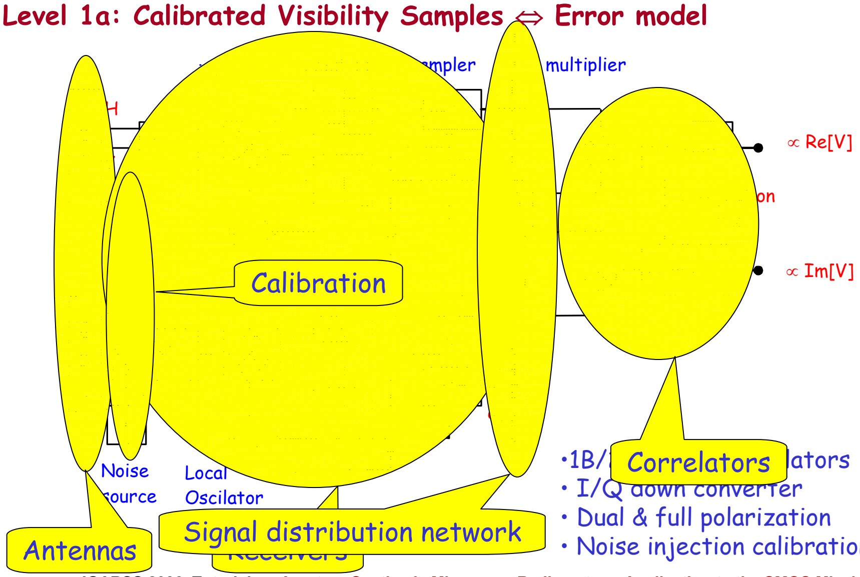

- 1B/2 correlators
- I/Q down converter
- Dual & full polarization
- Noise injection calibration

Level 1b: Calibrated T_B in antenna frame

Spatial frequencies smapled by an Y-array

Spatial frequencies (u,v)

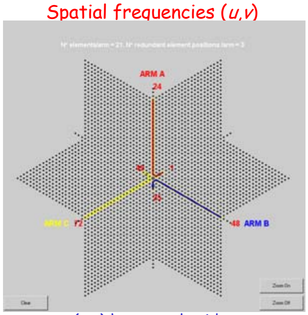

(u,v) hexagonal grid
Inter-element spacing $d = 0.875\ \lambda$
Nyquist criterion : $d/\lambda < 1/\sqrt{3}$

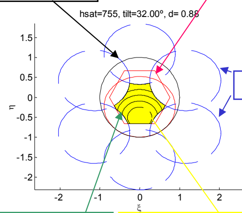

Nyquist criterion not satisfied:
- Aliasing in T_B images
- 6 Earth aliases overlap

$$\boxed{T(\xi,\eta) = F^{-1}[V(u,v)]}$$

Image reconstruction alg. includes redundant baselines, direct/reflected Sun cancellation (specular), sky imaging capability, "calibrated" fringe-washing funcs, blind correlations ...

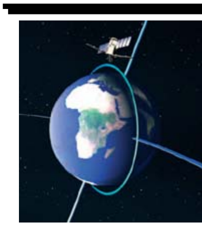

Antenna ref. frame:
X/Y-pol in (ξ,η)
$\Downarrow$
Earth ref. frame:
H/V-pol in (lat-lon)
uniform or ISEA grids

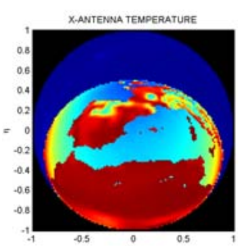

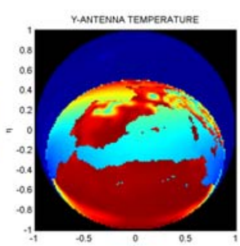

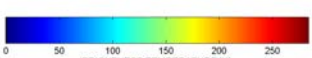

T_B images generated with SEPS

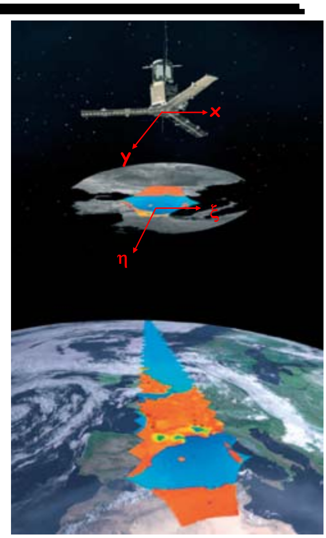

Higher levels: Calibrated T_B in Earth ref. frame
⇒ Faraday and geometric rotation corrections

- Dual-pol mode (X/Y):
  - all antennas at X-pol during 1.2 s, then at Y-pol
  - SINGULARITIES in the transformation T_{xx}, $T_{yy} \rightarrow T_{hh}$, T_{vv}
- Full-polarimetric mode:
  - Combinations among X and Y polarizations in different arms during 2.4 s.
  - NO SINGULARITIES in the transformation T_{xx}, T_{yy}, $T_{xy} \rightarrow T_{hh}$, T_{vv}, but:
  - LARGER NOISE

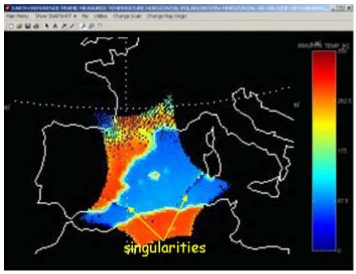

Dual-pol. mode

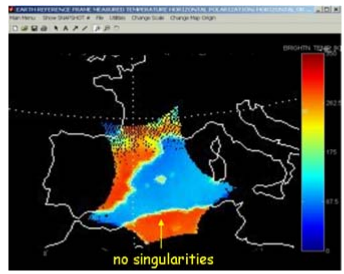

Full-pol mode

T_B representation in cartographic projections

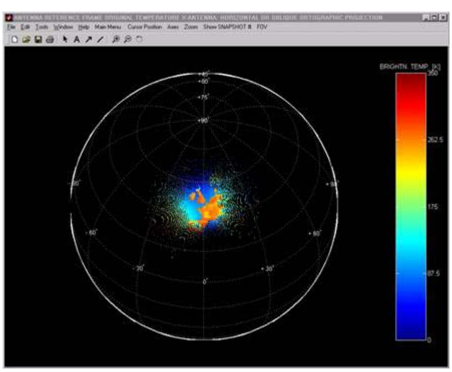

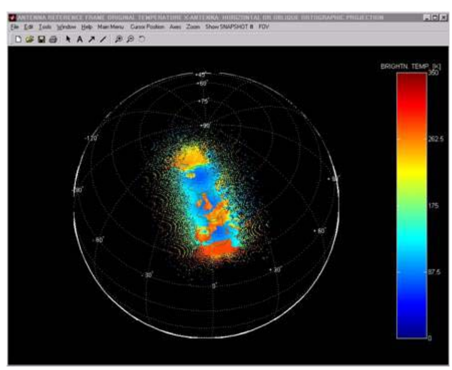

Show snapshot #:

projects a single snapshot of the simulation

Show multiple snap-shots with or without FOV:

Projects the alias-freeFOV contour line for each snapshot

SEPS Sample output

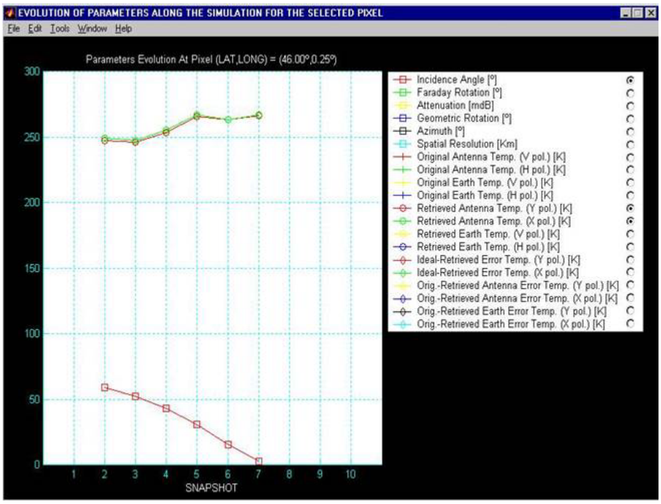

Parameter Values

vs. Snapshot

•Pixel selection by right-clicking mouse on Earth surface point

•Plot evolution of selected parameters and temperature results along the simulation

•Disabling params. available for friendly evaluation

Saving Results In A Text File:

Name of the file DATA_ascii with the following format

```
for iter=1:size(LAT,1),
  for i=1:size(LAT,2),
    fprintf(FID,'%6.0d %3.2f    %3.2f    %2.3f    %2.3f    %1.0d    %1.0d    %2.3f
                 %3.3f          %3.2f    %2.3f    %3.3f    %3.2f    %3.2f    %3.2f    %3.2f
                 %3.2f          %3.2f    %3.2f    %3.2f    %3.2f    %3.2f    %3.2f    %3.2f
                 %3.2f          %6.3f    %3.3f\n', (iter-1)*size(LAT,2)+i,LAT(iter,i),LON(iter,i),PX(1,i),PY(1,i),
                 OK(iter,i),fov4(1,i),TXant(iter,i),TYant(iter,i),TXrec(iter,i),TYrec(iter,i),THpix(iter,i),TVpix(iter,i),
                 deltaTX(iter,i),deltaTY(iter,i),FROT(iter,i),ATT(iter,i),PSI(iter,i));
  end
end
```

Can be read by other user applications for use in the development of geophysical parameters retrieval.

High-resolution TB generator and Level 2 prototype processor (UPC) to be added in potential future SEPS versions:

- T_B corrections (atmosphere, reflected galactic noise ...)

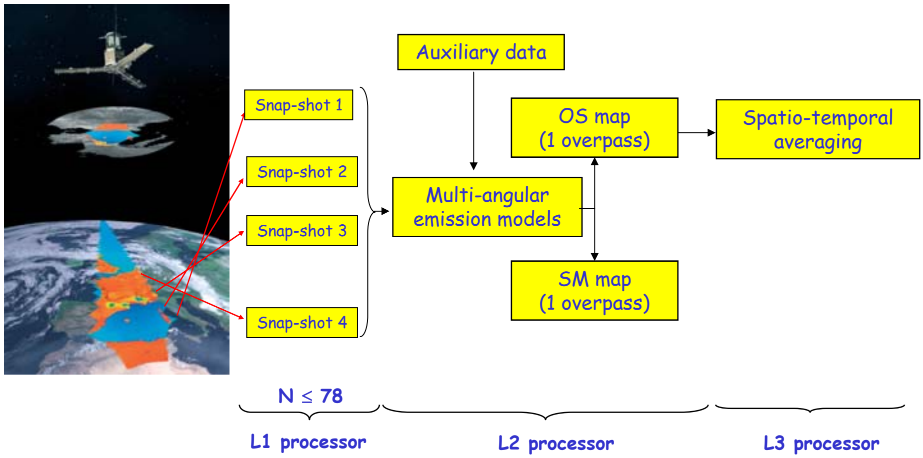

Conclusions:

- Fundamentals of Microwave Radiometer by Aperture Synthesis have been presented as well as the antecedents and context of ESA's SMOS mission.

- Instrument performance evaluated in terms of angular resolution, and radiometric performance (sensitivity, bias and accuarcy).

- Instrument Error Model and Internal/External Calibration Strategy have been presented.

- Visibility samples preprocessing and image reconstruction algorithms have been presented.

- Geophysical parameters retrieval algorithms and performance.

- SEPS 4.01 presented including an improved image reconstruction algorithm that reduces BT bias by decomposing the BT image into land and sea.

- New releases of SEPS will include a high resolution BT generator (to be used in SMOS Cal/Val activities) including the DEM and a new software tool to perform the retrieval of geophysical parameters from SEPS' outputs.

- More information in: http://www.esa.int/esaLP/LPsmos.html and in the documentation CD provided.

BACKUP

4.2. Elements

ANTENA:

The LICEF antenna provides best performance in terms of gain, bandwidth and differentiation of horizontal and vertical polarisation components of incoming microwaves.
It consists of four probes implemented as pairs, which are rotated 90 degrees to each other so as to acquire the two different signal polarisations.
Multi-layer 'microstrip' technology has been chosen for the circuit configuration. Each layer is dedicated to one polarisation.
Each LICEF antenna weighs 190 g, is 165 mm in diameter and is 19 mm high.

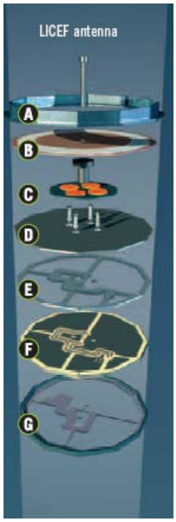

A) Carbon-fibre structure

B) Patch antenna

C) Feeding discs

D) Cavity floor to patch antenna

E) Alumninum spacer

F) Feed circuits (Multilayer microstrips on both sides of the grounding plane)

G) Aluminium spacer

Inter-elements spacing d = 0.88λ

LICEF

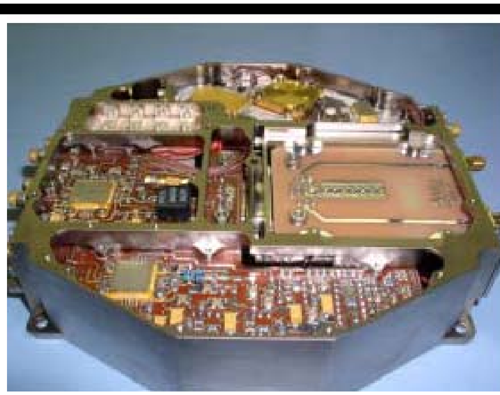

Lightweight Cost-Effective Front-ends
MIER (Spain) has overall responsibility for this integrated antenna-receiver unit, and has manufactured its electronics.
EADS-CASA has designed and manufactured the antenna and the receiver band-shaping RF filter, while UPC has provided key support in elaborating the technical specifications.

NIR

NIR is a polarimetric noise injection radiometer at 1.4 GHz.
Three NIR Flight Models will be included in the central hub of MIRAS. The main purposes of NIR are:
(A) to provide precise measurement of the average (fully polarimetric) brightness temperature scene for the absolute calibration of the MIRAS image map
(B) to measure the noise temperature level of the reference noise of Calibration Subsystem (CAS)

Thus, NIR is the absolute amplitude reference of MIRAS

Furthermore, NIR incorporates operational modes that allow it to form interferometric baselines with other receivers of MIRAS (so called mixed baselines).

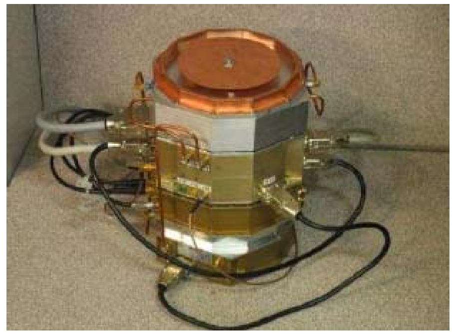

NIR

The Noise injection Radiometer consists of:
(A)Two radiometer receivers, one for vertical and one for horizontal polarization
(B)One controller, and
(C) Phase stable RF cables that connect the controller to the receivers.
The controller incorporates an antenna that receives the target noise.
The receivers of NIR are almost identical to the other receivers of MIRAS.
Also, the antenna is identical to those of the other antennas of MIRAS.

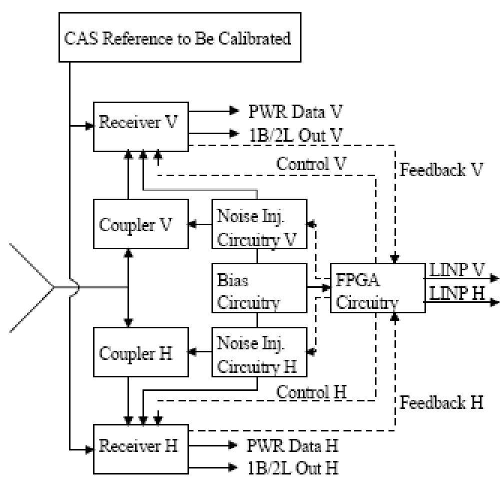

The functions of the controller are to
(A) inject reference noise into the two receiver chains,
(B) regulate the amount of the injected noise to keep the system balanced with antenna temperature or with the calibration noise from CAS, and
(C) control the switches of NIR (Dicke-switches of the receivers and the noise switches of the controller) according to the selected operation mode.

The basic blocks of the controller are
- bias circuitry, which generates the required voltages and provides EMC protection,
- two noise injection circuitries and couplers (for vertical and horizontal polarization channels),
- and an FPGA circuitry, which controls the noise injection circuitry and front-end switches of NIR receivers.

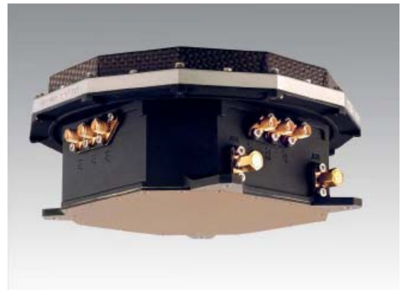

- 1B/2L stands for 1-bit/2-level digital output for the correlator of MIRAS,
- PWR is detector signal to retrieve system temperature,
- and LINP is Length of Injected Noise Pulse to retrieve antenna temperature.

Note that there are two paths for the noise injection into the receivers; through antenna branch for antenna temperature measurement and directly to the receiver's frontend switch for the calibration of the CAS' noise level.

Data organization in the L0 format

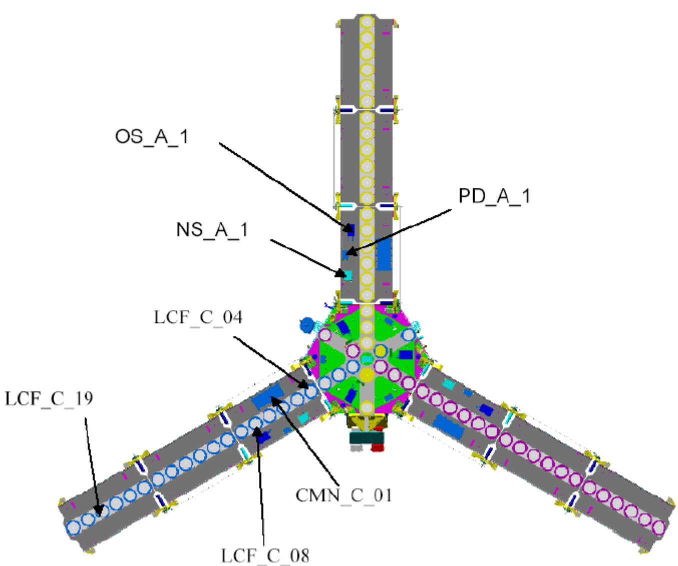

Data organization in the L0 format

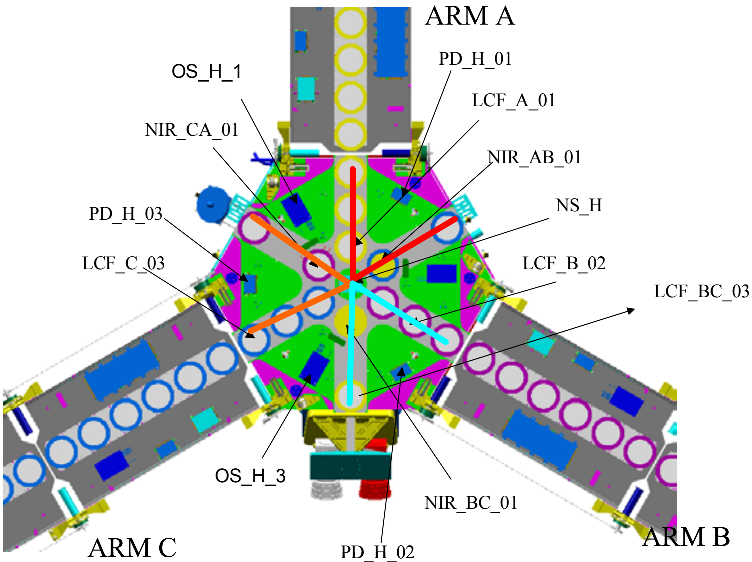

PMS CALIBRATION

Centralized calibration

This calibration is only done for LICEF units in the hub, except for those acting as NIR.

Input data: PMS voltages in CAL mode. 4 point method.

Amplitude of CAS S parameters

NIR measurement of CAS noise sources (warm and hot)

$$v_{offk}^{h} = \frac{v_{2k}^{h} v_{3k}^{h} - v_{1k}^{h} v_{4k}^{h}}{\left(v_{2k}^{h} - v_{4k}^{h}\right) - \left(v_{1k}^{h} - v_{3k}^{h}\right)} \qquad G_{PMS_k}^{hC} = \frac{v_{2k}^{h} - v_{1k}^{h}}{\frac{|S_{k0}|^2}{|S_{N0}|^2}\left(T_{sys_N}^{hC_2C} - T_{sys_N}^{hC_1C}\right)}$$

PMS CALIBRATION

Distributed calibration

The offset voltage can be computed independently for each case. Its final value for those receivers driven twice is the average of both.

1. Calculation of PMS offset from measurements with EVEN_NSs

$$v_{off\,0k}^{e} = \frac{v_{2k}^{e} v_{3k}^{e} - v_{1k}^{e} v_{4k}^{e}}{\left(ve_{2k}^{e} - v_{4k}^{e}\right) - \left(v_{1k}^{e} - v_{3k}^{e}\right)}$$

2. Calculation of PMS offset from measurements with ODD_NSs

$$v_{off\,0k}^{o} = \frac{v_{2k}^{o} v_{3k}^{o} - v_{1k}^{o} v_{4k}^{o}}{\left(ve_{2k}^{o} - v_{4k}^{o}\right) - \left(v_{1k}^{o} - v_{3k}^{o}\right)}$$

3. PMS offset as a mean of ODD and EVEN measurements (if LICEFs are driven twice)

$$v_{off\,0k} = \frac{1}{2}\left[v_{off\,0k}^{e} + v_{off\,0k}^{o}\right]$$

PMS CALIBRATION

Distributed calibration

4. System temperature at CIP plane of h LICEF with calibrated PMS

$$T_{sys_h}^{C} = \frac{v_h - v_{off_h}}{G_{PMSh}^{C}}$$

5. Calculation of PMS gain from measurements with ODD_NSs for receivers in first section LICEF ℓ and NIR-LICEF receivers

$$G_{PMS_l}^{C} = \frac{v_{2l} - v_{1l}}{\frac{\left|S_{l0}\right|^2}{\left|S_{h0}\right|^2}\left(T_{sys_h}^{C_2C} - T_{sys_h}^{C_1C}\right)}$$

Distributed calibration

System temperature at CIP plane of LICEF in the second section of each arm with calibrated PMS, ODD_NSs

(ℓ LICEF)

$$T_{sys_l}^{C} = \frac{v_l - v_{off_l}}{G_{PMS_l}^{C}}$$

Calculation of PMS gain from measurements with EVEN_NS for receivers in second section

(m LICEF)

$$G_{PMS_m}^{C} = \frac{v_{2m} - v_{1m}}{\frac{|S_{m0}|^2}{|S_{l0}|^2}\left(T_{sys_l}^{C_2C} - T_{sys_l}^{C_1C}\right)}$$

Distributed calibration

System temperature at CIP plane of LICEF in the third section of each arm with calibrated PMS, EVEN_NSs (m LICEF)

$$T_{sys_m}^{C} = \frac{v_m - v_{off_m}}{G_{PMS_m}^{C}}$$

Calculation of PMS gain from measurements with ODD_NS for receivers in second section (n LICEF)

$$G_{PMS_n}^{C} = \frac{v_{2n} - v_{1n}}{\frac{|S_{n0}|^2}{|S_{m0}|^2}\left(T_{sys_l}^{C_2C} - T_{sys_l}^{C_1C}\right)}$$